ANTI-OBESITY PHARMACOTHERAPY-INDUCED LOSS OF MUSCLE MASS AND FUNCTION IS RESCUED BY MODULATING DIETARY PROTEIN CONSUMPTION IN A MODEL OF ADOLESCENT OBESITY

Brooke A. Morris

A THESIS SUBMITTED TO THE FACULTY OF GRADUATE STUDIES IN PARTIAL FULFILLMENT OF THE REQUIREMENTS FOR THE DEGREE OF MASTER OF SCIENCE

Graduate Program in Kinesiology & Health Sciences

York University

Toronto, Ontario

August 2025

ABSTRACT

Pharmacological treatment options for obesity management, such as glucagon-like peptide-1 receptor agonists (GLP-1 RAs), yield significant weight loss. Lean mass accounts for a substantial proportion of weight loss, which is contraindicated owing to the reduced muscular mass and quality that presents in obesity, and may have particular implications in an adolescent model. This study determined the effect of semaglutide on body composition, skeletal muscle function, and bone deposition; and whether a protein-enriched dietary intervention could prevent negative effects of semaglutide on musculoskeletal health. Semaglutide treatment led to lower bodyweight, muscle mass, and maximal contractile function in adolescence, but did not affect submaximal contractile or mitochondrial function. Semaglutide improved load-bearing bone volume. Protein supplementation was able to restore bodyweight, muscle mass, and contractile function when used with semaglutide. This study reveals the effects of semaglutide on muscle health in an adolescent obesity model and presents protein supplementation as a viable solution.

ACKNOWLEDGEMENTS

This would not have been possible without the incredible support I have had surrounding me these past two years. I am unimaginably grateful, and I will try my very best to be concise.

To Mum, my biggest cheerleader. Your unwavering belief in me got me through the highs and the lows. Your active listening and thoughtful questions have allowed me to become a passable science communicator. To Dad, you have instilled in me the value of a strong work ethic from the start. You always said you saw me as a writer, so here is me fulfilling your vision, in my own way. To Jack, who was always the smarter sibling between the two of us, thank you for keeping me humble. I love you all immensely.

To Chris, I cannot encapsulate how much the last two years have positively impacted me, as a scientist, and as a human. Your passion for what you do is infectious, and it has been a joy to have you as a supervisor and mentor. Thank you for always making a homesick Nova Scotian feel a little closer to home, even if it came at the expense of being the butt of a joke.

To Gerry, thank you for nurturing my love for science and encouraging me to forge my own path, even if it meant leaving the world of physical chemistry (and thermodynamics). You taught me the importance of loving what you do and keeping the fun in science.

To Maddy and Shar (my girls), Adi, Sham, Luca, and Shiv, I greatly appreciate your patience with me. I will miss our numerous inside jokes, excellent British accents, and laughing so hard it hurts. Maddy, your work ethic is truly admirable, and you are an excellent teacher. Shar, this project would not have been possible without you, your time and dedication has not gone unnoticed. Adi, you saw me from the very start, thank you for helping me grow into myself. Sham, your energy for learning is rare, I am excited to see what the future has in store for you.

And finally, to little me. I hope that in some capacity, you can see us now. And I hope that you're proud.

TABLE OF CONTENTS

LIST OF ABBREVIATIONS

ACh	Acetylcholine
ADL	Activities of daily living
ADP	Adenosine diphosphate
AMP	Adenine monophosphate
AMPK	AMP-activated protein kinase
AP	Action potential
ATGL	Adipose triglyceride lipase
ATP	Adenosine triphosphate
Akt	Protein kinase B
BCAA	Branched-chain amino acids
BLEB	Blebbistatin
BMD	Bone mineral density
BMI	Body mass index
Ca^{2+}	Calcium ion
cAMP	Cyclic adenosine monophosphate
CCK	Cholecystokinin
CDNB	2,4-dinitrochlorobenzene
CHO	Carbohydrate
CI	Complex I
CII	Complex II
CIII	Complex III
CIV	Complex IV
CoQ	Coenzyme Q/Ubiquinone
CPT-1	Carnitine palmitoyltransferase-1
CPT-2	Carnitine palmitoyltransferase-2
CRP	C-reactive protein
CSA	Cross-sectional area
CV	Complex V/ATP Synthase
CVD	Cardiovascular disease
Cyt C	Cytochrome *c*
DHPR	Dihydropyridine receptor
DIO	Diet-induced obesity
DIT	Diet-induced thermogenesis
DMSO	Dimethyl sulfoxide
DPP-IV	Dipeptidyl peptidase IV
EAA	Essential amino acids
EDL	Extensor digitorum longus
ETC	Electron transport chain
e^-	Electron
FA	Fatty acid
FA Carnitine	Fatty acyl-carnitine
FA CoA	Fatty acyl-CoA
$FADH_2$	Flavin adenine dinucleotide
FFM	Fat-free mass
FM	Fat mass

GAS	Gastrocnemius
GLP-1	Glucagon-like peptide-1
GLP-1R	Glucagon-like peptide-1 receptor
GLP-1 RA	Glucagon-like peptide-1 receptor agonist
GLUT4	Glucose transporter, type 4
GPCR	G-protein coupled receptor
GTT	Glucose tolerance test
gWAT	Gonadal white adipose tissue
HSL	Hormone-sensitive lipase
H^+	Proton
H_2O	Water molecule
IL-6	Interleukin-6
IMM	Inner mitochondrial membrane
IMS	Intermembrane space
IR	Insulin receptor
IRS-1	Insulin receptor substrate-1
iWAT	Inguinal white adipose tissue
Kcal	KCalorie
KO	Knockout
K^+	Potassium ion
LCFA	Long-chain fatty acid
MCoA	Malonyl Coenzyme A
MHC I	Myosin heavy chain isoform I
MHC IIa	Myosin heavy chain isoform IIa
MHC IIb	Myosin heavy chain isoform IIb
MHC IIx	Myosin heavy chain isoform IIx
mH_2O_2	Mitochondrial hydrogen peroxide
microCT	Micro computed tomography
MnSOD	Mitochondrial isoform of superoxide dismutase
MPB	Muscle protein breakdown
MPS	Muscle protein synthesis
mtCK	Mitochondrial creatine kinase
mTOR	Mammalian target of rapamycin
NADH	Nicotinamide adenine dinucleotide
Na^+	Sodium cation
Na^+-K^+- ATPase	Sodium-potassium pump
OCT	Optimal cutting temperature
OMM	Outer mitochondrial membrane
OPG	Osteoprotegerin
OXPHOS	Oxidative phosphorylation
O_2	Oxygen molecule
$^{\bullet}O_2^-$	Superoxide anion
PBS	Phosphate-buffered saline
PCoA	Palmitoyl Coenzyme A
PGC-1α	Peroxisome proliferator-activated receptor gamma coactivator 1-α
PIP3	Phosphatidylinositol (3,4,5)-triphosphate

PI3K	Phosphoinositide 3-kinase
PKC	Protein kinase C
PLT	Plantaris
PRO	Protein
PYY	Peptide YY
QUAD	Quadriceps
RANKL	Receptor activator of nuclear factor κB ligand
RDA	Recommended dietary allowance
RyR	Ryanodine receptor
SEMA	Semaglutide
SERCA	Sarco/endoplasmic reticulum calcium ATPase
SOL	Soleus
SR	Sarcoplasmic reticulum
TA	Tibialis anterior
TAG	Triacylglycerol
TCA cycle	Tricarboxylic acid cycle
TFAM	Mitochondrial transcription factor A
TNF-α	Tumour necrosis factor-alpha
TRI	Triceps
T2D	Type 2 diabetes
VEH	Vehicle
VO_{2peak}	Peak oxygen uptake
WD	Western diet

LIST OF TABLES

LIST OF FIGURES

LIST OF SUPPLEMENTARY FIGURES

CHAPTER ONE: INTRODUCTION

Obesity is a chronic, often progressive disease characterized by the excessive accruement of adipose tissue, particularly in the visceral compartment of the body surrounding the abdominal organs.[1] This state of prolonged elevated adiposity leads to long-term, chronic exposure to low-grade inflammation, structural wear-and-tear, and dysfunctional metabolic and energy systems.[1] The consequences of obesity are severe, ranging from hypertension and joint pain up to and including cardiovascular failure, stroke, and even death.[1] The worldwide prevalence of obesity has increased steadily over the past several decades, significantly burdening the global healthcare system and economy.[2] While the rate of obesity appeared to be plateauing during the last decade, the COVID-19 pandemic has been associated with a surge in obesity prevalence once again.[3] Obesity tends to develop slowly, over multiple decades, and the chronic nature of this disease, in combination with myriad other contributing environmental, behavioural, and genetic factors have made it particularly difficult to treat.[4]

While obesity has historically developed in adulthood, in recent decades it has become increasingly common for obesity to present younger, during childhood and adolescence.[5] The causes of childhood obesity reflect those observed in adult-onset obesity: overconsumption of energy amidst a sedentary lifestyle, with genetic and environmental factors contributing as well[5]. Childhood obesity also comes with the associated risks for metabolic disease and dysfunction observed in adult-onset obesity, and the vast majority of obese children remain obese in adulthood.[5] Even when this is not the case, adults of a healthy weight who were obese as children remain at greater risk for obesity-related comorbidities throughout their lives.[5]

Obesity often presents alongside a reduction in relative skeletal muscle mass.[6] Reduced skeletal muscle mass is implicated in metabolic dysfunction independent of adiposity, negatively impacting muscle function at both the mitochondrial and whole-fiber level.[7,8] Furthermore, lower muscle mass is correlated with diminished quality of life and lifespan.[6] Sarcopenic obesity is defined as the simultaneous presence of elevated adiposity and low skeletal muscle mass.[6] In sarcopenic obesity, both the negative side effects of muscle atrophy and excess body fat can interact and further exacerbate one other in a feed-forward loop.[6]

Traditionally, it was thought that states of overweight and obesity were actually beneficial to bone health. This belief came from the observation that obese individuals tend to have greater

bone mineral density (BMD) than their lean counterparts, largely due to the load-bearing excess weight stimulating bone deposition. This does not correlate to better bone health outcomes, as obese individuals are at greater risk for bone injury and fracture, and non-specific joint pain.[9]

Glucagon-like peptide-1 receptor agonists, or GLP-1 RAs, were originally developed for the treatment of Type 2 Diabetes (T2D) to improve glycaemic regulation by stimulating insulin release from pancreatic β-cells.[10] The origins of T2D and obesity are closely related and the two commonly develop alongside one another, as both can occur resulting from prolonged energy intake exceeding energy expenditure.[11] A common side effect of GLP-1 RA prescription for T2D management was significant weight loss in overweight and obese individuals.[10,12] This led to the subsequent development of GLP-1 RAs as weight loss drugs.[12,13]

There are multiple mechanisms by which GLP-1 RAs induce bodyweight reductions, by inhibiting both appetite and hunger, increasing satiety signaling to the brain, and delaying gastric emptying and nutrient absorption; all of which contribute to a reduction in energy intake sufficient to reduce bodyweight.[12,13] Similar to other weight loss interventions, bodyweight reductions are not solely attributable to reductions in adipose tissue, and a decline in lean mass is also observed during GLP-1 RA therapy.[14,15] However, the unprecedented rate of weight loss observed with GLP-1 RA pharmacotherapy has been accompanied with reductions in lean mass greater than previously observed[16]. For context, with semaglutide, lean mass can account for up to 40% of weight loss[15]. Lifestyle interventions such as diet and/or exercise typically present with 14-22% of weight loss as lean mass, with surgical interventions exhibiting slightly greater declines in lean mass, ~17-31%.[16]

This is unfavourable for various reasons, namely that skeletal muscle is one of the body's most metabolically active organ systems, being responsible for over 80% of glucose uptake after an oral glucose load, signifying its importance for efficient glucose disposal.[17] When skeletal muscle atrophy occurs, individuals are at an increased risk for the disruption of normoglycaemia.[18] Likewise, skeletal muscle is a major contributor to energy expenditure at rest, and its loss makes it difficult to maintain the negative energy balance necessary to facilitate weight loss.[19] Also of concern is the induction of muscular atrophy in a population predisposed to low muscle mass, and the implications of this for long-term muscle function and health.

Semaglutide and other GLP-1 RAs are tremendously effective at stimulating weight loss in obesity and improving blood glucose regulation in T2D, two metabolic conditions known to

contribute to burdening the healthcare and economic systems.[2,12] The meaningful benefits experienced by those prescribed these drugs go considerably further than weight loss, extending to increased quality of life and expected lifespan, in addition to reduced rates of certain obesity-related comorbidities, such as cardiovascular events and stroke.[20,21] It is unlikely that, despite the substantial health detriments of skeletal muscle atrophy, prescription of these drugs for weight loss will slow, largely due to the fact that GLP-1 RAs are exceptionally efficacious at inducing weight loss.

This presents an opportunity for targeting the maintenance or promotion of skeletal muscle accretion during semaglutide prescription, thus making it possible to retain the beneficial reductions in body fat whilst maintaining lean mass, of which the majority is accounted for by skeletal muscle. Success in this endeavour is likely to lead to better health outcomes during prescription of anti-obesity pharmacotherapies, in addition to promoting long-term maintenance of weight following the initial weight loss period. Preserving skeletal muscle (and bone) mass during weight loss will lead to improved glycaemic control, maintenance of resting energy expenditure, and decreased risk for fracture and frailty.

We aim to target skeletal muscle preservation in a diet-induced mouse model of obesity undergoing semaglutide therapy through the manipulation of the dietary macronutrient profile. Elevating dietary protein, which is considered to be a lean mass-promoting, or anabolic, macronutrient, may be effective in combating the adverse effects of semaglutide given the ample literature demonstrating the beneficial effect of increased protein consumption on muscle and bone health. Whey and casein are high-quality, complete protein sources which have been previously effective in stimulating maintenance or growth of muscle tissue under many conditions, including weight loss or other circumstances that may compromise the body's ability to maintain its lean mass.

CHAPTER TWO: LITERATURE REVIEW

2.1. Glucagon-like peptide-1 receptor agonists (GLP-1 RAs)

2.1.1 Endogenous glucagon-like peptide-1 (GLP-1) and the GLP-1 receptor (GLP-1R)

Glucagon-like peptide-1 (GLP-1) belongs to a family of hormones that function largely in the role of appetite regulation.[22] GLP-1 is synthesized during the degradation of proglucagon in the L-cells of the intestinal mucosa, pancreatic α-cells, and neurons located in the nucleus of the

solitary tract, but is primarily secreted by the enteroendocrine L-cells.[22] It is responsible for inhibiting food intake and hunger cues via both mechanosensory mechanisms in the gut and modulation of hypothalamic regions responsible for regulation of feeding, where a high density of the GLP-1 receptors reside.[22] Peripherally, GLP-1 defers nutrient delivery through the gastrointestinal (GI) tract by temporarily paralyzing the smooth muscle lining it, delaying nutrient absorption after ingestion.[22] This reduction in gastric motility is known as the 'ileal brake' and also contributes to satiety following a meal **(Figure 1)**.[23]

Other hormones that contribute to appetite regulation are peptide YY (PYY), cholecystokinin (CCK), leptin, and ghrelin.[24] PYY is also secreted by the L-cells in response to the presence of nutrients in the GI tract and enhances the appetite suppressing effects of GLP-1.[24] CCK is secreted by the I-cells of the duodenum and participates in digestion.[24] GLP-1 may indirectly stimulate secretion of CCK as well.[24] Unlike the aforementioned hormones, leptin is secreted by adipocytes, and acts as a signal to the central nervous system (CNS) regarding the status of the body's energy stores.[24] Leptin regulates appetite at the level of the hypothalamus and can stimulate secretion of GLP-1.[24] GLP-1, PYY, CCK, and leptin are all classified as anorexigenic hormones, due to their negative regulatory effect on appetite.[24] Ghrelin, on the other hand, is considered a "hunger hormone".[24] Its actions oppose that of GLP-1 and other anorexigenic hormones as it stimulates appetite and food intake.[24]

GLP-1 does not function solely in appetite inhibition, and also plays a role in glucose homeostasis by stimulating secretion of insulin and inhibiting glucagon secretion following nutrient ingestion through the 'incretin effect', characterizing this peptide as an incretin hormone.[22] As such, GLP-1 contributes to metabolic control and regulation of nutrient intake through both centrally and peripherally mediated mechanisms, by direct and indirect signaling pathways.

The GLP-1 receptor (GLP-1R) is a G-protein-coupled receptor (GPCR) expressed across many tissues in the body, including the central and peripheral nervous systems, pancreas, cardiac and skeletal muscle, and potentially adipose tissue.[22] Endogenous GLP-1 has an incredibly short half-life, undergoing catalytic degradation by the enzyme dipeptidyl peptidase-IV (DPP-IV) within 1-2 minutes of its secretion, limiting its viability and duration at the active site of the receptor, and thus its ability to exert its downstream effects on satiety signaling and glucose homeostasis **(Figure 1)**.[22]

Activating the GLP-1R leads to the production of cyclic adenosine monophosphate (cAMP) and downstream activation of the classic insulin signaling cascade through activation of phosphatidylinositol-3 kinase (PI3K).[22] In rodent models, while GLP-1R knockout (KO) mice are viable, they exhibit dysregulated appetite control and feeding patterns leading to progressive weight gain.[22] Additionally, GLP-1 KO models have shown impairments in blood glucose homeostasis, cardiovascular function, and even altered cognitive function,[22] all of which are corroborated in the human Metabolic Syndrome.

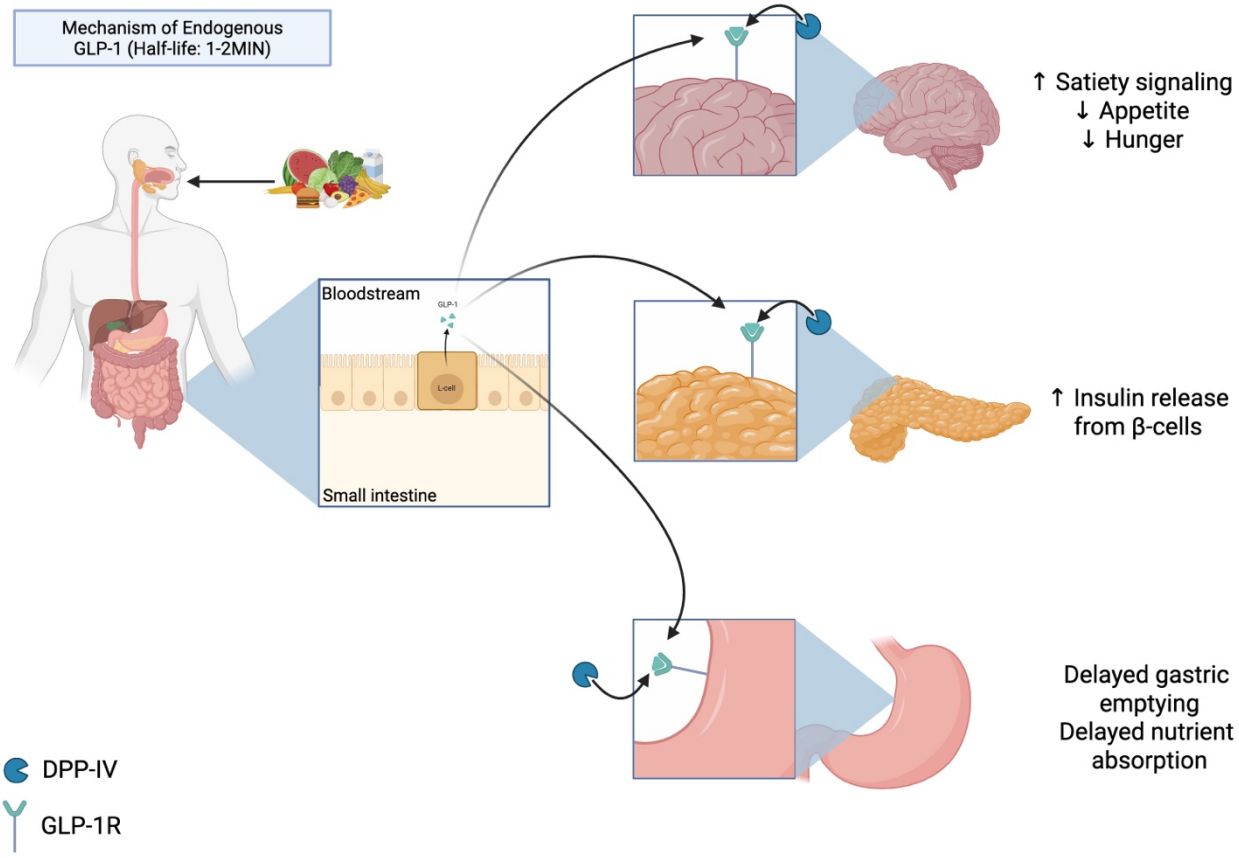

Figure 1. Functions of endogenously synthesized GLP-1. GLP-1, produced by the enteroendocrine L cells, is released to circulation where it can bind to its receptor on multiple tissues in the body and exert its effects. It is quickly catalytically degraded by the enzyme DPP-IV within a few minutes of its secretion, owing to issues with upregulating endogenous GLP-1 production not being effective diabetic or weight management treatment options. GLP-1 = glucagon-like peptide-1. GLP-1R = glucagon-like peptide-1 receptor. DPP-IV = dipeptidyl peptidase-IV.

2.1.2 Development of GLP-1 RAs as therapeutic agents

The short half-life of endogenously synthesized GLP-1 had previously presented as a barrier to the use of the peptide for therapeutic purposes but has since been circumvented by exogenous activation of the GLP-1R by a GLP-1 RA such as semaglutide **(Figure 1 & 2)**.[25] Semaglutide has a half-life of approximately one week, several orders of magnitude greater than

that of endogenously secreted GLP-1[22,25]. When semaglutide binds the N terminus of the GLP-1R, it mimics the actions of endogenous GLP-1 **(Figure 2)**.[25] The prolonged viability of semaglutide is owing to the addition of an acylated fatty acid in its structure, a therapeutic strategy commonly used to increase drug circulation time.[25] After entering circulation, semaglutide monomers reversibly bind to serum albumin via this acylated fatty acid.[25] Association with albumin prevents both enzymatic degradation and clearance by the kidneys until the GLP-1R is reached, when the active drug will dissociate from albumin to activate the GLP-1R.[25] Eventually, semaglutide faces the same fate as endogenous GLP-1, and is degraded by DPP-IV, despite its original resistance due to both its size and albumin-binding affinity.[25]

While originally developed to treat T2D because of its insulinotropic effects, a side effect of semaglutide prescription was moderate weight loss, leading to clinical trial implementation for the use of semaglutide as an anti-obesity pharmacotherapeutic aid.[10,12] Clinically meaningful weight loss is classified as a reduction in bodyweight >5% from baseline, which is considered the threshold for which improvements in health metrics are observed.[26] On average, obese individuals taking semaglutide for weight loss see reductions of 14.9% in bodyweight, greatly surpassing the minimum recommendations for improved metabolic health.[12]

The most common side effect associated with semaglutide and other GLP-1RAs is gastrointestinal distress in the form of nausea and diarrhea.[12] For this reason, the drug is often administered starting at a low dose, and dosage is increased every 2-4 weeks as tolerable until the desired maintenance dose is obtained.[12] Despite this, semaglutide displays a reliable safety profile, with severe adverse side effects being very rare.[12] There does appear to be increased risk for acute kidney injury and pancreatitis in genetically predisposed individuals.[12]

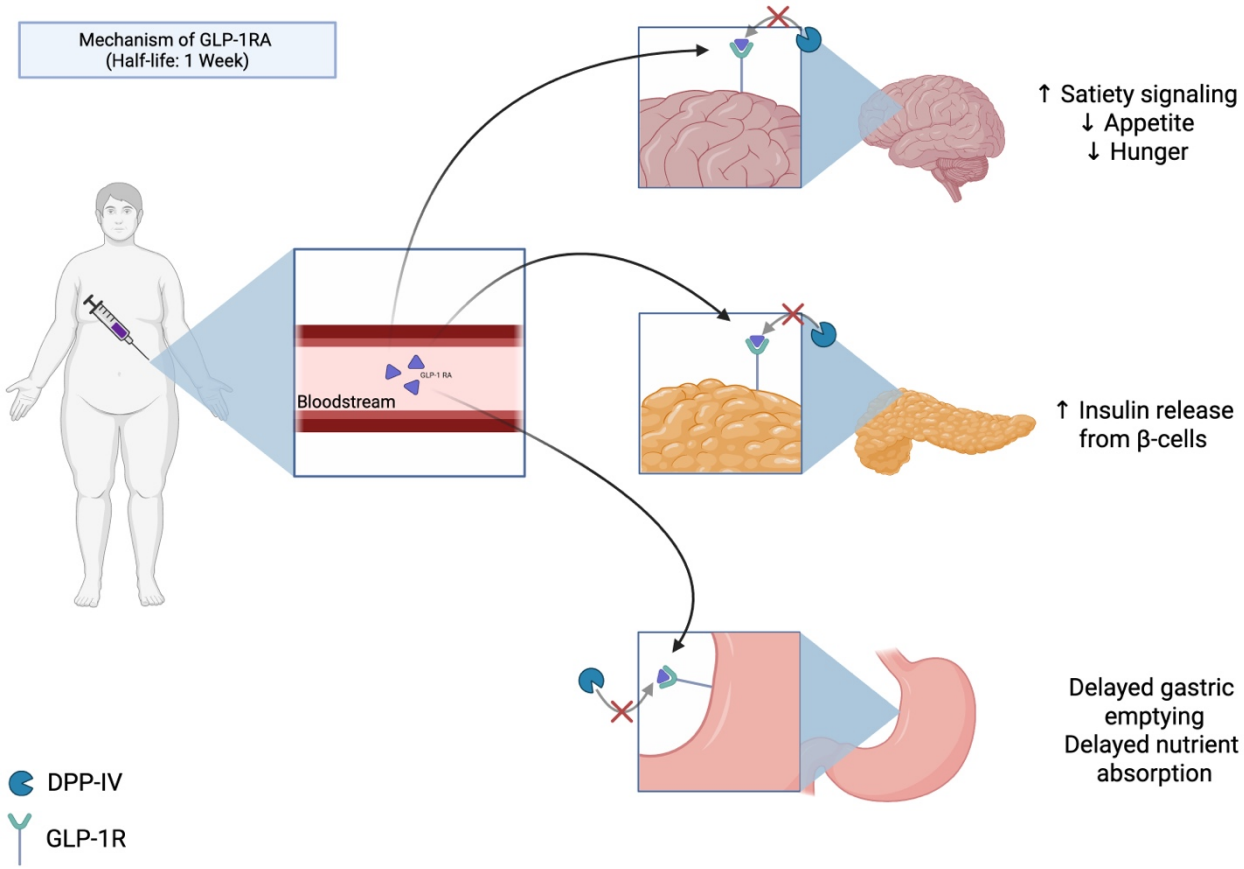

Figure 2. Exogenously administered GLP-1 RA mechanism. GLP-1 RAs are resistant to catalytic degradation by DPP-IV, extending their half-life to approximately 1 week, making them a viable option for diabetes and obesity management given they exert their effects in the same manner as endogenously synthesized GLP-1. GLP-1 = glucagon-like peptide-1. GLP-1R = glucagon-like peptide-1 receptor. GLP-1 RA = glucagon-like peptide-1 receptor agonist. DPP-IV = dipeptidyl peptidase-IV.

2.1.3 GLP-1 RA consequences for skeletal muscle health

Weight loss interventions with the objective of improving health and reducing the risk for developing chronic disease are sought out to reduce total body fat, or adipose, stores. However, total weight loss is typically not solely accounted for by reduced adipose mass and involves concurrent reductions in lean mass, mainly as skeletal muscle.[16] Though unavoidable, lean mass loss, often observed as skeletal muscle atrophy, should be minimized, because of its vital roles in glucose disposal, energy expenditure, and locomotion driven by contractile force generation.[17,19]

While effective in stimulating both weight and adipose reductions, GLP-1 RA medications can also exhibit greater reductions in lean mass compared to both lifestyle and surgical interventions.[16] Overweight and obese patients lose ~15.3kg within the first year of semaglutide treatment, with up to 40% of weight loss as lean mass.[12,15] The mechanism by which this occurs is yet to be elucidated but may be due in part to the rapidity at which weight loss is often observed,

or through another as yet undefined avenue. The high variability of lean mass reductions observed with pharmacological weight-loss treatments may be accounted for by differences in patient population, inclusion criteria, or drug dosage.

Oftentimes, the proportion of lean mass improves following chronic semaglutide use, known as the 'lean-fat ratio' (total lean mass/total adipose mass).[12] While improvements in the ratio of lean to fat mass are reliable predictors of improvements in health outcomes,[27] this does not negate that for reductions in bodyweight of approximately 15 kilograms (kg) in one year, up to 6kg (40%) of weight loss can be lean tissue. This reduction is significantly greater than the annual rate of muscle loss reported in conditions such as cancer cachexia and age-related sarcopenia.[28,29] Furthermore, this occurs in a population predisposed to low muscle mass and quality prior to treatment onset.[6]

Clinical trials investigating GLP-1 RA use have typically involved follow-up only within this first year of treatment, and often even less.[15] This is important as it signals not only are reductions in body and muscle mass significant, they are also incredibly rapid. Accelerated loss of muscle mass likely has negative consequences on skeletal muscle and mitochondrial health and function, which could lead to increased risk for frailty and early loss of independence in a clinical population predisposed to Metabolic Syndrome and early death.

2.1.4 GLP-1 RA consequences for bone health

The novelty of semaglutide use for treating overweight and obesity brings into question the breadth and depth of effects these drugs may have across the entire organism aside from adipose and skeletal muscle tissue. The GLP-1R is expressed across several different tissue types and has indirect effects in tissues where it is not present or has not been detected as of this writing.[30,31] As such, GLP-1 RA use may exert non-targeted effects on other tissue types, such as bone tissue. To receive the long-term benefits of sustained bodyweight reduction and lower risk for chronic disease, lifetime GLP-1 RA use is likely necessitated.

Bone turns over at a slower rate than other lean tissues, and any effect GLP-1 RA use for obesity may have on bone structure is unlikely to become apparent immediately.[32] While the current literature is still emerging and largely revolves around the first year of semaglutide treatment, this leaves much unanswered concerning how GLP-1 RAs may interact with bone health, both from a structural and functional scope. It is important to consider that non-pharmacologic weight loss interventions have shown increased risk for fractures in obese subjects,

likely attributable to increased circulating markers of bone turnover and reduced bone mineral density (BMD).[33] Accordingly, the question then becomes: does semaglutide therapy *further* exacerbate frailty and fracture risk beyond that seen during intentional non-pharmacologic weight loss?

Evidence in non-pharmacological weight loss interventions involving overweight and obese individuals suggests that negative consequences on bone metabolism appear in subjects who have lost >10% of initial bodyweight.[33] With semaglutide exhibiting, on average, ~15% bodyweight reductions from baseline within the first year on treatment,[12] this treatment falls within the critical threshold for impacting markers of bone health. The current limited body of evidence is inconclusive with respect to how GLP-1 RA treatment can affect bone metabolism and integrity.[32] Human studies in T2D patients have not shown negative effects of GLP-1 RA on bone health as outlined by maintenance of bone mineral density (BMD) and no change in risk for fracture occurrence.[32] GLP-1 RAs are prescribed at a lower dose to treat T2D, and thus if a dose-dependent effect of GLP-1 RAs on bone health is occurring, it has yet to be elucidated.[32]

2.2. Dietary weight-loss interventions, protein intake, and musculoskeletal preservation

Overweight and obese individuals undergoing weight loss interventions exhibit, to a degree, non-tissue specific reductions in bodyweight.[16] Meaning, that while the aim of weight loss interventions is to reduce total body fat mass (FM) and the relative proportion of the body attributed to fat, a certain degree of lean body mass loss occurs simultaneously, which is primarily attributed to skeletal muscle, but also includes bone mass and the organs as well.[16]

There is ample literature investigating the optimization of weight loss via non-pharmacological means, both through modification of dietary composition and as well as by reducing sedentariness.[16] The more powerful weight loss stimulus between these lifestyle interventions being reducing energy intake to a point below total energy expenditure.[16] Additionally, modulating dietary macronutrient composition can help preserve lean mass while maintaining meaningful reductions in adiposity by elevating both the relative proportion of protein in the diet in addition to increasing overall dietary protein intake.[34] Consideration of high-quality, complete protein sources is likely to be a highly efficacious means of preserving lean mass during weight loss interventions, leading to a more targeted approach in combating overweight and obesity.

2.2.1 Dietary weight loss interventions

In overweight and obese individuals, targeting reductions in total bodyweight have shown to improve several cardiometabolic health outcomes, expand quality of life, and ultimately extend lifespan.[26] Losing as little as 5% of initial bodyweight has shown to lead to improvements in these indices of health and is considered clinically significant.[26] Recommended weight loss targets for obese individuals range from 5-10% from baseline, according to the US's Obesity Guidelines from 2013.[35]

The degree of lean mass loss occurring with weight-loss interventions appears to be intervention-specific.[16] Pharmacological interventions, such as use of GLP-1 RA drugs, can exhibit up to 40% of weight loss as lean mass.[15] Bariatric surgery is a weight loss intervention that was historically considered to be associated with a significant degree of skeletal muscle atrophy, however, it preserves, on average, 25% *more* lean mass compared to GLP-1 RAs.[16] Weight loss interventions utilizing caloric restriction exhibit approximately half of the lean mass loss witnessed with some GLP-1 RAs.[16] Furthermore, in some circumstances, through an adjustment of the dietary macronutrient profile to elevate relative dietary protein intake, caloric restriction has not led to significant reductions in lean tissue.[34]

2.2.2 Long-term weight maintenance via lifestyle interventions

There is currently no generally accepted consensus for what is considered successful long-term weight maintenance following weight loss. Periods of long-term weight maintenance described in the literature range from 1-5 years.[36] ~20% of overweight and obese individuals who lose at least 10% of their starting bodyweight using lifestyle interventions such as diet and/or exercise are able to maintain it at the 1-year mark.[37]. In the ~80% of individuals unable to sustain a reduced bodyweight, weight regain occurs primarily as adipose tissue, and lean mass loss observed during the initial weight loss period is not recovered during the weight regain period.[38]

Thus, not only are the health and quality of life benefits attributed to weight reductions lost when weight regain occurs, but body composition has also been affected, with declines in relative lean mass accounted for by coincident increases in fat mass.[38] What this demonstrates is that lifestyle interventions, including nutritional interventions, are effective short-term weight loss strategies, in that they produce successful initial weight loss, but are not appropriate long-term solutions for the majority of individuals looking to maintain a reduced bodyweight. The complex mechanisms underpinning the struggle of weight maintenance following an initial period of weight

loss are multi-faceted, and the advent of long-term GLP-1 RA use may prove effective, when combined with other lifestyle factors, in sustaining long-term weight loss and the associated health and longevity benefits.

2.2.3 Efficacy of dietary protein in promoting weight loss

Protein is considered to be the most satiating macronutrient, and part of the importance of consuming protein regularly and in sufficient quantities is due to its ability to curb hunger and appetite in between feedings.[39] Even when weight loss is not the focus, when individuals consume diets higher in protein, feelings of satiety are improved in high-protein compared to high-carbohydrate diets.[39] As such, weight loss interventions targeting higher relative protein consumption alongside a caloric deficit may be more effective in sustaining long-term weight loss.[39] This outcome is likely due to the satiating effect of protein contributing to chronically reduced *ad libitum* energy intake sufficient to maintain a reduced bodyweight.[39] While likely minor, diet-induced thermogenesis (DIT) may contribute to the environment in which protein can contribute to weight loss.[40] Protein is the macronutrient which contributes the most to DIT, as it raises it to a greater degree than carbohydrates or fat, meaning that increasing protein consumption could support weight loss due to the greater energy utilization required to break down dietary protein.[40]

The current Canadian Recommended Dietary Allowance (RDA) for daily protein intake is prescribed as 0.8g protein/kilogram bodyweight/day. This intake is suggested to be sufficient for ~98% of individuals to maintain net muscle protein balance, but is not adjusted for age, sex, or other lifestyle factors, despite the blunted anabolic response in aged skeletal muscle to muscle protein synthesis (MPS).[41] Certain studies have shown that increased intakes above the RDA ranging from 1.2-1.6g protein/kilogram bodyweight/day can contribute to promotion and maintenance of skeletal muscle mass.[41] Increasing both the relative proportion of the diet attributable to protein and total dietary protein content is an effective strategy for preserving skeletal muscle mass during weight loss interventions.[34] These studies have typically included exercise protocols in addition to increasing dietary protein intake. Therefore, it is difficult to conclude that the skeletal muscle preservation observed is solely attributable to protein intake and not the exercise intervention or a synergetic response to both.

Not only is targeting protein consumption important for the long-term viability of sustaining meaningful weight loss, it is also useful for stimulating *quality* weight loss.[34,39] One of

the most important roles of dietary protein is in its provision of amino acids to the body's amino acid pool.[42] Once dietary protein has been degraded to its constituent amino acids, it can be utilized in a multitude of different bodily processes, one of them being muscle protein synthesis (MPS).[42] When muscle protein synthesis is increased sufficiently, it can drive the net rate of muscle protein turnover towards accretion.[39,43] Josse and colleagues have shown this can occur in overweight and obese premenopausal women even when calorie intake is restricted, demonstrating a capacity for the body to undergo a more target form of weight loss, where loss of lean mass can be minimized or even abolished by reducing total energy intake and elevating the total and/or relative contributions of protein to the diet.[34]

In addition to increasing overall or relative protein consumption, protein quality is of particular relevance. High-quality protein sources containing all essential amino acids (EAAs), in particular the amino acid leucine, are necessary to maximally stimulate MPS following nutrient ingestion.[44] Protein quality is furthermore determined by both its rate of digestion and bioavailability.[44]

2.2.3A Whey

Whey protein is a high-quality protein source derived from dairy, with a complete amino-acid profile that is particularly rich in the branched-chain amino acids (BCAAs) and cysteine, which play roles in whey's skeletal muscle-promoting properties.[41,44] Whey is often considered to be the 'superior' dietary protein for musculoskeletal and overall health benefits, even when compared against other complete protein sources.[41,44] Its superiority is multi-faceted, and attributable in part to its ability to shift muscle protein turnover towards net synthesis and fast rate of digestion and absorption.[41,44]

Leucine is part of the subgroup of amino acids known as BCAAs, and typically accounts for ~10% of amino acid content by weight in whey protein.[43] It is considered to be the most important single component in stimulating MPS, due to its ability to activate signaling cascades upstream of the anabolic growth regulator mammalian target of rapamycin (mTOR), resulting in an increase in its translation.[43] In aging rats, supplemented chow using leucine alone or as a component of whey protein is able to partially overcome the 'anabolic resistance' observed in aging muscle and effectively stimulate MPS.[43]

Another amino acid present in relatively high concentrations in whey protein is cysteine.[41,45] Cysteine is important for whole-body antioxidant defence as it is the rate-limiting

amino acid required for glutathione synthesis.[46] Glutathione neutralizes reactive oxygen species (ROS), becoming oxidized itself in the process.[46] It is then returned to its reduced form through the actions of glutathione peroxidase.[46] Infusing C2C12 cells with whey protein increases the concentration of reduced glutathione and the activity of glutathione peroxidase, which demonstrate improvement in the cellular antioxidant defence system.[45]

Ultimately, whey supplementation exhibits favourable effects from the molecular to whole body level.[40,41,44,45] It is able to increase total appendicular lean mass, muscle fiber cross-sectional area, and muscle protein turnover.[40,41] When utilized during a weight loss intervention, it has been effective in yielding high-quality weight loss, and more pronounced weight loss than energy restriction alone.[39] It may also be useful in the context of reducing the associated chronic low-grade inflammation characteristic of obesity due to its promotion of anti-oxidant buffering molecules.

2.2.3B Casein

Cow's milk protein is comprised predominantly of casein, accounting for the ~80% of its protein content.[41] While still relatively high in leucine, it is not as rich in the amino acid as is whey.[41] Casein is also considered to be cysteine-poor, thus not contributing significantly to the body's antioxidant pool.[47] Another difference between casein and whey protein is their rate of digestion and absorption, with casein protein ingestion exhibiting slower rates of both processes.[41]

Casein modulates muscle protein turnover by a different mechanism than whey.[48] It can increase MPS, albeit more modestly, by contributing its constituent amino acids to the amino acid pool following digestion and absorption.[48] While playing a more minor role in respect to the amount in which it is able to elicit hyperaminoacidemia, casein ingestion is associated with a more *prolonged* state of elevated plasma amino acids at the whole body level.[48] It affects muscle protein turnover to a greater degree on the opposite end of the equation, by inhibiting muscle protein breakdown (MPB), with its slow digestibility being an advantage in this instance, as casein is able to maintain the amino acid supply following its ingestion for an extended period of time.[44,48]

The combination of whey and casein, where the former is able to stimulate muscle protein synthesis and contributes a sharp, rapid increase in available amino acids, with the latter contributing a more modest increase in amino acids for a longer in duration in addition to inhibiting muscle protein breakdown; leads to a potent driver of the muscle protein turnover equation in the direction of net synthesis. For this reason, the combination of the two proteins may be more

powerful at eliciting benefits for musculoskeletal health during weight loss than either independently.

	Whey	**Casein**
Source?	Dairy products	Dairy products
Complete amino acid profile?	Yes	Yes
Rate of digestion?	Fast	Slow
Rate of absorption?	Fast	Slow
Leucine concentration?	High	High (lower relative to whey)
Cysteine concentration?	High	Low
Contribution to muscle protein turnover?	Strongly simulates MPS	Moderately stimulates MPS, Inhibits MPB

Table 1. Comparison of whey vs casein protein sources. MPS = muscle protein synthesis. MPB = muscle protein turnover.

2.2.4 The role of dietary protein in muscle function

The role of dietary protein has by now been established for its significance in skeletal muscle mass maintenance and promotion. What is less clear is protein's ability to improve skeletal muscle function independently. While a broad term, what is implied by 'skeletal muscle function' will be considered to be inclusive of strength, or contractile function, and endurance, or oxidative and glycolytic energy-producing capacity to keep up with the demands of the body.

In untrained healthy adults, protein supplementation is superior to energy-matched carbohydrate supplementation at improving whole body strength when used chronically alongside a resistance training regimen, although it is not thought to be a major contributor to strength gains in this context, and likely has a minor secondary role.[49] This has been replicated across multiple training modalities, lengths of training programs, and types of protein supplementation, with little variability.[49] Of note is that gains in strength typically occur concomitant to gains in lean mass, so it is difficult to elucidate whether gains in strength are attributable solely to greater muscle mass.[49] Additionally, chronic resistance training is known to elicit improvements in muscle strength independent of protein supplementation.[49] The key here is that protein supplementation may lead to greater improvements in strength, when combined with chronic resistance exercise, compared to resistance training alone, or resistance training in combination with non-protein-derived energy supplementation.[49]

The ability of protein supplementation to modulate aerobic muscular function has been investigated by Ferguson-Stegall et al.[50] While minimally effective in athletic populations, in clinical and sub-clinical populations where limitations such as intensity and volume are at play, protein supplementation has been shown to improve VO_{2peak} during an endurance exercise training regimen.[50] This may be especially relevant for the overweight and obese population, who may have limitations to the degree with which they can perform endurance exercise resulting from a sedentary lifestyle and prolonged strain on weight-bearing joints.

2.2.5 The role of dietary protein in structural and functional characteristics of bone

While the beneficial effects of protein consumption on skeletal muscle health are quite apparent, the picture is not so clear-cut in the context of bone health. Diets lacking in adequate protein may place individuals at risk for structural failure of bone, but increasing dietary protein consumption beyond the RDA does not elicit benefits in a dose-response manner, meaning that diets elevated in protein are not superior so long as baseline protein consumption is sufficient.[51]

Protein supplementation does not help or harm bone mineral density, markers of bone turnover, or fracture risk appreciably in human or animal models, indicating it is likely not the most important factor contributing to bone health in healthy or obese populations. [51]

2.3. Obesity, skeletal muscle, and mitochondria

2.3.1 Obesity

Obesity presents as significantly elevated body weight resulting from a chronic imbalance between energy intake and energy expenditure, to a point where energy consumption greatly exceeds disbursement.[1] The current primary diagnostic criterion for obesity is the body mass index (BMI) scale, where a BMI greater than 30kg/m^2 is defined as obese.[1] Obesity can further be divided into 3 subgroups, with Class I obesity falling within a BMI range of 30.0-34.9, Class II within 35.0-39.9, and Class III obesity classified as a BMI greater than 40.0kg/m^2.[52] While use of BMI to classify obesity has its own limitations as it reflects total body weight, not fat mass, there is a positive association between BMI, cardiometabolic complications, and all-cause mortality.[1] Whilst obesity can be calculated from height and weight measurements; it is the distribution of weight, and particularly adiposity, that is central to its negative health consequences.[1]

The waist-to-hip ratio is another commonly used diagnostic tool for obesity identification.[1] A ratio >0.9 for males and >0.85 for females is sufficient to diagnose obesity, as it provides an

indirect assessment of centralized adiposity[1]. Significant accumulation of adipose tissue in the abdominal compartment surrounding the organs, known as visceral adipose tissue, is most commonly related to adverse health outcomes observed in obese individuals.[53] Subcutaneous adipose tissue located just deep to the dermis, does not appear to contribute to the environment of chronic low-grade inflammation, illness, and premature death in the same manner.[53] Use of both BMI and waist-to-hip ratio together provides a better idea of the risk for adverse health outcomes in individuals who may be obese, as each has their own limitations.[1]

Additional stores of adipose tissue in and of themselves are not inherently harmful. However, adipose tissue is not solely a medium for energy storage.[54] Adipose tissue can be considered an endocrine organ due to its ability to synthesize and secrete hormones, such as adiponectin and leptin.[54] Adiponectin and leptin regulate inflammation and energy balance, respectively.[54] Interestingly, both of these hormones' quantity and efficacy are blunted in obesity. Adipose also secretes pro-inflammatory cytokines such as tumour necrosis-factor-α (TNF-α) and interleukin-6 (IL-6).

When adipose tissue is accrued so the proportion of bodyweight comprised of it significantly outweighs the physiological norm, its signaling and activity becomes dysregulated.[54] This is one way in which obesity has become associated with abnormal activation of the inflammatory signaling pathways involving TNF-α, IL-6, and C-reactive protein (CRP) in overweight and obese women, among others.[54,55] These inflammatory signaling pathways are also elevated in non-obese, but frail elderly populations,[56] likely explained by insufficient muscle mass. The obesogenic environment also contributes to elevated individual risk for developing cardiovascular disease (CVD), insulin resistance and T2D, multiple types of cancer, early mortality, and strongly promotes Metabolic Syndrome.[1,11,53]

2.3.2 Implications for muscle mass and health with obesity

The role of skeletal muscle as a key metabolic organ and primary driver of movement and balance makes its growth and preservation vital for health.[7,8,57] The lean, healthy human body consists of about 40% skeletal muscle mass by weight.[58] However, many diseases are associated with or exacerbated by significant muscular atrophy, including Duchenne muscular dystrophy and cancer cachexia.[28] The age-related loss of muscle mass and function, known as sarcopenia, increases morbidity and mortality as well.[6,59] Conversely, elevated skeletal muscle mass is linked

to improved health outcomes in diseased patient populations, and increased life expectancy in healthy populations, cementing its role as a biomarker of health.[60]

Obese individuals regularly present with a lower proportion of bodyweight as fat-free mass (FFM), which largely includes skeletal muscle.[6] As one of the largest and most metabolically active organ systems in the body, skeletal muscle is vital for glucose uptake and use, locomotion, and overall energy expenditure.[17,19] While obesity is often associated with a greater total amount of lean tissue due to what has been described as a 'training effect' of carrying excess weight on one's frame, the percentage of body mass occupied by lean mass is significantly reduced, and often of lower quality.[6]

Sarcopenic obesity is characterized by the manifestation of excess adiposity, reduced relative skeletal muscle mass, and muscle weakness.[6] Sarcopenic obesity is likely more dangerous than sarcopenia or obesity independently, as not only do the negative effects of each disease present concurrently, they are also likely to worsen one another. Low muscle mass and excess adiposity independent of one another exhibit several shared characteristics, including the activation of similar pro-inflammatory signaling pathways, elevated rate of connective tissue disorders and other chronic diseases, and lower quality of life and life expectancy.[6]

The origins of both sarcopenia and obesity also follow similar patterns, with both being linked to a sedentary lifestyle and low-quality nutrition.[6] As sedentariness has increased globally, physical activity, a major stimulus for skeletal muscle accrual, has declined. These factors interact and likely work in synergy to exacerbate one another, leading to further accumulation of adipose tissue, increasing the proportion of bodyweight attributed to fat mass and decreasing the proportion attributed to FFM and skeletal muscle.

2.3.3 Implications for muscle structural and functional capacity with obesity

2.3.3A Muscle contractile activity

A primary function of skeletal muscle is in the elicitation and control of body movement via contractile force production.[57] There are multiple stages of regulating skeletal muscle contraction, including through the coupling of neural impulses arriving externally to intracellular calcium handling, metabolic pathways that determine ATP supply, and pH regulation.[57]

Both preclinical and clinical literature has shown that overweight and obese phenotypes are associated with greater absolute force output compared to their lean counterparts.[61] This can be explained by two factors, firstly, a heavier bodyweight often requires more muscle to perform

activities of daily living (ADL), thus contributing to a 'training effect' of sorts where strength adaptations can lead to greater maximal force output.[61] Secondly, greater total lean mass that occurs in overweight and obesity is also likely to be a result of this training effect and is associated with a greater force-generating capacity.[61] However, when normalized to bodyweight, the previously observed 'advantage' of greater bodyweight on maximal contractile function disappears, with overweight and obese individuals producing reduced force per unit mass.[57]

Structurally, obese skeletal muscle shows marked differences that can affect its function as well. Significant fat infiltration, sometimes referred to as 'marbling', can occur, reducing muscle quality and displacing the structural components of individual fibers as well.[62,63] Fat infiltration can occur inter- and intra-muscularly, with excess accumulation of either type contributing negatively to transduction of neural impulses, the low-grade inflammatory environment, and overall force-generating capacity. [57,62,63]

At the fiber-level, obese skeletal muscle shows a preference for shifting toward a fast-twitch phenotype.[64,65] Mouse models of diet-induced obesity have demonstrated this by showing significant reductions in relative type I fiber content, accounted for by a shift towards more fast-twitch fiber types.[64,65] Type II muscle fibers display reduced mitochondrial concentrations, preferentially generate ATP using glycolysis, and are more fatigable owing to their greater force-generating capacity.[65] Type II fibers are also less sensitive to insulin-stimulated glucose uptake, and the higher incidence of these in obese skeletal muscle could contribute to peripheral insulin resistance.[65]

The transition towards a fast-twitch muscle fiber phenotype in obesity can be accounted for at numerous levels, such as disrupted calcium (Ca^{2+}) handling.[66] Diet-induced obese mouse models display reduced contractile function explained by impaired release of Ca^{2+} from the sarcoplasmic reticulum (SR) during contraction and impaired Ca^{2+} reuptake to the SR during the relaxation phase **(Figure 3)**.[66] Another potential contributing factor is the blunted activation of AMPK in obese skeletal muscle.[67] AMPK is an energy sensing molecule activated by AMP and competitively inhibited by ATP at the same site.[67] Obese skeletal muscle is in an environment of energy surplus, so activation of AMPK is diminished and thus its downstream effects contributing to oxidative slow-twitch fiber phenotypes are dampened in obese skeletal muscle.

Studies investigating the effects of GLP-1 RAs and/or nutritional interventions on muscle force-producing capacity may consider how these interventions could individually, and potentially

synergistically, modify skeletal muscle from a perspective that encompasses whole organ function down to individual fiber-type.

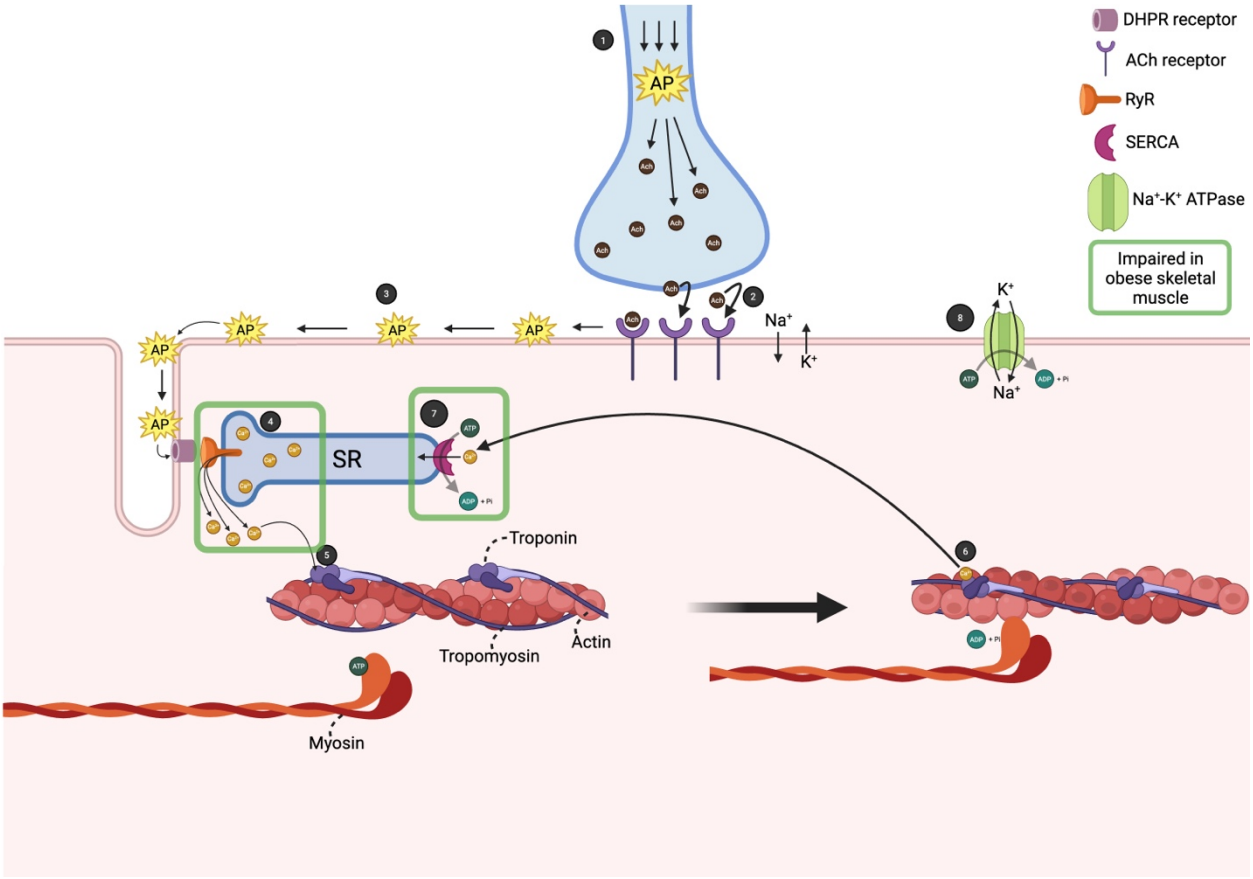

Figure 3. Locations of contractile impairment in obese skeletal muscle. Green box outlines steps in the contractile process that are impaired in obese skeletal muscle. **1)** An AP arrives at the neuromuscular junction, causing the neuron to release ACh, **2)** where it will bind with its receptor and depolarize the sarcolemma. **3)** The depolarization is propagated along the sarcolemma and enters the cell via DHPR receptors in t-tubules, **4)** catalyzing Ca^{2+} release from the SR via RyR; this is blunted in obesity. **5)** Intracellular Ca^{2+} binds troponin, moving tropomyosin away from actin's active site so myosin can bind to it. **6)** Upon binding actin, ATP hydrolysis allows myosin to exert force on actin, resulting in contractile force production. **7)** For relaxation to occur following contraction, Ca^{2+} must return to the SR, fulfilled by SERCA hydrolyzing ATP; Ca^{2+} uptake is also impaired in obesity. **8)** The Na^+-K^+ ATPase pumps Na^+ and K^+ against their electrochemical gradients to repolarize the cell and prepare it for the arrival of another AP. ACh = acetylcholine. ACh receptor = acetylcholine receptor. ADP = adenosine diphosphate. AP = action potential. ATP = adenosine triphosphate. Ca^{2+} = calcium ion. DHPR receptor = dihydropyridine receptor. K^+ = potassium ion. Na^+ = sodium ion. Na^+-K^+ ATPase = sodium-potassium ATPase. P_i = inorganic phosphate RyR = Ryanodine receptor. SERCA = sarcoplasmic-endoplasmic reticulum calcium ATPase. SR = sarcoplasmic reticulum.

2.3.3B Muscle metabolic capacity

The energy demands required by skeletal muscle to contract and perform other cellular functions are supplied by the mitochondrial ATP supply.[68] Diet-derived glucose and lipids are the primary substrates contributing to ATP generation in skeletal muscle.[67,69] These substrates are broken down via glycolysis and β-oxidation, respectively, before entering the tricarboxylic acid (TCA) cycle, where their electrons will be extracted as reducing equivalents through the

production of nicotinamide adenine dinucleotide (NADH) and flavin adenine dinucleotide ($FADH_2$). NADH and $FADH_2$ deliver electrons to the electron transport chain (ETC) to power the oxidative phosphorylation of ADP, yielding the energy-rich phosphate ATP.[70] The rate of ATP generation is regulated and matched to the requirement of muscle fibers based on the rapidity of its utilization.[68]

The main sites of ATP expenditure in the muscle fiber are the actomyosin ATPase, which hydrolyzes ATP so myosin crossbridges can exert force on actin monomers; sarcoplasmic-endoplasmic reticulum calcium ATPase (SERCA), which pumps Ca^{2+} ions back across the sarcoplasmic reticulum (SR) membrane during muscle relaxation; and sodium-potassium-ATPase, which pumps 3 Na^+ out and 2 K^+ into the muscle fiber to repolarize the sarcolemma during muscle relaxation **(Figure 3)**.[68] Thus, the reason for the high energy demand of skeletal muscle can be accounted for, in part, by its contractile properties, and impairments in obese skeletal muscle function could be related to dysfunction at any stage in the ATP-generating process.

Glucose and lipids derived from the diet are the primary fuel sources for skeletal muscle energy generation, and a major role of skeletal muscle is in taking these substrates up from the bloodstream and break them down to produce ATP.[68] Obesity is associated with impairments in both glucose and lipid metabolism at multiple steps in both the glycolytic and β-oxidation pathways **(Figure 4 & 5)**.[71,72]

Glucose Metabolism

Obese skeletal muscle frequently exhibits peripheral insulin resistance, meaning it experiences a diminished capacity to effectively take up glucose from the blood when stimulated by insulin.[71] Under conditions where insulin sensitivity is unaffected, stimulation of glucose uptake by insulin typically occurs as follows: insulin is secreted by the pancreatic β-cells in response to nutrient ingestion. It binds to its receptor on the muscle cell membrane, and the insulin receptor (IR) autophosphorylates itself to become fully activated **(Figure 4-A)**.[67] From here, it can exert its kinase properties on insulin receptor substrate-1 (IRS-1), which reacts with phosphoinositide 3-kinase (PI3K) to yield phosphatidylinositol 3,4,5-triphosphate (PIP3).[67] PIP3 activates pyruvate dehydrogenase kinase 1 (PDK1), mammalian target of rapamycin complex 2 (mTORC2), and atypical protein kinase C (PKCζ). PDK1 and mTORC2 can each phosphorylate and activate Akt, and both Akt and PKCζ activity can lead to phosphorylation of AS160.[67] AS160 is responsible for release of the GLUT4 glucose transporter from its intracellular storage vesicles,

where it translocates to the cell membrane and glucose uptake into the cell is elevated **(Figure 4-A)**.[67]

Where obese skeletal muscle is often resistant to insulin stimulation, there are many intermediates in the insulin signaling cascade between insulin binding its receptor and GLUT4 translocating to the cell membrane which are negatively impacted. The kinase activity of the IR targets tyrosine residues on itself and IRS-1.[73] However, obese skeletal muscle exhibits increased serine phosphorylation at both locations amidst reduced tyrosine phosphorylation.[73] Elevated serine phosphorylation of IRS-1 reduces its affinity for PI3K, and is one of the primary molecular mechanisms behind peripheral insulin resistance.[74] Likewise, Akt activation is also blunted,[73] likely as a result of what is occurring upstream **(Figure 4-B)**. The overall effect of this becomes a reduction in glucose uptake and oxidation for energy generation in the muscle fiber, concurrent with elevated insulin secretion from the pancreas necessitated to take up and oxidize the same amount of glucose as would be observed in a lean subject's muscle tissue. Hence, the muscle has become resistant to the actions of insulin.

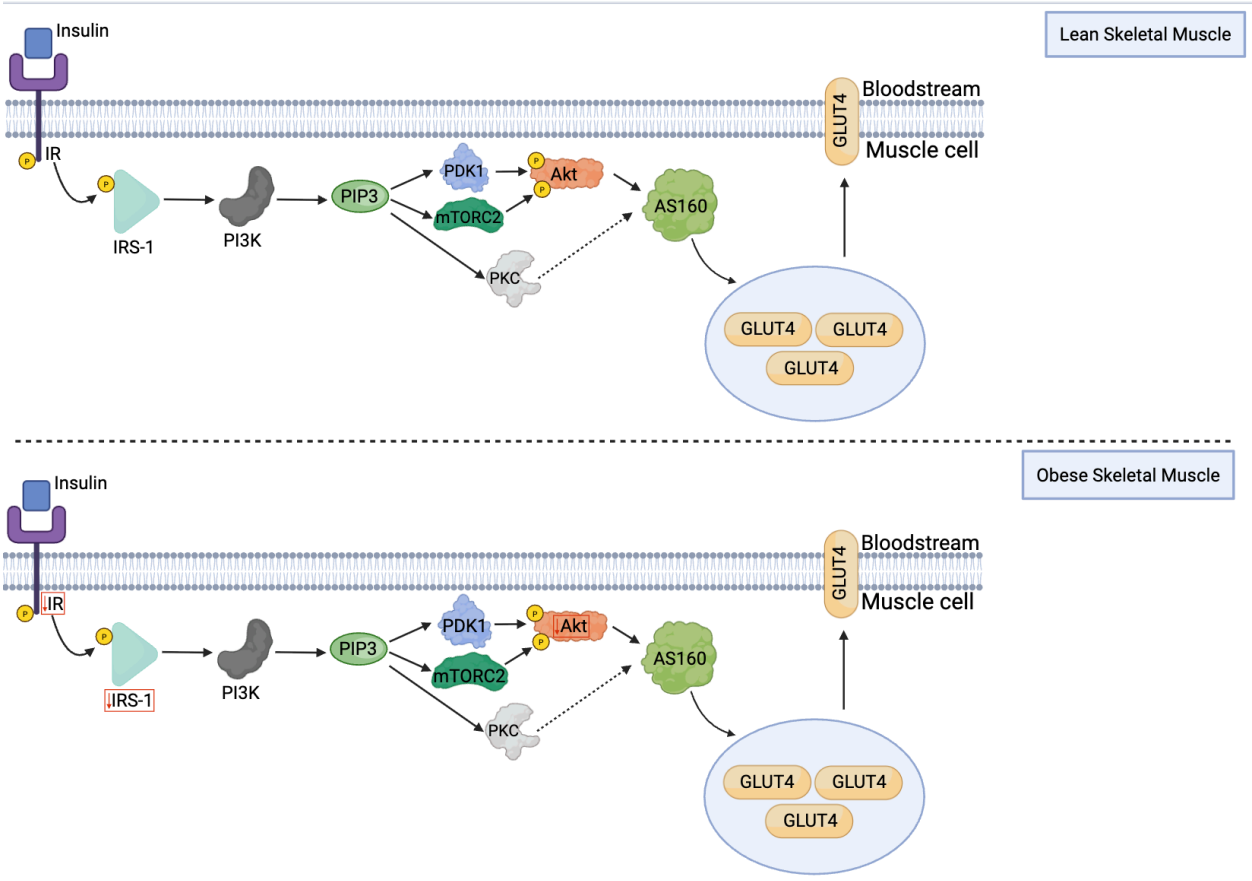

Figure 4. Insulin-mediated GLUT4 translocation in lean vs obese skeletal muscle. A) Insulin binds its receptor, activating itself and IRS-1 both via phosphorylation. IRS-1 and PI3K react to generate PIP3, PIP3 recruits PDK1 to

the membrane to activate Akt, which phosphorylates AS160. PIP3 may also cause downstream phosphorylation of AS160 via mTORC2 and atypical PKC. AS160 releases GLUT4 from its intracellular vesicle, where it can translocate to the membrane to take up glucose into the muscle cell. **B)** Obese skeletal muscle is resistant to insulin stimulation. IR phosphorylation is dysfunctional, reducing its ability to autophosphorylate on the proper residues and IRS-1. Akt activation is also diminished. Akt = protein kinase B. GLUT4 = glucose transporter type 4. IR = insulin receptor. IRS-1 = insulin receptor substrate-1. PIP3 = phosphatidylinositol 3,4,5-triphosphate. PI3K = phosphoinositide 3-kinase. PKC = protein kinase C.

Lipid Metabolism

Obese skeletal muscle also presents with dysregulated lipid metabolism, with fatty acids (FAs) being shuttled away from oxidation for energy and toward esterification and storage as triacylglycerols (TAGs) in abundance in both adipose tissue and skeletal muscle.[72] FA esterification protein and enzyme content is upregulated in obese skeletal muscle.[75] Not only does obese skeletal muscle show preference for storing dietary fat, it also is less effective at breaking down FAs for energy utilization, with impairments apparent at multiple locations in the skeletal muscle lipolytic pathway.[72,75]

Healthy, lean skeletal muscle undergoes lipolysis as so: stored TAGs are broken down into their constituent 3 FAs and glycerol by removing one FA at a time, mainly through the activity of the enzymes hormone-sensitive lipase (HSL) and adipose triglyceride lipase (ATGL).[69] Once FAs are freed and have crossed the outer mitochondrial membrane (OMM), becoming fatty acyl CoA, they are converted to fatty acylcarnitine by carnitine palmitoyl transferase 1 (CPT-1), where they can cross the inner mitochondrial membrane (IMM) before reverting back to fatty acyl CoA molecules through the actions of carnitine palmitoyl transferase-2 (CPT-2).[69] Mitochondrial fatty acid transport is regulated by CPT-1, which is inhibited by malonyl CoA.[69] Malonyl CoA effectively prevents crossing of FA lipolytic intermediates across the IMM.[69,75] Fatty acyl CoA then enter the β-oxidation pathway, where it will be broken down, 2 carbon atoms at a time, to generate acetyl CoA units for the TCA cycle **(Figure 5-A)**.[69]

Obese skeletal muscle shows repressed CPT-1 activity explained by an increased inhibitory effect of malonyl CoA,[72,75] thus leading to a reduction in FA import to mitochondria for β-oxidation, which is likewise impaired in obesity, and ultimately diminished energy generation **(Figure 5-B)**. Conversely, human studies show elevated intramuscular TAG (IMTG) content, with studies in obese skeletal muscle and myotubes harvested from obese individuals showing amplified FA uptake.

FA uptake to skeletal muscle is facilitated by a number of FA transporter proteins, including FAT/CD36, which can also localize to the mitochondrial OMM and work alongside

CPT-1 to regulate FA transport and subsequent oxidation.[76] Despite elevated FA uptake in obese skeletal muscle, FAT/CD36 expression remains unchanged.[76] However, obese skeletal muscle does exhibit increased localization of this transporter protein to the sarcolemma, facilitating further FA uptake, but also diminishing the proportion of FAT/CD36 at the OMM.[76] Lower mitochondrial localization of FAT/CD36 combined with CPT-1 inhibition leads to an increase in FA shuttling toward esterification and storage as IMTG.[76,77] IMTG amassment in obese skeletal muscle is linked to elevated concentrations of lipid metabolism intermediates, such as diacylglycerol (DAG) and ceramides, both of which are implicated in the development of insulin resistance.[77]

Methods used to assess the ability of mitochondria to produce ATP should therefore carefully consider the design of experimental assays that compare different substrate effects on mitochondrial oxidative phosphorylation. The effect of semaglutide on substrate-specific oxidation in mitochondria is currently unresolved, so measurement of both glucose and fatty acid oxidation is vital. This is important not solely for determining the effect of semaglutide on mitochondrial respiration, but furthermore, by taking a substrate-specific approach, it is possible to assess that if a change in utilization of one substrate is found, whether an adaptation has occurred in the other energy-generating pathway to compensate for this. Thus, is a change in substrate utilization preventing significant changes in electron transport chain (ETC) flux and ATP generation, that would not otherwise be apparent by taking a single substrate approach?

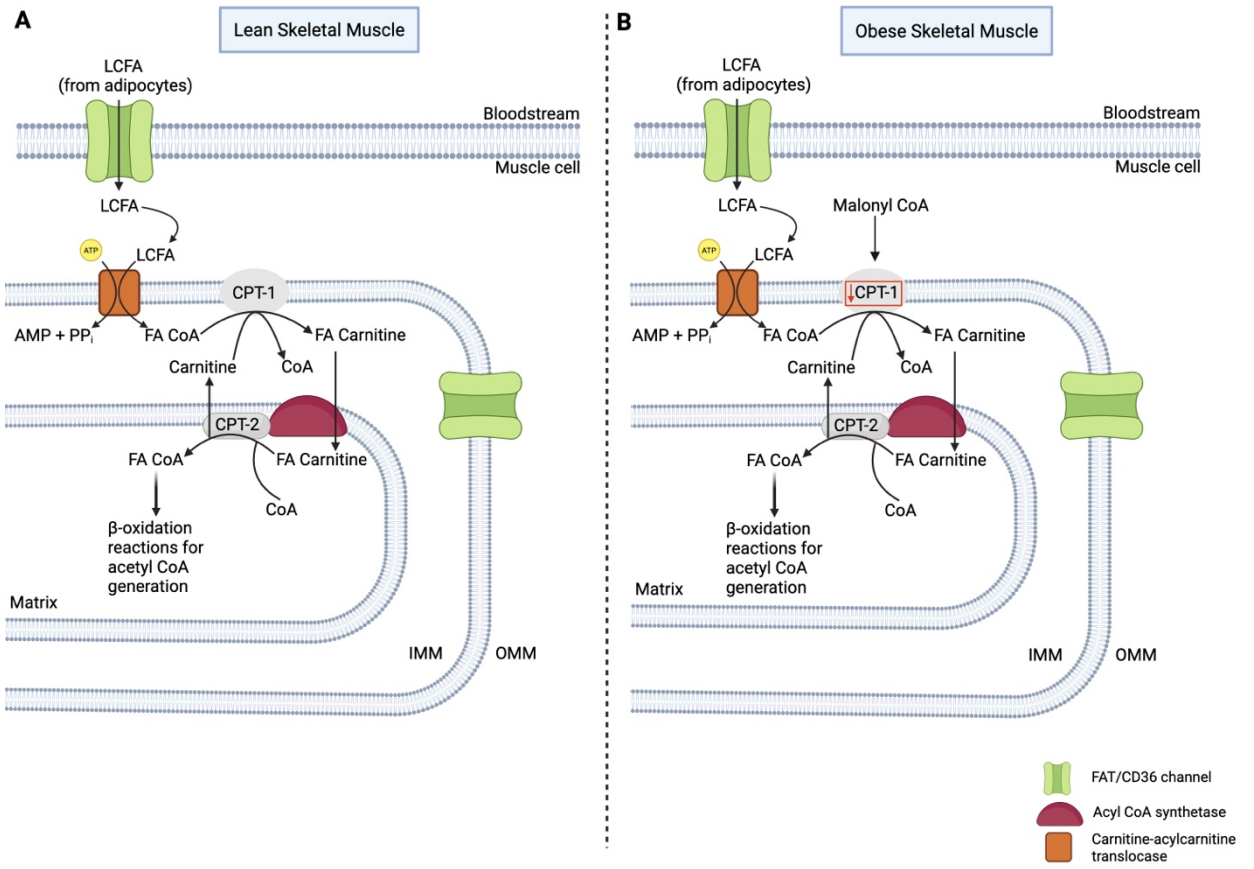

Figure 5. Lipid transport in lean vs obese skeletal muscle. A) In lean muscle, LCFAs are converted to FA CoA by acetyl CoA synthetase upon uptake by FAT/CD36 transporters. CPT-1 catalyzes FA CoA exchange with carnitine to yield FA carnitine, which can cross the IMM in exchange for carnitine via carnitine-acylcarnitine translocase. FA carnitine then reacts with CPT-2 to recover FA CoA, which can then enter beta-oxidation to yield acetyl CoA for entry to the TCA cycle and be completely oxidized for energy generation. **B)** CPT-1 activity is inhibited by malonyl CoA, which is elevated in obese skeletal muscle, leading to reduced transport of lipolytic intermediates to the matrix and impaired fat oxidation. AMP = adenosine monophosphate. ATP = adenosine triphosphate. CoA = coenzyme A CPT-1 = carnitine palmitoyl transferase-1. CPT-2 = carnitine palmitoyl transferase-2. FA CoA = fatty acyl CoA. FA carnitine = fatty acyl carnitine. IMM = inner mitochondrial membrane. LCFA = long-chain fatty acid. OMM = outer mitochondrial membrane. PP_i = inorganic pyrophosphate.

Oxidative Phosphorylation

Obese skeletal muscle displays reduced mitochondrial content compared to lean muscle, which is maintained when normalizing mitochondrial content to muscle mass and cross-sectional area.[78] Reductions in mitochondrial content can be explained by evidence of impaired mitochondrial protein transcription, translation, and import.[78] Peroxisome proliferator-activated receptor γ coactivator-1α (PGC-1α) has been nicknamed the 'master regulator' of mitochondrial biogenesis, and its protein content is reduced in obese skeletal muscle, contributing further to lower mitochondrial content via reduced synthesis of new mitochondria.[78] Mitochondrial transcription factor A (TFAM) is an important component for initiating transcription of proteins encoded by mitochondrial DNA.[78] Reductions in TFAM content in obesity shows that transcription of both

nuclear- and mitochondrially-encoded proteins is disrupted in obese skeletal muscle. The overwhelming evidence for reductions in mitochondrial concentration in obese skeletal muscle has implications for overall mitochondrial health within muscle fibers, where fewer mitochondria are present to generate ATP, lower mitochondrial content has potential consequences for mitochondrial functional capacity. Reductions in mitochondrial content do not necessitate reductions in mitochondrial function if a lower concentration of mitochondria can maintain the energy demands of a muscle fiber. However, obese skeletal muscle does exhibit reduced mitochondrial capacity and efficiency.[78–80]

In lean, healthy muscle, NADH and $FADH_2$ generated from either glycolysis, the TCA cycle, and β-oxidation transport protons and electrons to the ETC **(Figure 6)**.[70] NADH passes off its electrons and is oxidized at Complex I to NAD^+, with $FADH_2$ doing the same at Complex II.[70] Coenzyme Q shuttles these electrons to Complex III, and then cytochrome *c* does the same from Complex III to IV.[70] Complex IV is known as the final electron acceptor, as it transfers electrons to oxygen to yield water.[70] As electrons flow down the ETC, the energy released as each Complex is reduced is used to pump protons across the matrix against their electrochemical gradient via Complexes I, III, and IV **(Figure 6)**.[70] The oxygen-consuming step at Complex IV is the "respiratory" step. Respiration occurs as protons return to the matrix by flowing down their concentration gradient.[70] When protons re-enter the matrix via ATP synthase to phosphorylate ADP, respiration is coupled to ATP generation, known as State III respiration.[70] When protons re-enter the matrix through leak channels, such as UCP3, respiration is uncoupled to ADP phosphorylation, known as State II **(Figure 6)**.[68] Skeletal muscle from obese subjects exhibit reduced State III, or respiration coupled to ADP phosphorylation, and State II, or uncoupled respiration compared to non-obese sedentary and trained individuals.[79] In HFD-induced obese mice, both State II and III respiration of the soleus muscle are similarly affected.[80]

Mitochondrial energy generation is reduced in obese compared to lean skeletal muscle. The mechanisms behind this are multi-faceted, but can, in part be explained by the lower energy demand that is placed on the muscular and organismal level with obesity.[76] Sedentary lifestyles associated with obesity do not make significant energy demands on skeletal muscle, and so ATP generation is reduced accordingly to account for this. Energy balance is also dysregulated at the level of energy intake. Thus, an excessive supply of energy-generating substrates in addition to a

reduction in energy demand leads to the shuttling of these fuel sources toward long-term storage as adipose tissue.[76]

Obese skeletal muscle may also exhibit compromised mitochondrial energy generation independent of an energetic supply-and-demand imbalance. Obese skeletal muscle is commonly insensitive to insulin-stimulated glucose uptake, and preferentially shuttles FAs toward esterification and away from oxidation.[71,72,81] When substrates for energy generation do arrive to the muscle cell, there are fewer mitochondria available to oxidize them, and these mitochondria are less capable of generating ATP during respiration even in the presence of adequate substrate supply.[78–80]

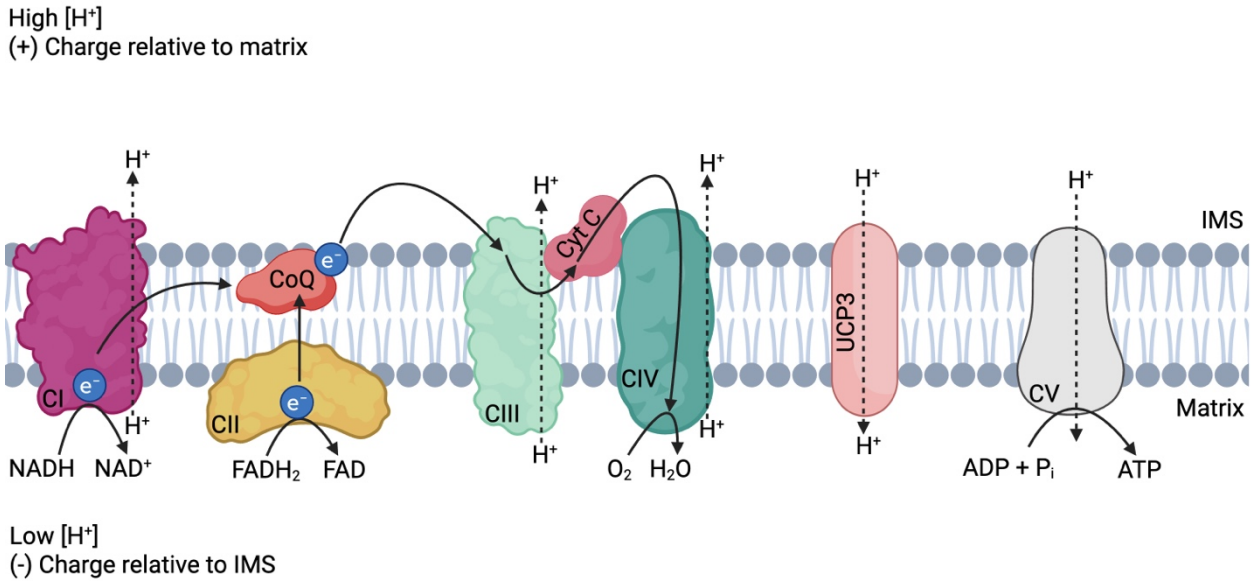

Figure 6. Mitochondrial oxidative phosphorylation representative figure. NADH and $FADH_2$ provide electrons to CI and CII, respectively, which then shuttle the electrons to CIII via CoQ. CIV is considered the final electron acceptor, as when it accepts 2 electrons from cyt c and reacts with oxygen, it generates a water molecule. Protons are pumped against their electrochemical gradient at CI, CIII, and CIV to the intermembrane space. They can leak back to the matrix via UCP or be used in the phosphorylation of ADP and P_i to generate ATP. ADP = adenosine diphosphate. ATP = adenosine triphosphate. CI = Complex I, CII = Complex II, CIII = Complex III, CIV = Complex IV, CV = Complex V/ATP synthase. CoQ = Coenzyme Q. Cyt c = cytochrome c. e^- = electron. FAD = oxidized flavin adenine dinucleotide. $FADH_2$ = reduced flavin adenine dinucleotide. H_2O = water H^+ = proton. IMS = intermembrane space. NADH = reduced nicotinamide adenine dinucleotide. NAD^+ = oxidized nicotinamide adenine dinucleotide. O_2 = oxygen. P_i = inorganic phosphate. UCP3 = uncoupling protein-3.

Reactive Oxygen Species (ROS) Generation

The ETC is a major site for ROS generation in the muscle fiber.[82] Low levels of ROS generation are vital for maintaining the muscle's homeostatic environment, as they play roles in cell signaling.[82] When ROS generation is increased, however, this is unfavourable due to their high reactivity and ability to activate apoptotic processes.[82] Superoxide, a type of ROS, is produced from electron slip at Complexes I and III on the ETC **(Figure 7)**.[82] Electron slip is lowest during

State III respiration, as flux through the ETC is rapid in order to keep up with ATP demands.[82] When ATP demands are lower, such as in obesity due to factors such as chronic overfeeding and sedentariness, electron flux slows, increasing the risk for electron slip to occur at Complexes I and III. Likewise, State II respiration is associated with maximal ROS generation.[82] When an electron slips off the ETC, it can react with oxygen to yield superoxide.[82] Superoxide is scavenged by the mitochondrial isoform of superoxide dismutase (MnSOD) to generate the less volatile H_2O_2.[82] H_2O_2 is membrane permeable, so it can cross the mitochondrial membrane and be detected **(Figure 7)**.

Diet-induced obesity is associated with systemic oxidative stress.[83] In skeletal muscle specifically, MnSOD expression is reduced,[84] lowering mitochondrial antioxidant defence capacity and lengthening the lifetime of superoxide, giving it the opportunity to further oxidize the matrix environment.

Insulin resistance and low muscle mass are also accompanied by increased oxidative stress,[82,85] and the prevalence of insulin resistance and sarcopenia in obesity likely contributes to this environment as well. High-fat diet feeding in both human and rodents' skeletal muscle displays significantly elevated mitochondrial hydrogen peroxide (mH_2O_2) emission, indicating a more oxidized mitochondrial environment.

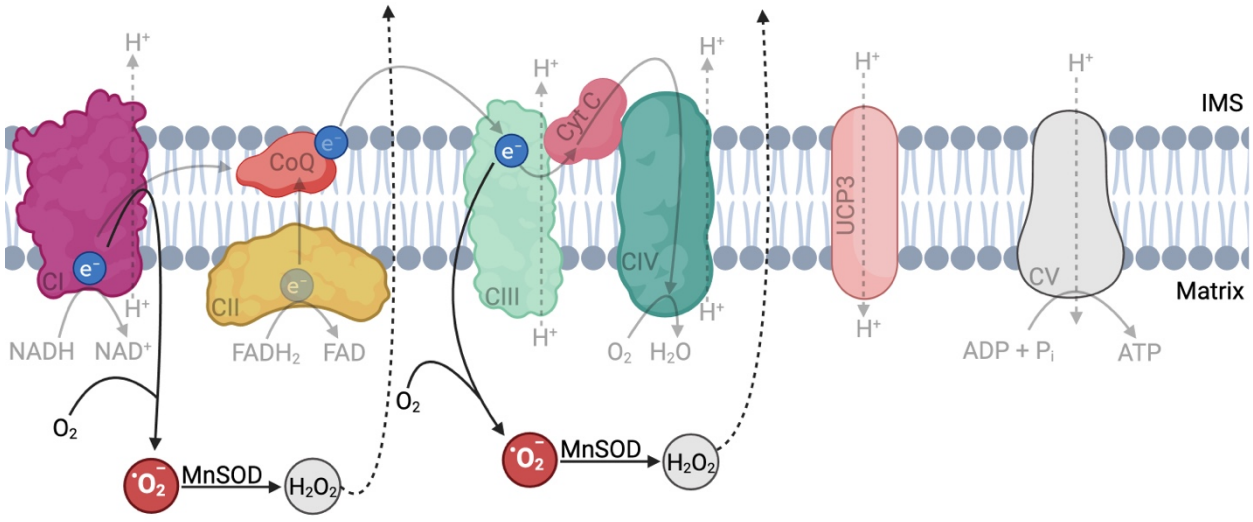

Figure 7. Mitochondrial hydrogen peroxide emission representative figure. Electron slip occurs at CI and CIII, which reacts with oxygen in the matrix to produce a superoxide radical. MnSOD dismutates superoxide to H_2O_2, a less volatile ROS which can leave the matrix and be detected. ADP = adenosine diphosphate. ATP = adenosine triphosphate. CI = Complex I, CII = Complex II, CIII = Complex III, CIV = Complex IV, CV = Complex V/ATP synthase. CoQ = Coenzyme Q. Cyt c = cytochrome c. e^- = electron. FAD = oxidized flavin adenine dinucleotide. $FADH_2$ = reduced flavin adenine dinucleotide. H_2O = water. H_2O_2 = hydrogen peroxide. H^+ = proton. IMS = intermembrane space. MnSOD = mitochondrial superoxide dismutase. NADH = reduced nicotinamide adenine

dinucleotide. NAD^+ = oxidized nicotinamide adenine dinucleotide. O_2 = oxygen. $^{\bullet}O_2^-$ = superoxide anion. P_i = inorganic phosphate. UCP3 = uncoupling protein-3.

2.3.4 Implications for bone structure and function with obesity

The traditional perspective on obesity and bone has been that the obesogenic phenotype is beneficial to bone.[9] Overweight and obese individuals experience increased mechanical load on bones due to their greater body mass.[9] Thus, obesity has been considered to promote the deposition of bone, in the same manner previously mentioned with respect to skeletal muscle, where weight bearing was thought to induce a training effect, leading to greater muscle mass. While a plausible theory, this has been disproven in leptin KO mice, which exhibit reduced BMD and bone volume despite their obese phenotype.[86]

The chronic inflammatory environment attributed with obesity contributes to the decline in bone quality observed in obese subjects.[9] The bone metabolic environment experiences a shift towards overall bone resorption through upregulation of several proinflammatory cytokines, including TNF-α and IL-6.[9] These molecules modulate the RANKL/OPG pathway, ultimately stimulating osteoclastogenesis.[9] At the same time, osteoblast formation is downregulated, and this is in part due to their shared lineage of mesenchymal stem cells.[9] The preferential formation and storage of TAGs in obesity thus leads to a shift in stem cell differentiation away from osteoblasts.[9] Thus, obesity's effects on the bone metabolic environment are two-fold through the downregulation of bone formation and surge in bone resorption.

CHAPTER THREE: RATIONALE, AIMS, AND HYPOTHESES:

3.1 Rationale

Obesity, characterized by the excessive accumulation of adipose tissue, and sarcopenic obesity, which includes the above definition in addition to reduced skeletal muscle mass and function, both contribute to lower quality of life, increased incidence and severity of chronic disease and death, and significant healthcare and economic burden. Semaglutide is an exceptionally powerful stimulus for weight loss in overweight and obese individuals Unfortunately, semaglutide does not specifically reduce adipose tissue, and its use has been associated with an unprecedented degree of lean mass reduction, greater than that observed with lifestyle or surgical weight loss interventions. The impact semaglutide has on skeletal muscle *function* and bone morphology is less understood and remains to be explored, in both the context of semaglutide independently and in conjunction with targeted lean tissue preservation. Given the

evidence that the macronutrient protein is able to preserve musculoskeletal content and health under other lean tissue-compromising conditions, its usage may be key for the optimization of high-quality pharmacologically-induced weight loss, that is, weight loss maximizing adipose reduction.

Semaglutide is increasingly being prescribed in childhood and adolescent obese populations, despite the lack of evidence for how it may impact musculoskeletal growth and development at this age.

3.2 Specific Aims

Aim 1: Identify the effect of semaglutide on body composition, muscle force production, and bone volume in an adolescent model of diet-induced obesity.

Aim 2: Determine the ability of a nutritional intervention manipulating dietary protein content to preserve muscle mass, muscle function, and bone volume during semaglutide therapy; while maintaining meaningful reductions in adiposity

3.3 Detailed Specific Aims

Aim 1: Identify the effect of semaglutide on body composition, muscle force production, and bone volume in an adolescent model of diet-induced obesity.

Objective: Assess body composition via semi-weekly bodyweight measurement, pre- and post-intervention *in vivo* microCT analysis, individual muscle and organ weights, and muscle cross-sectional area to identify differences in whole-body and tissue-specific composition resulting from semaglutide. Perform voluntary measures of muscle function weekly from animal arrival to endpoint and carry out *in situ* TA maximal contractile function at endpoint to assess if impairments in muscle contractile function are present across the protocol duration.

Expected Results: In mature models of DIO, semaglutide significantly impacts bodyweight and lean mass. We expect that semaglutide will significantly reduce body, muscle, and bone size compared to no treatment at this age. There is a known link between muscle mass and muscle strength, and we believe semaglutide will significantly impair force output, although it is unclear whether this will be solely a result of muscle atrophy.

Limitation: The use of multiple analysis techniques can lead to divergent results. MicroCT analysis for lean tissue is not specific to skeletal muscle volume, so it cannot be compared directly against skeletal muscle mass. Likewise, absolute tissue and organ weights are only

harvested at endpoint, so we cannot see the longitudinal effect on individual muscles. Similarly, the *in situ* force protocol involves almost complete dissection of the TA muscle and as such is a non-survival measure. It can only be assessed at one timepoint, and so maximal contractile function can only be assessed at endpoint, and not in the intermediate weeks or pre-intervention.

Aim 2: Determine the ability of a nutritional intervention manipulating dietary protein content to preserve muscle mass, muscle function, and bone volume during semaglutide therapy; while maintaining meaningful reductions in adiposity.

Objective: We will perform the same measures outlined in the Objective section of Aim 1; to identify if protein supplementation is a feasible solution for the optimization of GLP-1 RA use.

Expected Results: Protein is known to prevent lean mass reductions when supplemented during non-pharmacological weight-loss interventions. What is currently unknown, is whether it can mitigate pharmacologically-induced lean mass loss. We expect that high-quality protein supplementation using a blend of whey and casein will lead to preserved reductions in adipose tissue to a similar degree as we predict will occur with semaglutide alone in this age-group. We also expect that protein supplementation will preserve muscle mass and contractile function, given the established anabolic role of this macronutrient.

Limitation: While we are considering high-quality protein sources, the use of a blend of whey and casein will not allow the determination of whether both are necessary or the ratio (60% whey, 40% casein) is optimal. Likewise, other high-quality protein sources, such as soy protein, were not included in the study design and so it is not possible to extrapolate findings outside of this specific blend.

3.4 Hypothesis

We hypothesize that a protein-supplemented dietary intervention will preserve muscle mass, muscle contractile function, and bone volume during semaglutide pharmacotherapy in an adolescent model of diet-induced obesity, given its previously established efficacy in promoting musculoskeletal content and health under both healthy and diseased conditions.

3.5 Author Contributions

The majority of the experiments in this project were carried out by Brooke A. Morris. *In vivo* microCT analysis was performed by Shahrzad Khajehzadehshoushtar. *In vivo* microCT statistical testing was shared between B.M. and S.K. Mice morphometric data were collected by B.M. and

S.K. over four months. Muscle histology was shared between B.M. and S.K. Mitochondrial functional assays were performed by S.K., Ihtisham A. Rana, Aditya N. Brahmbhatt, and Madison C. Garibotti. All other assays were completed by B.M.

3.6 Additional Contributions

Co-author published

Ghandi S, Delfinis LJ, Bhatt PD, Garibotti MC, Bellissimo CA, Goli AN, **Morris BA**, Brahmbhatt AN, Yakobov-Shimonov S, Rahman FA, Quadrilatero, J, Simpson, JA, Sweeney G, Abdul-Sater, AA, Backx, PH, Hsu HH, Perry CGR. Adiponectin-receptor agonism prevents right ventricular tissue pathology in a mouse model of Duchenne muscular dystrophy.

Co-author in progress

Delfinis, LJ, Khajehzadehshoushtar S, Flewwelling LD, Andrews NJ, Garibotti MC, Gandhi S, Brahmbhatt AN, **Morris BA**, Garlisi B, Lauks S, Aitken C, Cheng AJ, Petrik J, Perry CGR. Mitochondrial-targeted plastoquinone therapy prevents early onset muscle weakness that occurs before atrophy during ovarian cancer.

Khajehzadehshoushtar S., Delfinis LJ, Rahman FA, Garibotti MC, Gandhi S, Brahmbhatt AN, **Morris BA**, Garlisi B, Lauks S, Aitken C, Ogilvie LM, Zhang ZX, Simpson, JA, Quadrilatero J, Petrik JJ, Perry CGR. The mitochondrial-targeted antioxidant SkQ1 prevents skeletal muscle mitochondrial- apoptotic but not necroptotic signalling during ovarian cancer.

CHAPTER FOUR: METHODS

4.1 Study Approval

All procedures performed herein were approved by York University's Animal Care Committee under protocol 2024-05: "Non-pharmacological methods of attenuating loss of muscle mass and function occurring with use of semaglutide as an anti-obesity treatment". This was in compliance with the Canadian Council on Animal Care Guidelines

Study Design

Male C57Bl/6J diet-induced obesity (DIO) mice were obtained from Jackson Laboratories at 7 weeks old. Prior to arrival at our animal facility, animals were raised on a high-fat diet (60% calories from fat, 20% from carbohydrate, 20% from protein) in an effort to induce the obese phenotype. All animals were placed on a 'Western Diet' (WD), designed to mimic the standard North American diet, upon arrival to York University's Animal Facility for a 2-week acclimatization period prior to being randomized to any treatment group. The WD was comprised

of 15% kcalories (kcal) from protein, 43% from carbohydrate (CHO), and 42% from fat. The protein component of the WD was derived from mixed sources: 50% isolated soy protein, 30% casein, 19% wheat gluten, and 1% collagen. Females were excluded from the study design given female mice do not gain appreciable weight in diet-induced obesity mouse models.

Group randomization and assignment occurred upon completion of the aforementioned acclimatization period, at 9 weeks of age. Groups were designed as follows: 1) WD + vehicle (obese control), 2) WD + semaglutide, and 3) WD with protein increased by 60% utilizing a 60:40 whey and casein blend + semaglutide; with an allocation of n=12/group. The obese control received vehicle injections (18% dimethyl sulfoxide (DMSO) dissolved in saline) and the drug groups received 10nM semaglutide (dosed by bodyweight) 5 days per week for 6 weeks. All injections were administered subcutaneously in the subscapular region. The protein-enriched diet remained isocaloric to the WD by reducing its CHO content to account for the protein supplementation. Absolute dietary fat was unmodified across all groups.

4.2 Animal Care

4.2.1 Animals

Male C57Bl/6J DIO mice, obtained from Jackson Laboratories at 7 weeks old, were housed in a temperature-controlled environment with a 12hr light-dark cycle and received *ad libitum* access to food and water. Animals were accommodated in cages of 3 in an effort to obtain a rough estimate of food intake while minimizing the stress associated with individual housing.[87] Mice were housed without access to running wheels.

One week into the acclimation period, a glucose tolerance test was performed to assess the ability of peripheral tissues to handle a glucose stress. No more than 48hr before initiation of the intervention, a micro-computed tomography (microCT) scan for body composition was taken. Finally, at 9 weeks old, following completion of the 2-week acclimatization period, the nutrition and/or injection protocols began. To ensure uniformity in age and measures across experimental groups, animal arrivals were staggered by 2-3 weeks at a time, arriving in groups of 12-15. The endpoint for all animals occurred at 15 weeks of age, upon completion of 6 weeks of injections.

Semi-weekly food intake was recorded from arrival up until sacrifice, and bodyweight was recorded 5x/wk during treatment. Bodyweight was recorded twice weekly during acclimatization so as to minimize excess stress due to handling during adjustment to both a new environment and food modification (two other potential sources of stress).

4.2.2 Semaglutide preparation and administration

Semaglutide was administered subcutaneously 5 days/week on Wednesday, Thursday, Friday, Sunday, and Monday. 5mg semaglutide (MedChemExpress, HY-114118) was dissolved in 10mL DMSO to make a stock concentration of 0.5mg/mL. It was stored at -20°C in 50uL aliquots until needed. Fresh aliquots were used each day and thawed on a rocker. Once thawed, a 50uL aliquot of semaglutide was dissolved in 2.450mL saline and mixed well.

Semaglutide treatment was initiated using a ramp protocol, so as to minimize often observed side effects such as nausea, vomiting, and diarrhea. On day 1, a dose of 3nM was administered. Day 2: 6nM. Day 3 and onward: 10nM. Injection volume was calculated using the animal's bodyweight, desired dose, and stock concentration (0.5mg/mL). For the 3nM dose, the animal's bodyweight was multiplied by 1.2341, for the 6nM dose, the animal's bodyweight was multiplied by 2.4682, and for the 10nM dose, the animal's bodyweight was multiplied by 4.1136.

4.2.3 Vehicle preparation and administration

Vehicle injections were administered on a schedule identical to semaglutide injections, and similarly made fresh the morning of injections. Vehicle preparation consisted of dissolving 100uL DMSO in 4.900mL saline and mixing thoroughly. Volume of vehicle injections was calculated using the same formula(s) as for the semaglutide injections, and a ramp protocol was followed for consistency.

4.3 Body Composition and Functional Assays

4.3.1 Timeline of Measures

Several tests were performed on animals prior to the surgical endpoint. They are outlined as follows for clarity. Prior to treatment onset and following treatment completion, body composition and glucose tolerance were measured at 9 and 15 weeks old, respectively. Starting at 9 weeks old, on a weekly basis, whole body voluntary functional testing was performed, which included cage hang time and forelimb grip strength testing.

4.3.2 Body composition via micro-computed tomography (microCT) scanning

Body composition analysis was performed at 2 timepoints: before treatment onset and upon treatment completion utilizing the Bruker SkyScan 1278 *in-vivo* x-ray microtomography unit.

Animals were anesthetized under isoflurane for the duration of the scan. Animals were laid supine in the unit's animal cassette, with hindlimbs straight and forelimbs extended overhead and

secured in place. Scans were completed with a 100μm resolution using a 0.5mm aluminum filter at 50kV and 996uA, with a 30ms exposure time and a 0.75° rotation step.

Following scans, body composition metrics were analyzed by first reconstructing the image using Nrecon (software version 1.7.0.4, Bruker micro-CT) where the region of interest was selected and analyzed. Whole body volume, trunk volume, whole body fat mass (FM), trunk FM (visceral FM), non-trunk FM (subcutaneous FM), percent (%) FM, total fat-free mass (FFM), % FFM, hindlimb volume, hindlimb FFM, and whole body bone volume were separately analyzed by separating them according to their respective densities in this manner. Thresholds for different tissues were used as follows: 25-50 for adipose, 51-90 for FFM, and 91-255 for bone.

4.3.3 Glucose tolerance testing (GTT)

Animals were removed from their cages and placed in fresh cages with *ad libitum* access to water, but not food, for 5hr prior to the beginning of the GTT protocol. This 5hr fast mimics an overnight fast in humans. Following the 5hr fast, EMLA cream (containing lidocaine) was applied locally to the tail to numb it. It was reapplied every 45 minutes throughout the duration of the procedure. During this time, animals were kept warm on a heating pad to promote vasodilation of the tail vein.

15 minutes after EMLA cream application, baseline blood glucose was obtained using a glucometer (FreeStyle Lite, Abbott) by pricking the tail vein with a 23G needle and collecting the blood on a glucose strip. Once the baseline blood glucose measure was obtained, a glucose bolus was intraperitoneally injected in the lower abdominal region, and the animal returned to its cage for 30 minutes. At 30, 60, 90, and 120 minutes following glucose administration, blood glucose as taken identically as during the baseline measure

Glucose solution preparation and dosing

The glucose solution was prepared at 20% w/v by dissolving 2g glucose in 10mL saline. It was then left to rock until fully dissolved. Once dissolved, the solution was passed through a 0.2μm filter. Individual dosage was calculated according to bodyweight, with animals receiving 1.5g/kg bodyweight.

4.3.4 Cage hang time

Animals were placed on top of a large metal cage-top held horizontally ~30cm above a cage filled with soft bedding. Upon ensuring all 4 limbs were grasping the bars of the cage-top,

the cage lid was then inverted so the animal was hanging, and a timer started. Cage hang time was recorded for a maximum of 180sec. animals that fell off prior to 180sec were given 60sec to recover before up to 2 more attempts were provided. Following the third attempt (if necessary), the maximum hang time from each animal was noted. All trials were recorded.

4.3.5 Forelimb grip strength

A metal grid was attached to the force transducer (Mark 10 Digital Force Gauge, Copiague, NY) set to the 'peak tension' setting. The force transducer was placed on the edge of a countertop so as to allow the metal grid to extend past it. Animals were placed in proximity to the grid so they could grip it with their forepaws. Upon grasping, animals were gently pulled away from the grid by their tail until their grip was broken, ensuring the hindlimbs did not come in contact with the grid at any point. Peak tension was recorded, and the procedure was repeated for a total of 3 attempts, with 60sec of recovery between each attempt. If the animal did not show resistance to the experimenter, (if they did not exhibit a pulling motion on the grid with their forepaws) the trial was not recorded. Maximum peak tension from the best of the 3 trials was used for analysis

4.3.6 Muscle force protocol

The *in situ* tibialis anterior (TA) muscle force production protocol has been adapted from previous literature and refined by LD and MG. Animals were anesthetized under isoflurane, and following this hair and superficial connective tissue was removed from the hindlimb to expose the TA tendon. Once exposed, the TA tendon was carefully cut and secured with a double suture. After the knot was securely in place, the TA was gently cut up the length of the muscle toward the knee joint. The suture was then attached to the muscle level arm of the force transducer (Aurora Scientific 305C) with a hook. The knee was secured with a vertical knee clamp and the paw taped in place sole-down. The needle electrodes were inserted into the fascia underneath the TA, following which current optimization took place. Resting length of the TA was measured with a ruler and then single twitches (pulse width = 0.2ms) were sent until maximal twitch force was achieved. One minute of rest was allocated prior to onset of the force protocol to avoid twitch potentiation.

The force frequency protocol then proceeded, in which 10 isometric contractions of increasing stimulation frequency (1, 10, 20, 30, 40, 50, 60, 80, 100, 120, 200Hz) followed. Upon completion of the force frequency protocol, 5 minutes of rest followed before initiation of the fatigue protocol, where a 60Hz stim was sent every 0.7sec for 2 minutes. Recovery from fatigue

was measured at the 5, 10, and 15 minute timepoint following completion of the fatigue protocol by sending a single 100Hz stim. The TA was then excised and weighed for normalization of force production, known as 'specific force'.

4.4 Surgery Procedure

Immediately prior to sacrifice, the *in situ* TA force protocol, as described above, was performed under isoflurane anesthesia. This TA was then excised, weighed, and embedded in optimal cutting temperature (OCT) solution prior to being frozen in liquid nitrogen and stored at -80°C. The other TA was immediately removed and placed in ice cold BIOPS for bioenergetic analysis (see below). Blood was then collected via cardiac puncture and set aside for 10min before being centrifuged for serum collection and subsequent snap freezing.

Mice were euthanized under isoflurane via exsanguination. The extensor digitorum longus, quadriceps, soleus, gastrocnemius, plantaris, and triceps from both limbs were quickly collected. From one side of the body, these tissues were snap frozen in liquid nitrogen and stored at -80°C. For the gastrocnemius muscle only, prior to snap freezing, the red portions were gently cut away and frozen separately from the white portions. Muscles from the contralateral side of the body were then weighed and embedded in OCT solution prior to snap freezing in liquid nitrogen. Both tibiae bones were collected after carefully stripping away remaining muscle and connective tissue. One was placed in a Falcon tube containing bleach and stored at room temperature, the other placed in a Falcon tube containing saline and stored at -20°C.

Diaphragm, heart, spleen, kidneys, liver, lungs, inguinal (subcutaneous) fat pads, and gonadal (visceral) fat pads were then weighed and snap frozen in liquid nitrogen at -80°C.

4.5 Mitochondrial Bioenergetic Assessments

4.5.1 Preparation of permeabilized muscle fibers

Preparation of permeabilized muscle fiber bundles (pmfb), mitochondrial oxygen consumption, and mitochondrial hydrogen peroxide (mH_2O_2) analysis was performed as previously established in our lab. Immediately following surgical excision, the TA was placed in ice cold BIOPS, containing (mM) 50 MES Hydrate, 7.23 K_2EGTA, 2.77 CaK_2EGTA, 20 imidazole, 0.5 dithiothreitol, 20 taurine, 5.77 Na_2ATP, 15 Na_2PCr, and 6.56 $MgCl_2 \cdot 6H_2O$ (pH 7.1). Under 1X magnification, muscle was trimmed of fat and connective tissue, and divided into 8 smaller bundles (4 for oxygen consumption measures and 4 for mH_2O_2 analysis). All bundles were

made from the center of the TA muscle and gently separated along the longitudinal axis. Pmfb were weighed in ~1.5mL of ice-cold tared BIOPS (ATP-containing relaxing media) to ensure they remained relaxed

Bundles then underwent permeabilization, being treated with 40μg/mL saponin in BIOPS on a rotator for 30 minutes at 4°C. For bundles intended for mH_2O_2 emission measurement related to Complex I, an additional treatment with 35μM 2,4-dinitrochlorobenzene (CDNB) was applied during the permeabilization step. This step served to deplete glutathione, establishing detectable rates of mH_2O_2.

Following permeabilization, all bundles were transferred to Buffer Z, comprising (in mM) 105 K-MES, 30 KCl, 10 KH_2PO_4, 5 $MgCl_2 \cdot 6H_2O$, 1 EGTA and 5mg/mL BSA (pH 7.4) on a rotator at 4°C for a minimum of 15 minutes (but no longer than 4hr) until measurements began.

4.5.2 Mitochondrial oxygen consumption

High-resolution oxygen consumption measurements were conducted in 2mL of respiration medium (Buffer Z) using the Oxygraph-2k (Oroboros Instruments, Corp.) with stirring at 750rpm at 37°C. Buffer Z contained 20mM creatine to saturate mitochondrial creatine kinase (mtCK) and promote phosphate shuttling through mtCK. For ADP-stimulated respiratory kinetics, standard procedures to determine Complexes I and II-supported respiration were employed. All experiments were conducted in the presence of 5μM Blebbistatin (BLEB) in the assay media to prevent spontaneous pmfb contraction, which can occur in response to addition of ADP at 37°C and confound respiration rate data. Each protocol was initiated with a starting oxygen concentration of at least 350μM and was completed before the Oxygraph chamber oxygen concentration reached 150μM as performed previously. Polarographic oxygen measurements were acquired in 2s intervals with the rate of respiration derived from 40 data points and expressed as pmol/s/mg wet weight.

4.5.3 Carbohydrate oxidation protocol

2M pyruvate and 2mM malate were added as Complex I-specific substrates (saturating electron entrance to Complex I via NADH production) followed by titrations of submaximal ADP (25, 100, 300, and 500μM) and maximal ADP (1000, 5000, and 7000μM). 10mM glutamate is added to ensure complete saturation electron entrance to Complex I via NADH. Cytochrome *c* was added to test for mitochondrial membrane integrity, with experiments demonstrating a <15%

increase in respiration. Finally, 20mM succinate was added to saturate electron entrance to complex II via $FADH_2$ production. Polarographic oxygen measurements were acquired in 2s intervals with the rate of respiration derived from 40 data points and expressed as $pmol \cdot s^{-1} \cdot mg\ wet\ weight^{-1}$. Pmfb were weighed in ~1.5mL of ice-cold tared BIOPS (ATP-containing media) to ensure they remained relaxed.

4.5.4 Fatty acid oxidation protocol

This protocol has been previously described by Smith and colleagues and was used to determine rates of palmitoyl coenzyme A-supported (PCoA) respiration followed by the capacity of malonyl coenzyme A (MCoA) to suppress PCoA-supported respiration. 500mM L-carnitine and 1M malate were added following fiber background stabilization and acquisition in the reaction medium (20mM creatine Buffer Z). 5mM ADP was then added to the respiration medium to stimulate state III respiration. PCoA-stimulated respiration was measured by sequential additions of increasing concentration of PCoA to the chamber on the order of 5, 10, 15, 20, and 40μM. If maximal respiration was not achieved at a concentration of 40μM, titrations continued by adding 20μM PCoA at a time, until a plateau in respiration was obtained. Fiber sensitivity to respiration inhibition by MCoA was then assessed by adding MCoA to the chamber in a manner similar to that performed in the PCoA portion of the protocol. 0.5, 1, 2.5, 5, 7.5, 10, and 20μM MCoA was added in sequence to the chamber. If maximal respiratory inhibition was not obtained at a concentration of 20uM MCoA, titrations continued by adding 10μM MCoA at a time, until a plateau in respiration was obtained. Cytochrome *c* was added to test for mitochondrial membrane integrity.

4.5.5 Mitochondrial H_2O_2 emission (mH_2O_2)

mH_2O_2 was determined fluorometrically (QuantaMaster 40, HORIBA Scientific, Edison, NJ, USA) in a quartz cuvette with continuous stirring at 37°C, in 1mL Buffer Z supplemented with 10μM Amplex Ultra Red, 0.5U/mL horseradish peroxidase, 1mM EGTA, 40U/mL Cu/Zm-SOD1, 5μM BLEB, and 20mM creatine. Site-specific induction of H_2O_2 was measured through the addition of either 10mM pyruvate and 2mM malate (NADH, Complex I) or 10M succinate ($FADH_2$, Complex I via reverse electron flux from Complex II).

Following the induction of state II mH_2O_2 by Complex I and II substrates, 3 successive ADP titrations (25, 100, and 500μM) were added to progressively attenuate mH_2O_2. All

measurements were made in the presence of 1μM BLEB to prevent ADP-induced rigour as described earlier. The rate of mH_2O_2 emission was calculated from the slope (F/min) of a standard curve established with the same reaction conditions and normalized to pmfb dry weight. Upon completion of mH_2O_2 experiments, the fibers were rinsed in deionized H_2O, lyophilized in a freeze-dryer (Labconco, Kansas City, MO, USA) for >4 hours and weighed on a microbalance (Sartorius Cubis Microbalance, Gottingen, Germany).

4.6 Histology

4.6.1 Sample preparation

Soleus muscle embedded in OCT medium (Thermo Fisher Scientific_ was cut into 10μm sections with a cryostat (HM525 NX, Thermo Fisher Scientific) at -20°C. cryosections were used for immunofluorescence analysis and histology.

4.6.2 Immunofluorescence analysis

Muscle fiber type analysis followed the methodology described by Delfinis et al. (2023), allowing determination of fiber-type-specific atrophy. All primary antibodies were purchased from the Developmental Studies Hybridoma Bank (University of Iowa), and secondary antibodies were purchased from Invitrogen, Thermo Fisher Scientific. Briefly, slides were blocked with 5% goat serum (MilliporeSigma) in phosphate-buffered saline (PBS) for 1 hour at room temperature. Next, slides were incubated with primary antibodies against MHC I (BA-F8; 1:25), MHC IIA (SC-71; 1:1000), and MHC IIB (BF-F3; 1:50) for 2 hours at room temperature. Slides then underwent 3 washes in PBS for 5 minutes and were incubated with secondary antibodies (MHC I; Alexa Fluor 350 IgG2b; 1:1000), (MHC IIa; Alexa Fluor 488 IgG1; 1:1000), and (MHC IIb; Alexa Fluor 568 IgM; 1:1000) for 1 hour at room temperature. Following incubation, slides underwent 3 additional 5 minute washes in PBS before being mounted with ProLong antifade reagent (Life Technologies, Thermo Fisher Scientific).

Images were acquired after 24 hours with EVOS FL Auto 2 Imaging System (Invitrogen, Thermo Fisher Scientific). Individual images were taken across the entire cross section and assembled into a composite image. Fibers were selected randomly throughout the cross section and traced with ImageJ software to assess CSA after calibrations with a corresponding scale bar. Muscle fibers exhibiting a black appearance were classified as MHC IIX. For type I and type IIA fibers, 30 were selected per fiber per slide due to their abundance throughout the soleus muscle.

For type IIB and type IIX fibers, between 0-30 fibers were selected per fiber per slide due to their relative rarity in the soleus muscle.

4.6.3 Fiber counting

On the same slides used to calculate CSA of the soleus muscle, total and relative (%) fiber count for each of type I, type IIA, type IIB, and type IIX fibers was conducted using ImageJ software.

4.7 Statistics

Results are expressed as mean ± standard deviation (SD). The level of significance was established at $P < 0.05$ for all statistical tests performed. All data was first subject to the ROUT test to identify and exclude outliers. The D'Agostino-Pearson omnibus normality test was then performed to determine whether data resembled a Gaussian distribution. Depending on the number of independent variables being measured, one- and two-way ANOVAs were performed. When performing statistical testing involving a singular independent variable, if data passed normality testing, a one-way ANOVA was performed; if data failed normality testing, the Kruskal-Wallis test was performed. For assessments comprised of two independent variables, if data passed normality testing, a two-way ANOVA was performed; if data failed normality testing, it was log-transformed before proceeding with a two-way ANOVA. When a significant interaction was observed, Benjamini, Krieger and Yekutieli's post-hoc analysis was performed. All statistical analyses were performed with GraphPad prism Software 8.4.2 (La Jolla, Ca, USA).

CHAPTER FIVE: RESULTS

5.1 Elevated dietary protein consumption rescues semaglutide-associated bodyweight reductions

7-week old male C57Bl/6J DIO mice initially arrived at York University's animal facility for a 2-week acclimation period. (See **Figure 8-A** for overview of study timeline). Bodyweight was not significantly different at this age **(SFigure 1-C)**. At 9-weeks old, mice were randomized to receive 6 weeks of either semaglutide (SEMA) or vehicle (VEH; n=12) treatment 5 days per week administered subcutaneously in the subscapular region. Of those receiving SEMA injections, half remained on a Western Diet (WD+SEMA; n=12; comprised of 15% kcalories (kcal) from protein, 43% from carbohydrate (CHO), and 42% from fat) identical to that of the VEH group, and the other half were placed on a protein-enriched diet (PRO+SEMA; n=12; protein content was elevated 60% compared to WD, both diets remained isocaloric by reducing carbohydrate content accordingly).

Bodyweight was measured twice weekly during the following 6-week injection protocol **(Figure 8-B)**. All groups experienced increases in bodyweight from baseline **(Figure 8-B)**. There were no significant differences in bodyweight prior to randomization and treatment initiation **(Figure 8-B & 8-D)**. This was not explained by approximate measures of food intake **(SFigure 1-B)**. Upon completion of treatment, the SEMA group exhibited significantly reduced bodyweight compared to VEH **(Figure 8-C)**. In the PRO group, bodyweight was restored to the degree observed in the VEH group **(Figure 8-B – 8-D)**. While not statistically significant, SEMA treatment alone tended to inhibit weight gain at this age (P=0.0601; **SFigure 1-E)**.

5.2 Semaglutide reduced inguinal but not gonadal white adipose tissue depots

The inguinal white adipose tissue (iWAT) depot was harvested from one side of the body, in the region surrounding the pelvis and quadriceps (QUAD). The iWAT depot is classified as subcutaneous as it is located deep to the skin. The gonadal white adipose tissue (gWAT) depot was identified by its physical attachment to the testes and was harvested in its entirety. The gWAT depot is classified as visceral, due to its location surrounding the organs of the abdominal region.

6 weeks of SEMA treatment led to smaller iWAT mass, however, iWAT was not significantly smaller in PRO- compared to VEH-treated animals **(Figure 8-F)**. SEMA and PRO treatment did not significantly alter gWAT size compared to VEH treatment **(Figure 8-F)**. These

observations remained true for both adipose depots when normalized to bodyweight and tibial length **(SFigure 2-E & 2-F)**.

5.3 Semaglutide reduces absolute hind- and fore-limb muscle mass

Upon completion of the 6-week protocol, animals were sacrificed, and several muscles were harvested and weighed to assess changes in tissue size resulting from SEMA treatment.

The extensor digitorum longus (EDL), soleus (SOL), plantaris (PLT), gastrocnemius (GAS), and triceps (TRI) all exhibited a significant reduction in absolute weight following 6 weeks of SEMA injections compared to non-treated (VEH) muscle weights **(Figure 8-E)**. Conversely, in the PRO group, all aforementioned muscles showed at least some degree of restoration in muscle weight **(Figure 8-E)**. The tibialis anterior (TA) and QUAD muscle were unaffected by SEMA treatment, and similarly, PRO treatment did not result in significantly greater muscle size compared to VEH-treated TA and QUAD muscles **(Figure 8-G)**.

When normalized to tibial length, an identical pattern was observed **(SFigure 2-B)**. When muscle weights were normalized to total bodyweight, the reduction in weight observed with SEMA was preserved in the EDL, PLT, and TRI muscles **(SFigure 2-A)**. Interestingly, PRO was only able to rescue mass in the PLT **(SFigure 2-A)**.

5.4 Semaglutide reduces liver mass, but not other non-muscle lean tissue size

In addition to skeletal muscle dissection, several organs were harvested and weighed at the protocol's endpoint. Similarly the observation made in several muscles, SEMA treatment led to a significantly smaller liver mass, and which was abolished in PRO-treated animals **(Figure 8-H)**. The kidney, lung, heart, and spleen showed no effect of SEMA or PRO on organ size **(Figure 8-H)**. When organ masses were normalized to tibial length, the results remained the same **(SFigure 2-D)**, except for the reduction in liver size, which disappeared when normalized to bodyweight (**SFigure 2-C**).

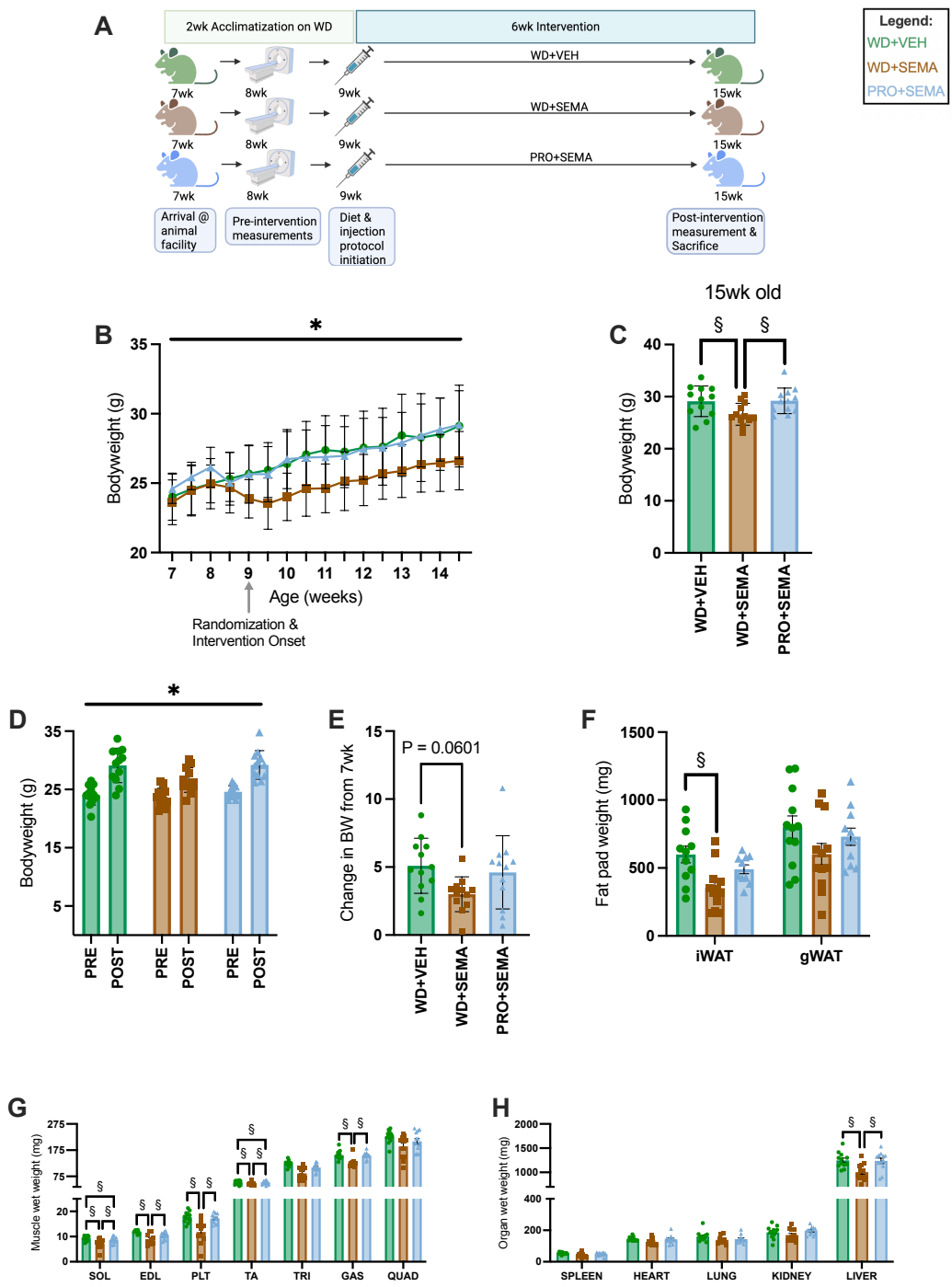

Figure 8. Bodyweight and morphometrics. A) Representative image of protocol timeline. **B)** Whole-body weight was taken 2x/week (n=12). **C)** Absolute bodyweight at 15wk old (n=12). **D)** Pre- vs. post-intervention body mass (n=12). **E)** Change in bodyweight from baseline (n=12). **F)** Subcutaneous fat from the inguinal white adipose tissue depot and visceral fat from the gonadal white adipose tissue depot were weighed (n=9-12). **G)** Hind- and fore-limb muscle wet weights (n=11-12). **H)** Abdominal organ wet weights (n=11-12). Results represent mean ± SD. A two-way ANOVA was used to determine the difference between WD+VEH vs WD+SEMA vs PRO+SEMA for **A & B**. A one-way ANOVA was used to determine the difference between WD+VEH vs WD+SEMA vs PRO+SEMA for **C,**

D, E, & **F**. When a significant interaction was present, post-hoc analysis was performed using the Benjamini, Krieger, and Yekutieli test. *P<0.05 main effect of time. §P<0.05.

5.5 Elevated protein intake does not further improve semaglutide-induced enhancement in glucose tolerance

Semaglutide has been previously established as an insulin-sensitizing drug. Glucose tolerance tests (GTTs) provide an *index* of insulin sensitivity by measuring the tissues' (specifically skeletal muscle and the liver's) ability to take up glucose from circulation following administration of a glucose load. GTTs were administered at 2 timepoints: 1 week prior to initiation of the 6-week injection protocol (intervention; PRE; defined by the unbroken lines in **Figure 9-A**), and during week 5 of the 6 week injection protocol (post-intervention; POST; defined by the dashed lines in **Figure 9-A**).

All groups demonstrated similar blood glucose responses during the PRE GTT **(Figure 9-A & 9-B)**. Both SEMA and PRO groups demonstrated considerably lower blood glucose responses compared to the VEH group during the POST GTT **(Figure 9-A & 9-B)**. Both SEMA and PRO groups experienced improved glucose tolerance indicated by significantly dampened responses in blood glucose concentration following 6 weeks of drug treatment **(Figure 9-A & 9-B)**. Conversely, VEH animals showed no change in glucose tolerance following 6 week of injections **(Figure 9-B)**. There were no significant differences between SEMA and PRO GTT response PRE or POST-intervention, indicating protein did not further improve glucose tolerance during SEMA treatment **(Figure 9-B)**.

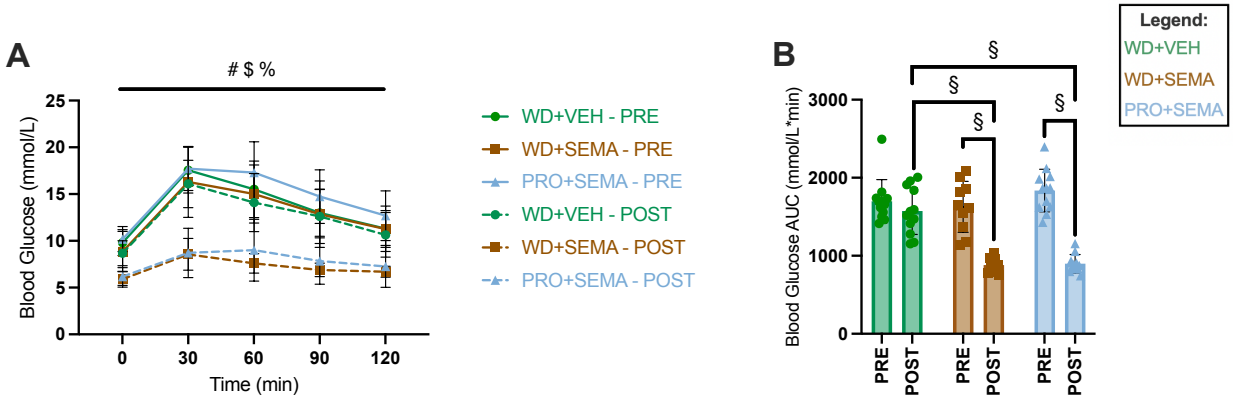

Figure 9. Changes in glucose tolerance following 6wk of semaglutide treatment. A) Blood glucose concentration (mmol/L) response to a glucose bolus following a 5hr fast. Straight lines indicative of pre-intervention glucose tolerance testing (GTT), dashed lines indicative of post-intervention GTT (n=10-12). **B)** Area under the blood glucose concentration response curve (n=10-12). Results represent mean ± SD. A two-way ANOVA was used to determine the difference between WD+VEH vs WD+SEMA vs PRO+SEMA. When a significant interaction was present, post-hoc analysis was performed using Benjamini, Krieger, and Yekutieli test. $^{\#}$P<0.05 PRE vs POST in all SEMA-treated groups. $^{\$}$P<0.05 WD+VEH post vs WD+SEMA post. $^{\%}$P<0.05 WD+VEH post vs PRO+SEMA post. §P<0.05.

5.6 Semaglutide did not improve lean-to-fat ratio

The lean-to-fat ratio was assessed *in vivo* pre- and post-intervention via microCT scan **(Figure 10-B)**. Multiple body compartments were considered via CT analysis and are outlined in **Figure 10-A**. Lean-to-fat ratio was also calculated *ex vivo* by summing hindlimb muscle and fat pad weights, respectively, then dividing total hindlimb muscle mass by total fat pad mass **(Figure 10-C)**.

There were no differences in *in vivo* lean/fat ratio between groups prior to onset of the intervention **(Figure 10-B)**. Similarly, following completion of the intervention, no group exhibited changes in lean/fat ratio from baseline **(Figure 10-B)** and likewise there were no significant differences at the endpoint between groups in the *in vivo* lean/fat ratio **(Figure 10-B)**. These results were identical across whole body, upper body, and crus compartments **(Figure 10-B)**.

The same pattern was observed *ex vivo* in the calculated lean/fat mass ratio from absolute tissue weights **(Figure 10-C)**. SEMA significantly reduced total hindlimb muscle wet weight and total fat pad wet weight **(Figure 10-D & 10-E)**, with PRO treatment preserving hindlimb muscle wet weight **(Figure 10-D)**.

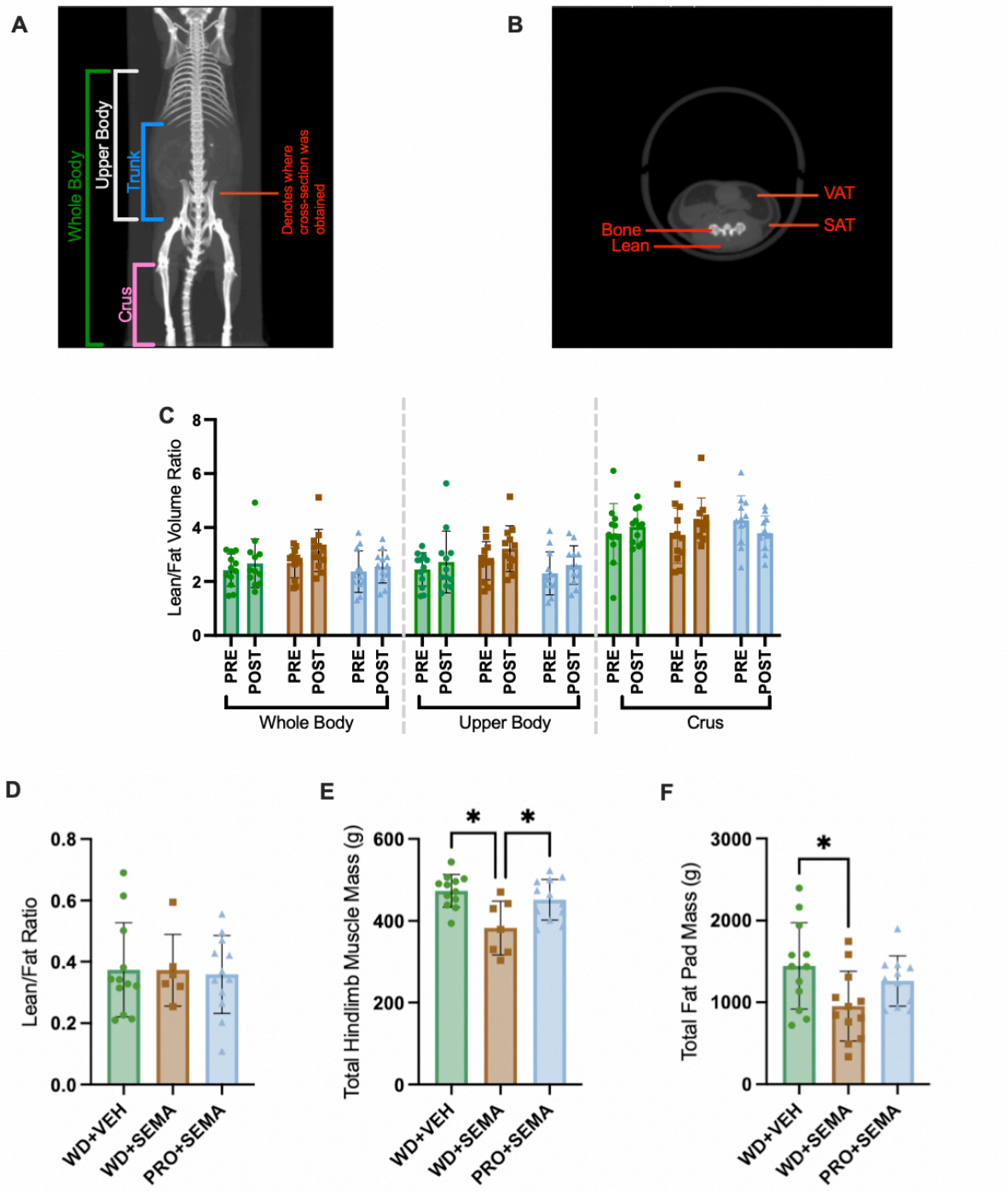

Figure 10. ***In vivo*** **and** ***ex vivo*** **lean/fat ratio. A)** Representative image depicting how each compartment was defined for microCT analysis. The whole body compartment is defined from the bottom of the shoulder blades to the ankle joint. The upper body department is defined from the bottom of the shoulder blades to the hip joint. The trunk compartment is defined from the bottom of the ribcage to the hip joint. The crus compartment is defined from the knee joint to ankle joint. All analysis excluded the tail and any body parts residing above the bottom of the shoulder blade region. **B)** Representative cross-sectional image denoting lean, bone, visceral adipose, and subcutaneous adipose tissue. **C)** Lean/fat volume ratio before (PRE) and after (POST) 6wk intervention in respective body compartments (n=12). **D)** Absolute lean/fat ratio comparing total sum of collected hindlimb muscles (TA, EDL, QUAD, SOL, PLT, GAS) against total sum of collected fat depots (iWAT, gWAT) for each animal (n=6-12). **E)** Total cumulative mass of collected hindlimb muscles (n=7-12). **F)** Total cumulative mass of collected fat pads (n=11-12). Results represent

mean ± SD. A two-way ANOVA was used to determine WD+VEH vs WD+SEMA vs PRO+SEMA for **C)**. A one-way ANOVA was used to determine WD+VEH vs WD+SEMA vs PRO+SEMA for **D)**, **E)**, & **F)**. When a significant interaction was present, post-hoc analysis was performed using Benjamini, Krieger, and Yekutieli test. *P<0.05.

5.7 In-vivo body composition changes in response to 6 weeks of semaglutide treatment during adolescence

Body composition was evaluated pre- and post-intervention via microCT scan to assess tissue-specific responses to SEMA treatment with (PRO) and without (WD; SEMA control) whey and casein supplementation, compared to VEH on adipose, lean, and bone tissue volume in multiple body compartments (whole-body (WB), upper-body (UB), trunk, and crus, respectively). **Figure 10-A** provides a representative image of how each body compartment was defined and separated for analysis.

There was no difference in WB change (Δ) in volume from baseline with SEMA compared to VEH treatment, irrespective of dietary modification **(Figure 11-A)**. The same observation was made when looking at change specific to WB tissue type, with no difference in Δlean, Δadipose, or Δbone volume from baseline **(Figure 11-A)**. However, there was an, albeit non-significant (P=0.0770), benefit of SEMA on Δbone volume percentage (%) of the WB compartment that was also observed in the PRO-treated group **(Figure 11-B)**. There were no significant between group differences pre- or post-intervention in total WB volume **(SFigure 3-A)**. This remained the case for absolute and relative individual tissue types across the WB compartment **(SFigure 3-A & 3-B)**. There was a main effect of time leading to increased total, lean, and bone volume of the WB compartment **(SFigure 3-A)**.

The UB compartment displayed no significant between group differences in Δvolume, absolute Δlean volume, absolute Δbone volume, or Δlean volume % **(Figure 11-C & 11-D)**. While not significant, VEH-treated animals exhibited a greater absolute Δadipose volume of the UB compartment (P=0.0797; **Figure 11-C**).

Additionally, both SEMA and PRO-treated groups elicited a trend toward a greater positive Δbone volume of this compartment (P=0.0692**; Figure 11-D)**. There were no differences in total volume, absolute lean volume, lean volume %, absolute adipose volume, adipose volume % or absolute bone volume of the UB chamber at baseline **(SFigure 3-C & 3-D)**. These tissues were similarly not different from one another post-intervention **(SFigure 3-C & 3-D)**. However, bone volume % was significantly greater in VEH and SEMA compared to PRO-treated animals at baseline **(SFigure 3-D)**. This interaction had disappeared by the post-intervention period in all

groups, indicated by a reduction in VEH-treated animals' bone volume % that wasn't observed in SEMA-treated animals **(SFigure 3-D)**. There was a main effect of time on total, absolute lean, and absolute bone volume from pre- to post-intervention **(SFigure 3-C)**.

Total trunk volume was not changed to a greater extent in any group from baseline **(Figure 11-E)**. However, absolute and % visceral adipose volume increased to a greater degree in the VEH compared to PRO group **(Figure 11-E & 11-F)**. In the absolute visceral depot, this was not significant for SEMA treated animals (P=0.0606; **Figure 11-E)**. Absolute Δsubcutaneous adipose tissue were appreciably greater for VEH and PRO groups compared to SEMA **(Figure 11-E)**. Likewise, there was a non-significant trend toward a greater reduction in subcutaneous adipose tissue % in SEMA compared to VEH and PRO groups (P=0.0963; **Figure 11-F)**. There were no significant differences between any group in any measure of trunk body composition pre- or post-intervention **(SFigure 3-E & 3-F)**. There was a main effect of time with respect to total trunk volume and relative subcutaneous adipose volume **(SFigure 3-E & 3-F)**.

The crus compartment was defined as the area spanning the knee to ankle joint. Absolute Δlean, Δadipose, and Δbone volume was not significantly different between any group in this compartment **(Figure 11-G)**. VEH-treated animals exhibited a non-significant greater increase in total crus volume compared to SEMA (P=0.0691) and PRO (P=0.0537; **Figure 11-G)**. VEH administration led to a greater crus Δlean volume %, but SEMA administration led to a greater Δbone volume % in both SEMA-receiving groups, favouring greater bone volume **(Figure 11-H)**. No difference was present in total, absolute lean, absolute adipose, adipose %, or absolute bone volume was present pre- or post-intervention between any group. **(SFigure 3-G & 3-H)**. An increase in lean volume % of the crus compartment was apparent only in the VEH group **(SFigure 3-H)**, and VEH vs PRO lean volume % was significantly different at baseline, but not post-intervention **(SFigure 3-H)**. Bone volume % of the crus compartment was elevated at baseline in VEH compared to SEMA and PRO groups, but not at the endpoint **(SFigure 3-H)**. Likewise, VEH animals exhibited significantly reduced bone volume %, while SEMA-treated animals exhibited significant improvements in bone volume % **(SFigure 3-H)**.

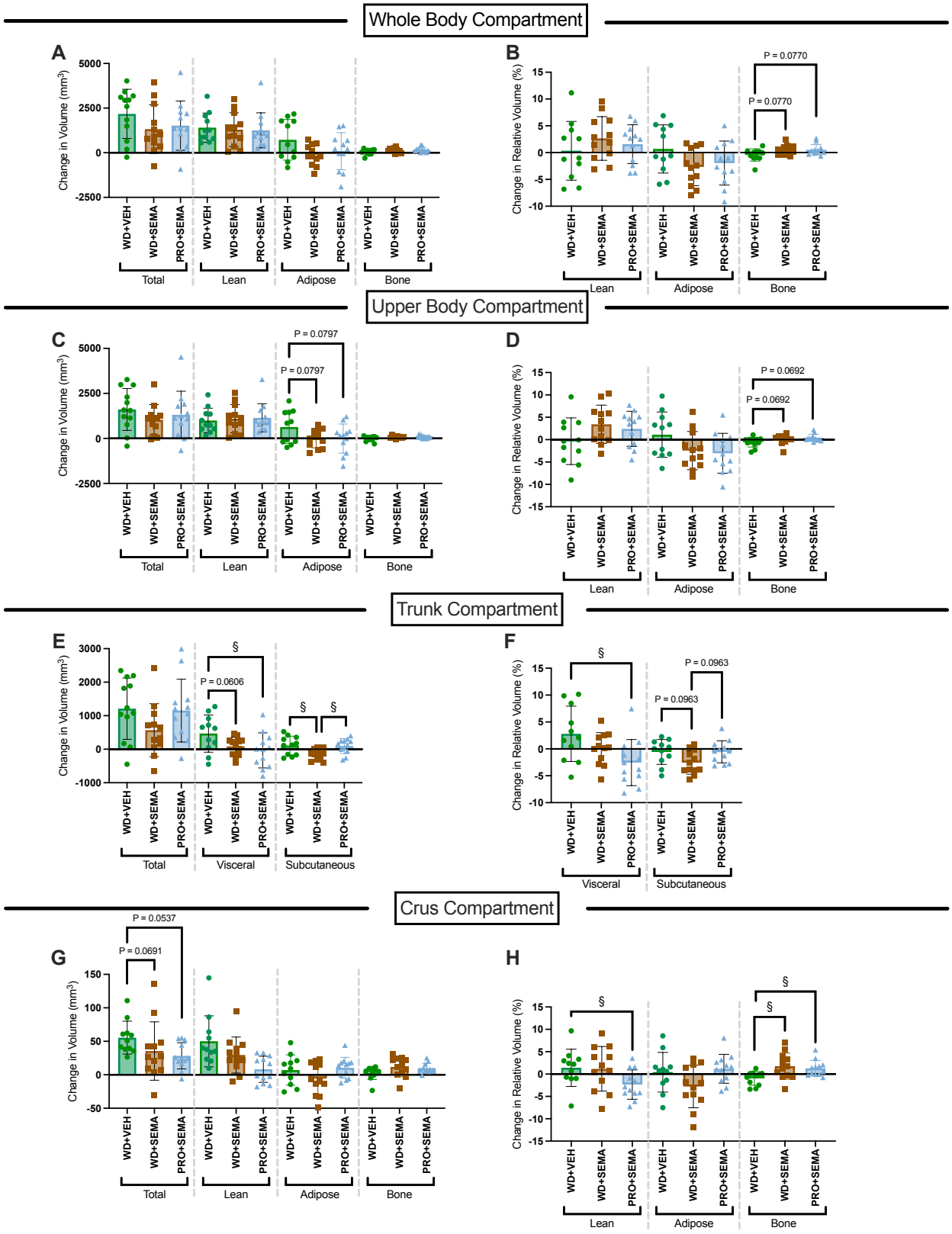

Figure 11. Body composition changes from baseline in response to 6 weeks of vehicle or semaglutide injections. All values are expressed as the change (Δ) in total **(A, C, E, & G)** or relative **(B, D, F, & H)** volume from pre- to post-intervention. **A)** Whole-body (WB) volume was defined from the bottom of the shoulder blade to the ankle joint. Total

volume was measured and then divided according to density into lean, adipose, and bone components. Tail volume was excluded from all analysis (n=11-12). **B)** Proportions of lean, adipose, and bone of the WB compartment (n=11-12). **C)** Upper-body (UB) volume was defined from the bottom of the shoulder blade to the hip joint and. Total volume was first measured and then sectioned to lean, adipose, and bone volumes (n=11-12). **D)** Proportions of lean, adipose and bone of the UB compartment (n=11-12). **E)** Trunk volume was defined from the bottom of the ribs to the hip joint. Total and adipose volume was measured, and adipose volume was subsequently divided into visceral and subcutaneous depots (n=10-12). **F)** Proportions of visceral and subcutaneous adipose relative to total trunk adipose volume (n=10-12). **G)** The crus compartment was defined from the knee joint to the ankle joint and was analyzed identically to **A)** and **C)** (n=11-12). **H)** was analyzed identically to **B)** and **D)** (n=11-12). Results represent mean ± SD. A one-way ANOVA was used to determine WD+VEH vs WD+SEMA vs PRO+SEMA. When a significant interaction was present, post-hoc analysis was performed using Benjamini, Krieger, and Yekutieli test. $^{\S}P<0.05$.

5.8 Reductions in soleus mass are not explained by reductions in cross-sectional area or fiber number

Following harvesting of the soleus muscle, it was embedded in optimal cutting temperature (OCT) embedding solution for histological analysis. Significant freeze fracturing occurred between tissue harvest and imaging of the soleus slides, which has negatively impacted the quality of the analysis and interpretation of results.

Semaglutide did not reduce cross-sectional area (CSA) across any fiber type, or average fiber CSA throughout the entire fiber **(Figure 12-B & 12-C)**. Likewise, PRO-treatment did not contribute to any meaningful differences in fiber-type specific CSA **(Figure 12-B & 12-C)**. Furthermore, SEMA did not change total fiber number, the amount of any particular fiber type, or the proportion of each fiber type making up the soleus section **(Figure 12-D & 12-E)**. The PRO group likewise did not change total fiber count, individual fiber number, or relative contribution of each fiber to total fiber number **(Figure 12-D & 12-E)**.

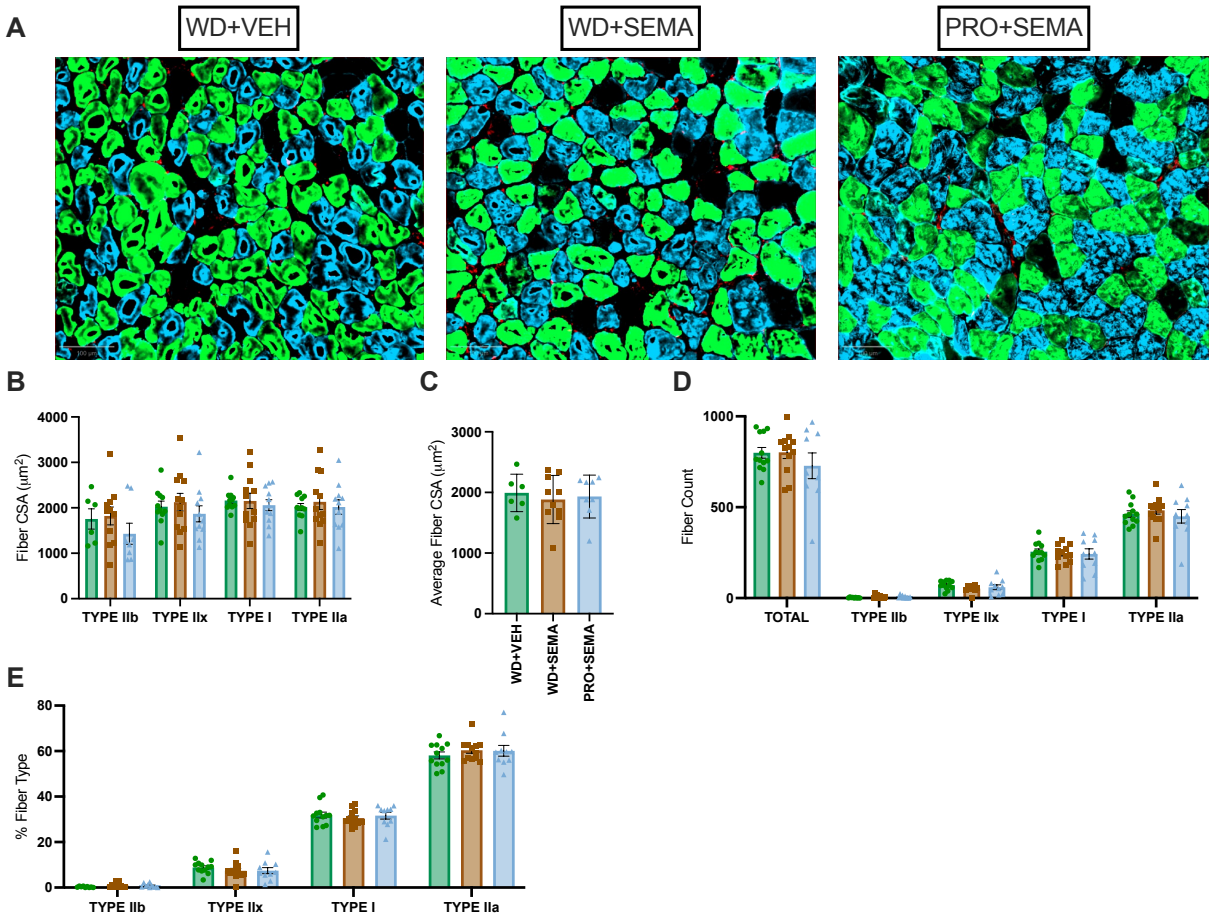

Figure 12. Histological analysis of the soleus muscle. A) Representative images from (L) to (R) showing WD+VEH, WD+SEMA, and PRO+SEMA soleus sections. The blue stain depicts Type I muscle fibers, the green stain depicts Type IIa muscle fibers, and fibers that do not fluoresce are Type IIx. A red stain was used to detect Type IIb fibers, however, these fibers are sparse in murine soleus muscle and were undetectable in several slides. **B)** Fiber-type specific cross-sectional area (CSA) (n=7-11). **C)** Average CSA for all fibers analyzed (n=7-11). **D)** Total number of fibers per soleus as well as total number of each respective fiber type (n=9-12). **E)** Relative proportion of fiber type present in soleus sections (n=9-12). Results represent mean ± SD. A one-way ANOVA was used to analyze **B)** & **C)**. **D)** & **E)** were not normally distributed and thus were analyzed using a Kruskal-Wallis test.

5.9 Semaglutide pharmacotherapy impairs maximal contractile force production in the tibialis anterior

Immediately prior to sacrifice at 15 weeks of age, an *in situ* force procedure was performed consisting of force frequency, fatigue, and recovery from fatigue protocols administered sequentially in the TA muscle (outlined in **Figure 13-A**).

Following 6 weeks of SEMA administration, absolute force production was reduced at maximal frequencies of stimulation in the TA muscle **(Figure 13-B)**. This reduction in absolute force output was prevented with PRO treatment **(Figure 13-B)**. When normalized to muscle cross-sectional area (CSA), the effect of SEMA on force output was eliminated. **(Figure 13-C)**. There

were no between-group differences at frequencies of stimulation associated with submaximal contraction **(Figure 13-B & 13-C)**.

A sub-analysis was performed of contractions at 80, 100, 120, and 200Hz, which are known to elicit maximal force output. Across all of these contraction frequencies, SEMA treatment was associated with an impairment in force output **(SFigure 4-A – 4-D)**. PRO treatment once again rescued absolute force at the SEMA-affected stimulation frequencies **(SFigure 4-A – 4-D)**. Specific force remained unaffected at 80 and 200Hz (P>0.1), but a trend toward significance was observed at contractions stimulated by 100 (P=0.0611) and 120Hz (P=0.0600; **SFigure 4-E – 4-H)**. All groups demonstrated increasing force production with increasing frequency of muscle stimulation until maximal force output was achieved **(Figure 13-B & 13-C)**.

When individual force frequency contractions were expressed relative to maximal force output, SEMA administration produced a greater proportion of maximal force at lower frequencies of stimulation compared to VEH- and PRO-treated groups **(Figure 13-D)**.

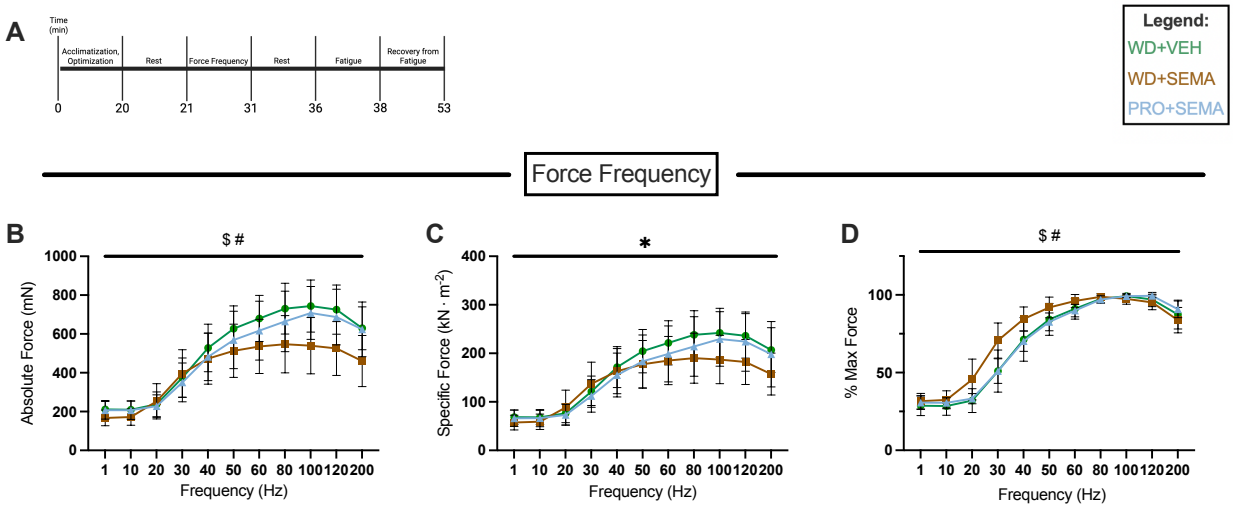

Figure 13. Semaglutide reduces maximal contractile force output. A) Outline of *in situ* tibialis anterior (TA) force set up and procedure. Force protocols included force frequency (FF), fatigue, and recovery from fatigue. **B)** Absolute FF was measured by stimulating the TA once per minute for 0.2ms at increasing stimulation frequencies (1Hz – 200Hz) (n=10-12). **C)** Specific FF was calculated by dividing the absolute force at each stimulation frequency by muscle cross-sectional area (n=10-12). **D)** Each contraction of the FF protocol was expressed relative to maximal force output. Left-ward shift of the curve indicates a shift toward a type I fiber phenotype (n=10-12). Results represent mean ± SD. A two-way ANOVA was used to determine WD+VEH vs WD+SEMA vs PRO+SEMA. When a significant interaction was present, post-hoc analysis was performed using Benjamini, Krieger, and Yekutieli test. $^{\$}$P<0.05 WD+VEH vs WD+SEMA. $^{\#}$P<0.05 WD+SEMA vs PRO+SEMA. *P<0.05 main effect of time.

5.10 Semaglutide treatment does not affect voluntary or involuntary submaximal measures of muscle contraction

SEMA treatment did not significantly impair force output during fatiguing contractions **(Figure 14-A)**, nor did PRO improve fatiguability **(Figure 14-A)**. The same effect was observed following CSA normalization **(Figure 14-B)** and when considering force output expressed relative to the initial fatiguing contraction **(Figure 14-C)**.

A sub-analysis performed on individual contractions from the first 1/3rd of the fatigue protocol shows that while no between-group differences were apparent upon protocol initiation, **(SFigure 6-A & 6-F)**, SEMA treatment was associated with diminished absolute force output 20 and 30 contractions into the protocol **(SFigure 6-C & 6-D)**, with non-significant reductions evident at contractions 10 and 40 (P=0.0813 and P=0.0826, respectively; **SFigure 6-B & 6-E**). Upon normalization to muscle CSA, this was absolved **(SFigure 6-F – 6-J)**.

Irrespective of treatment, all groups exhibited similar total and relative reductions in force output from baseline to protocol completion **(Figure 14-A – 14-C)**. Likewise, area under the curve was not significantly different between any groups for either absolute or specific force from fatigue **(SFigure 5-B & 5-D)**.

Recovery from fatigue was measured 5, 10, and 15 minutes following the final fatiguing contraction by sending a single tetanic stimulation. Absolute and specific force output during the 15 minute window succeeding fatiguing contractions exhibited no differences amongst any groups **(SFigure 5-E & 5-F)**. Likewise, recovery expressed relative to the initial fatiguing contraction exhibited no differences between groups **(Figure 14-F)**.

In addition to involuntary measures of skeletal muscle function, submaximal voluntary measures of muscle function, including forelimb grip strength and maximal cage hang duration were assessed. There was no effect of time on forelimb grip strength, defined by peak tension normalized to bodyweight, for any group **(Figure 14-D)**. There were also no differences between animals receiving VEH, SEMA, or PRO treatment either pre- or post-intervention **(Figure 14-D)**. The same observations were made for maximal cage hang time, with no significant changes from pre- to post-intervention or between groups at either timepoint **(Figure 14-E)**. These measures were made on a weekly basis throughout the 6-week intervention, with changes in voluntary submaximal function unaffected during the intermediate weeks as well **(SFigure 7-E & 7-F)**. Absolute values for forelimb grip strength showed similar results **(SFigure 7-A & 7-D)**.

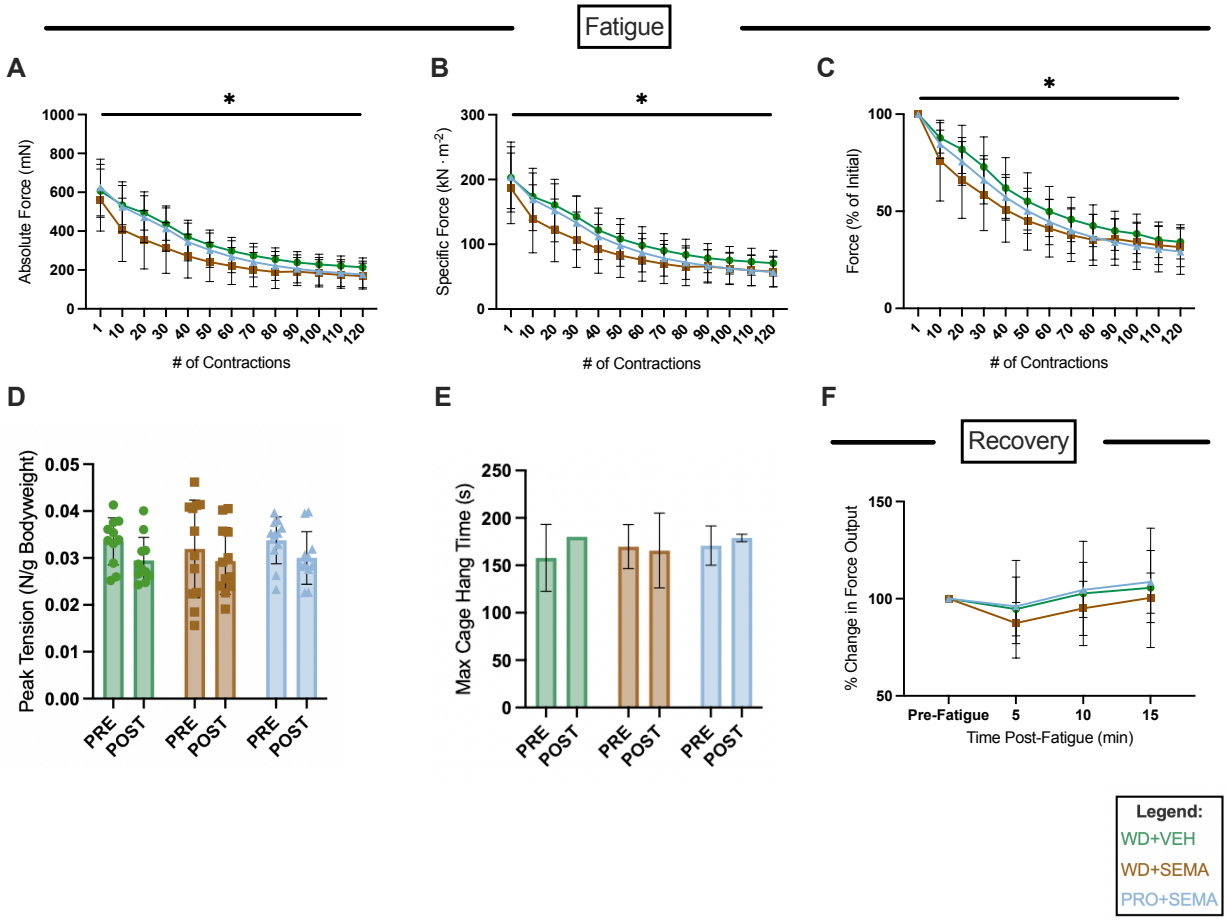

Figure 14. Semaglutide did not influence submaximal measures of force generation. A) The fatigue protocol consisted of 120 twitches sent every 0.3s at a stimulation frequency of 60Hz, expressed as total force output (n=9-10). **B)** Absolute force during the fatigue protocol normalized to muscle cross-sectional area (n=9-10). **C)** Force output expressed relative to initial force produced during first contraction of the fatigue protocol (n=9-10). **D)** Forelimb grip strength normalized to bodyweight as an index of submaximal voluntary muscle function (n=12). **E)** Maximal cage hang time duration (capped at 180sec) as an index of submaximal voluntary muscle function (n=12). Under certain instances, all animals in a group reached 180s for cage hang time. When this occurred, no error bars were drawn **F)** The recovery protocol consisted of 1 twitch sent every 5 minutes for 15 minutes at a stimulation frequency of 100Hz following completion of the fatigue protocol, expressed relative to initial force produced during the first contraction of fatigue (n=9-10). Results represent mean ± SD. A two-way ANOVA was used to determine WD+VEH.

5.11 Semaglutide does not alter mitochondrial hydrogen peroxide (mH_2O_2) emission

Complex I-supported and Complex II-supported mH_2O_2 emission were measured using pyruvate and malate (NADH, Complex I), and succinate ($FADH_2$, Complex I via reverse electron flux from Complex II), respectively in TA permeabilized muscle fibers. Initially, State II (maximal) mH_2O_2 emission was recorded in the absence of ADP. State III mH_2O_2 emission was then measured following 3 subsequent titrations of ADP. 25µM ADP was titrated to measure mH_2O_2 emission under basal, or resting, conditions. 100µM ADP was titrated to measure mH_2O_2

emission under conditions of increased energy demand, e.g. exercise. Finally, 500μM ADP was titrated to measure mH_2O_2 emission in the presence of supraphysiological ADP concentrations.

Complex I-supported State II mH_2O_2 emission was unaffected by SEMA or PRO treatment **(Figure 10-A)**. Likewise, both absolute and relative (expressed as a % of state II) Complex I-supported mH_2O_2 emission following ADP administration were not significantly different in any group **(Figure 15-B & 15-C)**. ADP significantly reduced mH_2O_2 to a similar degree in VEH, SEMA, and PRO groups **(Figure 15-B & 15-C)**.

Complex II-supported state II mH_2O_2 emission was similar between SEMA and VEH groups, but the PRO group presented with significantly elevated mH_2O_2 emission **(Figure 15-D)**. Both absolute and relative Complex II-supported mH_2O_2 emission rates were not significantly different in any group **(Figure 15-E & 15-F)**. Similarly, ADP significantly reduced mH_2O_2 emission to a similar degree in all groups **(Figure 15-E & 15-F)**.

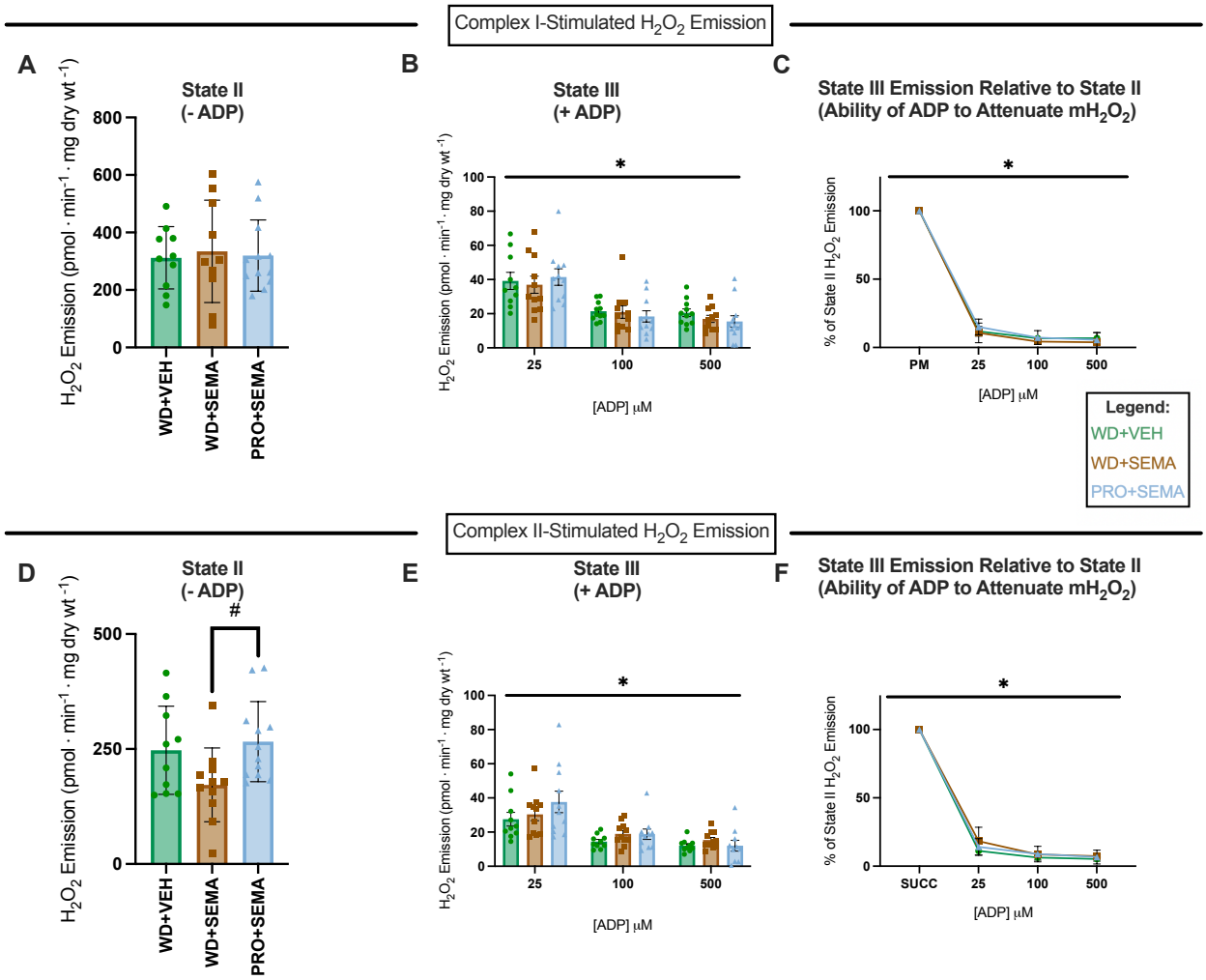

Figure 15. State II and State III mH2O2 emission in C57Bl/6 DIO mice via Complex I and Complex II. Following 6 weeks of VEH or SEMA treatment, tibialis anterior permeabilized muscle fiber bundles underwent 1 of 2 mH_2O_2 protocols: either by being supplied with 10mM pyruvate and 2mM malate (to support Complex I-stimulated mH_2O_2 emission) or with 10mM succinate (reverse electron transfer from Complex II to Complex I via Coenzyme Q). All experiments were performed with 20mM creatine in the reaction medium. **A)** Maximal mH_2O_2 emission was assessed through provision of pyruvate and malate (n=11-12). **B)** Adding multiple ADP titrations was done in an effort to observe changes in Complex I-stimulated mH_2O_2 emission across various states of energy demand, expressed as absolute reduction in emission (n=10-12). **C)** Shows the ability of ADP to attenuate Complex I-stimulated mH_2O_2 emission, relative to maximal mH_2O_2 emission (n=9-12). **D)** Maximal mH_2O_2 emission was assessed through provision of succinate (n=11-12). **E)** Absolute reduction in Complex II-stimulated mH_2O_2 emission (n=10-12). **F)** Relative reduction in Complex II-stimulated mH_2O_2 emission expressed as a percentage of State II emission (n=9-12). Results represent mean ± SD. A one-way ANOVA was used to determine WD+VEH vs WD+SEMA vs PRO+SEMA for **A** and **D**. A two-way ANOVA was used to determine WD+VEH vs WD+SEMA vs PRO+SEMA for **C** and **F**. *P<0.05 main effect of [ADP]. #P<0.05 WD+SEMA vs PRO+SEMA.

5.12 Semaglutide treatment leads to improved sensitivity to ADP-stimulated respiration at submaximal concentrations

Permeabilized muscle fiber bundles were made from the non-contracted TA muscle immediately upon completion of the *in-situ* force protocol. Half of the bundles slated for

respiration were used for oxygen consumption stimulated by CHO-derived substrates, with the other half being utilized for FA-stimulated respiration, described below.

There was no significant differences across any group in submaximal (25-500μM) or maximal (1000-7000μM) coupled (State III) respiration, an index of coupled ATP generation **(Figure 16-A)**. Uncoupled (State II) respiration also was unchanged across any treatment group **(Figure 16-B**). Further addition of reducing equivalents as NADH **(Figure 16-C)** or $FADH_2$ **(Figure 16-D)** likewise did not result in differences between groups in further oxygen consumption. However, analysis of Michaelis-Menten kinetics reveals that SEMA treatment led to significantly elevated sensitivity in TA permeabilized muscle fiber bundles to ADP-stimulated respiration **(Figure 16-F)** despite no significant differences in maximal respiratory reaction rate **(Figure 16-E)**. There was a main effect of ADP concentration **(Figure 16-A)**.

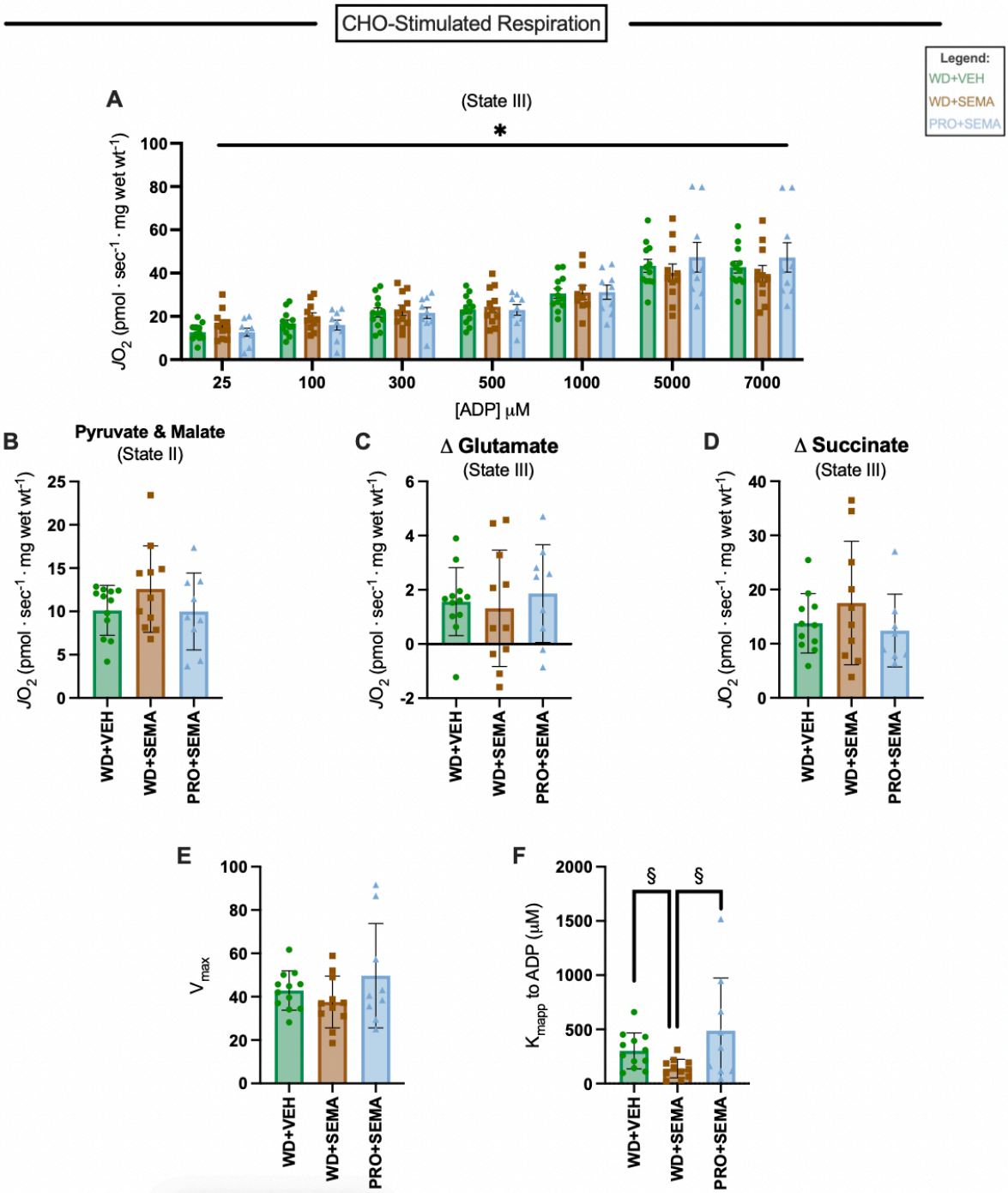

Figure 16. Carbohydrate substrate-stimulated respiration of the TA muscle. A) State III respiration under a range of basal, physiological, and supraphysiological ADP concentrations, supported by 5mM pyruvate and 2mM malate (n=9-12). **B)** State II (uncoupled) respiration stimulated by adding pyruvate and malate to supply the reaction chamber with NADH (n=9-12). **C)** State III respiration further stimulated through addition of 10mM glutamate as another source of NADH (n=9-12). **D)**. 20mM Succinate was added to the reaction chamber as a further source of reducing equivalents, this time in the form of $FADH_2$, for respiration (n=9-12). **E)** Maximal respiration rate (n=9-12). **F)** K_M reflects the substrate concentration at which the reaction rate is at half of its maximal capacity (n=9-12). Results represent mean ± SD. A two-way ANOVA was used to determine WD+VEH vs WD+SEMA vs PRO+SEMA for **A)**. A one-way ANOVA was used to determine WD+VEH vs WD+SEMA vs PRO+SEMA for **B-F)**. When a significant

interaction was present, post-hoc analysis was performed using Benjamini, Krieger, and Yekutieli test. *P<0.05 = main effect of [ADP]. §P<0.05.

5.13 Semaglutide treatment did not lead to changes in fatty acid-stimulated respiration

Respiration stimulated by FAs was stimulated by adding L-carnitine and malate to the reaction medium (State II), followed by a maximal ADP titration to stimulate State III respiration. SEMA and PRO treatment did not significantly differ with respect to State II or State III FA-derived respiration **(Figure 17-A & 17-C)**. Addition of MCoA to the reaction medium led to substantial variability between permeabilized muscle fiber bundles, and there was ultimately no observed ability of MCoA to inhibit coupled respiration **(Figure 17-B)**. Likewise, there were no differences between groups with titration of MCoA **(Figure 17-B)**. Maximal respiratory reaction rate and K_m were not different across treatment groups **(Figure 17-D & 17-E)**. There was a main effect of PCoA concentration on fatty acid-stimulated respiration **(Figure 17-A)**, but otherwise no apparent effect of SEMA or PRO on State II or State III respiration stimulated by FA-supplied substrates.

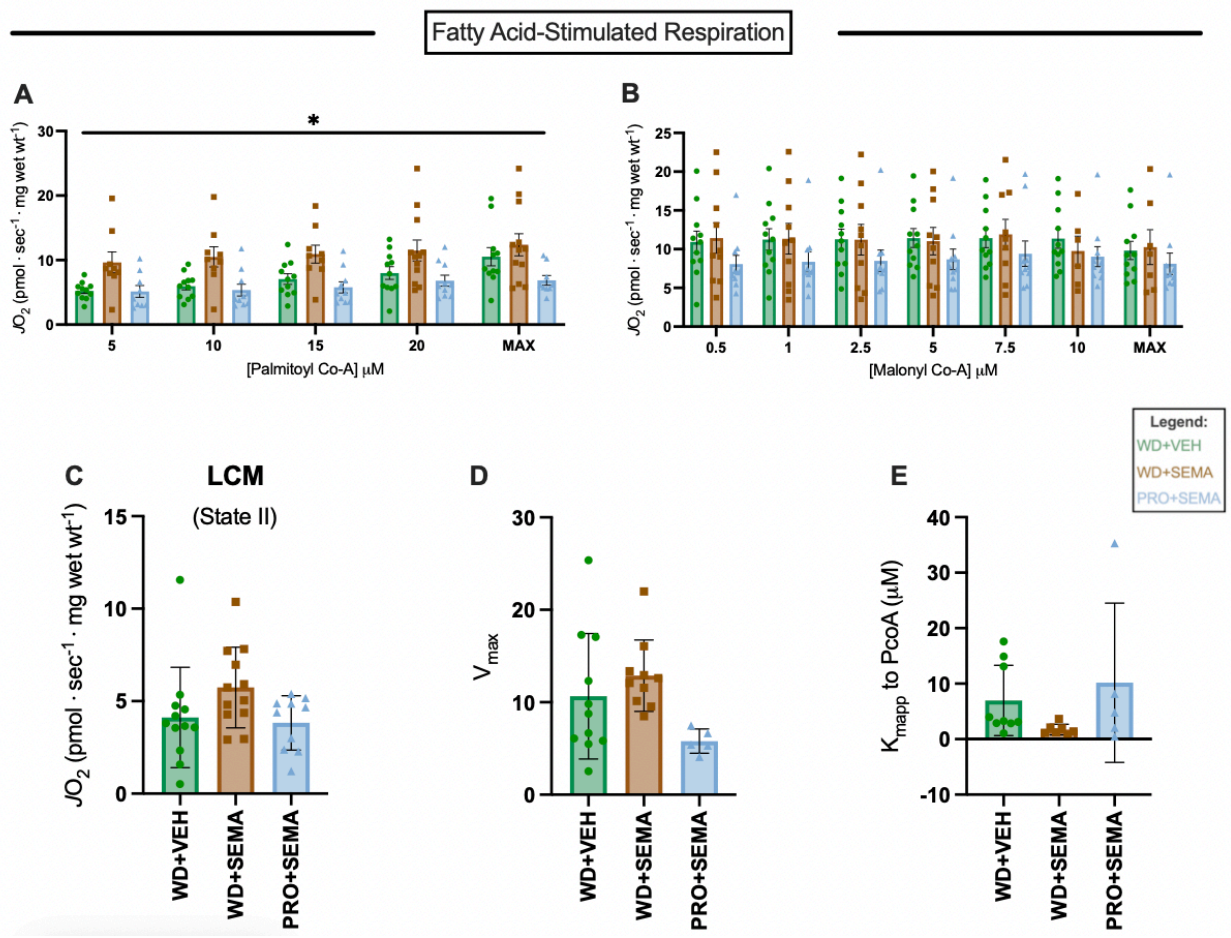

Figure 17. Fatty acid-substrate stimulated respiration of the TA muscle. The fatty acid protocol is initiated by titrating L-carnitine and malate to generate reducing equivalents for the ETC. A single maximal ADP titration is then administered to stimulated oxygen consumption coupled to ATP generation before the first palmitoyl CoA (PCoA) titration is administered. **A)** State III respiration stimulated by titrating increasing concentrations of palmitoyl CoA. Following 20µM PCoA titration, PCoA continued to be added, 20µM at a time, until maximal respiration has been achieved (n=9-12). **B)** Immediately after achieving maximal PCoA-stimulated respiration, Malonyl CoA (MCoA) is titrated at increasing concentrations to inhibit oxygen consumption. Following 10µM MCoA titration, MCoA continued to be added, 10µM at a time, until maximal inhibition was obtained (n=9-12). **C)** State II (uncoupled) respiration stimulated by adding 500mM L-carnitine and 1mM malate to supply the reaction chamber with reducing equivalents (n=9-12). **D)** Maximal respiration rate (n=5-11). **E)** K_M reflects the substrate concentration at which the reaction rate is at half of its maximal capacity (N=5-11). Results represent mean ± SD. A two-way ANOVA was used to determine WD+VEH vs WD+SEMA vs PRO+SEMA for **A) & B)**. A one-way ANOVA was used to determine WD+VEH vs WD+SEMA vs PRO+SEMA for **C-E)**. *P<0.05 = main effect of [PCoA]. LCM = L-carnitine and malate.

CHAPTER SIX: DISCUSSION

The state of chronic energy imbalance favouring storage of surplus energy as adipose tissue characteristic of obesity is implicated in the development of other weight-related comorbidities, millions of annual deaths, and preventable global economic and healthcare hardships.[1,2,6] Due to the complex physiological, behavioural, environmental, and genetic components underpinning the

development of obesity, it has historically been notoriously treatment-resistant.[37,88] GLP-1 RAs present the dawn of a new era, whereby they contribute to meaningful weight loss in overweight and obese individuals and reduce the incidence and severity of weight-related comorbidities such as T2D, cardiovascular events, and stroke.[12,20,21]

While the prevalence of obesity nears epidemic proportions, a lesser-considered consequence of an increasingly sedentary world has arisen as well: that is, inadequate muscle mass.[1,3,6,52] These two are not mutually exclusive, and often go hand-in-hand. The simultaneous incidence of obesity and low relative muscle mass and function has been coined sarcopenic obesity and is associated with worse outcomes than abdominal obesity on its own.[6] What do GLP-1 RAs have to do with this? Their use has been linked to a significant proportion of weight loss as lean mass, above what is observed with other, non-pharmacological interventions.[15,16] The use of an atrophy-inducing agent in a population predisposed to low muscle mass and quality is unfavourable considering the vital role of skeletal muscle in glucose uptake, energy expenditure, and locomotion/proprioception.

Despite this profound negative side effect, GLP-1 RAs are still an incredibly efficacious weight loss treatment option.[12] By improving the ratio of fat to muscle loss with GLP-1 RA treatment and elucidating other possible effects GLP-1 RAs may have on skeletal muscle function, it may be possible to optimize weight loss interventions utilizing GLP-1 RAs. Non-pharmacological weight loss interventions have had success in this by manipulating the dietary macronutrient profile in an effort to yield 'high quality' weight loss – that is – fat loss not at the expense of muscle atrophy.[34] By utilizing previously effective methods of skeletal muscle mass preservation, we aimed to optimize weight loss elicited by GLP-1 RAs.

Ultimately, semaglutide treatment resulted in lower bodyweight and individual muscle wet weights. Submaximal measures of contractile function were unimpeded, but maximal contractile function was reduced following the 6-week semaglutide treatment protocol. Concurrent protein supplementation ameliorated semaglutide-induced reductions in bodyweight, muscle mass, and maximal force output. Semaglutide did not greatly affect mitochondrial function, although it may enhance sensitivity to ADP-stimulated respiration.

6.1 Establishing an appropriate semaglutide dose in a model of adolescent obesity

Semaglutide was originally developed for treating T2D due to its insulin-sensitizing effects.[89] T2D and obesity often present together, and in T2D patients who were also overweight and obese, modest weight loss was observed with semaglutide doses ranging from 0.5-1.0mg, administered via subcutaneous injection once per week.[89] This finding led to clinical trials whereby the viability of semaglutide was tested and the dosage optimized for inducing weight loss in obese subjects. The average demographic in the seminal clinical study testing semaglutide for weight loss was 46 (age cut off was 18 years of age), and this cohort was administered 2.4mg via subcutaneous injection at the same injection frequency.[12]

In rodent studies, dosing is variable and calculated according to bodyweight. Typical doses fall within the range surrounding 100μg/kg bodyweight.[90,86] We utilized a more conservative dose, for a number of reasons. Firstly, our collaborators from the Wright lab at University of British Columbia have validated this dose was effective in stimulating weight loss in adult mice, without any apparent gastrointestinal side (GI) effects common to this drug. Secondly, we erred on the side of caution. Where, to the best of our knowledge, there is no known appropriate dose for adolescents, many non-weight loss medications used in youth and adulthood scale the quantity down to adjust, in part, for smaller body size.

We also selected a dosing schedule of 5 days per week owing to the heightened metabolic rate in mice. Doses were administered over the course of an entire week so the drug would not be cleared from circulation. We selected a 5 day dosing schedule following consultation with our collaborators and a literature search. Frequency of administration of GLP-1 RAs in rodent studies ranges from every other day to twice per day.[90,92] We selected 5 days weekly as an intermediate between these two. There were never 2 consecutive days where injections were not administered.

We can be confident that our drug was delivered properly and was active when it entered circulation given the improvement glucose tolerance in all groups receiving 6 weeks of semaglutide that was not observed in the obese control group.

6.2 Elucidating the effect of semaglutide and protein intake on body composition

Use of absolute tissue weights versus in vivo body composition analysis

Body composition was measured utilizing multiple methods: physically weighing animals twice per week; collecting muscle, fat pad, and organ wet weights at endpoint; and by pre- and post-intervention microCT scans. Each measure has its limitations; hence all were utilized in an effort to minimize the margin of error and confidently present results. As such, the absolute weights, at times, diverged from what was observed with microCT analysis.

Prior to treatment initiation, all groups exhibited similar bodyweight, semaglutide-treated (SEMA) animals demonstrated significantly lower bodyweight at endpoint. Most individually weighed muscles, exhibited the same finding; as well as iWAT. Protein supplementation alongside semaglutide administration (PRO) demonstrated a preservative effect on total bodyweight and all affected muscle weights. Due to the nature of dissection, muscle weights could only be taken at the endpoint, so it was not possible to measure the change (Δ) in individual muscle wet weights from pre- to post-intervention.

Due to the non-invasive nature of microCT scanning, we were able to show changes from pre- to post-intervention and between groups in lean, adipose, and bone volume across multiple body compartments. Separation of lean, adipose, and bone tissue was performed by differentiating each tissue based on its density, with bone tissue being the most dense, absorbing x-rays to the greatest degree and appearing brightest on the CT scans, and adipose tissue being the least. Lean tissue is of intermediate density, but differentiating between skeletal muscle and non-skeletal muscle lean tissue volume was not possible with the analysis tools and software.

Thus, lean tissue encompassed skeletal muscle in addition to the abdominal organs, water, and connective tissue. The majority of lean tissue is still considered to be skeletal muscle, particularly in rodents,[93] but CT analysis of lean volume in each compartment cannot be solely attributed to skeletal muscle volume, which may account for some of the divergent results between absolute tissue weights and body composition analysis. Areas where these analysis techniques affirmed or diverged in their findings are summarized in **Table 2**.

Results of *in vivo* and *ex vivo* analysis matched	
	in vivo WB total volume vs bodyweight – pre-intervention
	in vivo WB total volume vs bodyweight – post-intervention
	in vivo ΔWB volume vs Δbodyweight
	in vivo visceral adipose volume vs *ex vivo* visceral fat pad weight – post-intervention

Results of *in vivo* and *ex vivo* analysis diverged	
	in vivo trunk subcutaneous adipose volume vs *ex vivo* subcutaneous fat pad weight – post-intervention
	in vivo crus lean volume vs *ex vivo* total hindlimb weight – post-intervention
Not comparable: results were not obtained with both techniques	
	in vivo pre-, post-, or Δbone volume – no *ex vivo* bone weights were obtained
	in vivo pre-, post-, or ΔWB lean, adipose, bone volume – no *ex vivo* weights were taken for collective WB weight of these individual tissues
	in vivo pre-, post-, or ΔUB whole, lean, adipose, bone volume – only the triceps muscle weight was obtained *ex vivo*
	in vivo pre-, post-, or Δtrunk total volume – it was not possible to obtain an *ex vivo* weight for this body region
	In vivo pre- or Δtrunk visceral and subcutaneous adipose volume – it was not possible to obtain an *ex vivo* weight for the fat pads at this timepoint

Table 2. Comparison of in vivo vs ex vivo body composition analysis. Divergent responses were observed between *in vivo* and *ex vivo* measures of body composition and are listed according to whether *in vivo* vs *ex vivo* measures agreed with one another, disagreed with one another, or were not comparable. Instances that were not comparable included all pre-intervention and Δ *in vivo* analysis (aside from WB total volume which could be compared against total bodyweight), and all bone volume analysis. UB = upper body. WB = whole body. Δ = change from baseline.

Use of semaglutide to prevent weight gain in a model of adolescent obesity

While mice reach sexual maturity at ~7 weeks of age, the onset of adulthood is later, at approximately the 12-week mark.[94] It is for this reason that animals of this age were selected, to gain an understanding of the effects of semaglutide treatment before and during the transition from adolescence to adulthood. In older models of diet-induced obesity (DIO), where a more robust phenotype has been allowed to develop, semaglutide treatment leads to substantial weight reduction in both rodent and human studies.[12,92] The effects of semaglutide treatment for obesity in a developing body remain under-explored, especially considering it is a vital time for musculoskeletal growth.

The prevalence of DIO at younger ages has increased significantly in recent decades.[3,5] Similarly to adult-onset obesity, adolescent obesity exhibits elevated risk for the development of several weight-related chronic diseases, although the length of time one remains obese appears to play a role in this, as these effects tend to not be as severe in youth.[5] Nevertheless, obese children and adolescents consistently grow up to be obese adults. Even when this is not the case, lean adults that were obese in their youth are still at higher risk for developing weight-related comorbidities compared to their lean counterparts who were never obese. Sarcopenic obesity can also present in childhood and adolescence, and thus the question becomes: is it more dangerous to experience

significant muscle atrophy in adulthood and later in life, or to never deposit sufficient muscle mass in the first place?

We demonstrated that, while semaglutide treatment did not induce weight loss during adolescence, it prevented weight gain, to a degree, evidenced by diminished bodyweight in the SEMA group at 15 weeks old. Interestingly, the combination of semaglutide and protein supplementation did not yield the same results. The effects of escalated adiposity during adolescence can span a lifetime, even when leanness is achieved later in life. Thus, preventing the induction of obesity in at all ages should be considered to instil the greatest improvements in morbidity and mortality. While the pathogenesis of obesity is relatively simple: a chronic increase in energy intake greater than energy expenditure, there are many different factors contributing to this imbalance, on both sizes of the equation.

Therefore, while not necessarily 'optimal', there may be a case for, in certain circumstances, the use of GLP-1 RAs to prevent obesity development in youth and adolescents who may be at greater risk for becoming obese. The progression of obesity is influenced by genetic, behavioural, and environmental factors that exacerbate this state of energy imbalance. While some of these may be considered preventable or adjustable, the unique vulnerability of childhood and adolescence brings into question the feasibility of lifestyle or environmental changes. As such, GLP-1 RAs may prevent lifelong negative consequences of adolescent obesity. Although we observed that semaglutide may be able to prevent weight gain in a younger cohort, our SEMA-group also exhibited reduced individual muscle size. Semaglutide did not hinder muscle deposition with PRO treatment, so pharmacological and non-pharmacological methods of obesity prevention and management may work better together when considering skeletal muscle health.

Muscle fiber analysis - Inconclusive

In an effort to explain the reduction in muscle mass with SEMA that was preventable with PRO treatment, we then performed fiber-type specific cross-sectional area (CSA) analysis on the soleus muscle. This muscle was selected because 1) it exhibited atrophy with SEMA that was rescued with PRO; 2) it has a low concentration of type IIb fibers, which are not present in human skeletal muscle tissue; and 3) it has a large proportion of type I fibers, permitting us to investigate if the obesity-associated type II fiber shift was prevented with SEMA.

There were no evidence of between-group differences in average or fiber-type-specific CSA, total fiber number, or a fiber-type shift present in the soleus muscle. This is contradictory to

what the absolute soleus weight showed. A few possible explanations for this could be that when individual muscles are harvested and weighed, they are not dried, and differences in water weight may make up the difference in absolute tissue mass that is not apparent in the histological analysis of CSA and fiber count. So, perhaps the SEMA-treated animals hold less water weight in their muscles than VEH- or PRO-treated animals. This would mean that fiber CSA and total fiber number is not different with SEMA, but that there may be an effect of SEMA on hydration.

Another potential reason we did not see a difference in CSA between groups comes down to the freezing of the samples. The small size of the soleus muscle makes it particularly prone to freeze fracturing, which can cause shrinkage or swelling of muscle fibers.[95] This was not considered at the time this tissue was selected for histological analysis. At some point between muscle dissection and imaging, significant freeze-fracturing occurred in the majority of the soleus samples, resulting in large 'holes' in a significant portion of the cross-sections. This can be visualized by looking at the representative images in **Figure 14**, where the VEH and SEMA images exhibit instances of freeze fracturing, but the PRO image does not. The freeze fracturing present in our soleus cross-sections may be hiding a reduction in CSA in SEMA-treated animals.

Semaglutide may enhance skeletal volume during growth in load-bearing bones

MicroCT analysis of the crus compartment, defined from the knee to ankle joint corresponding with the tibia and fibula bones, revealed that the obese control (VEH) group exhibited reduced relative bone volume following completion of the protocol, with SEMA treatment significantly improving relative bone volume, and both SEMA and PRO treatment exhibiting a greater positive Δbone volume % of the crus compartment. Both the WB and UB compartments exhibited greater, albeit non-significant, relative Δbone volume % as well.

The improvement in bone volume over 6 weeks is quite remarkable, given the slow turnover rate of bone. Much is unknown about the effects of semaglutide treatment in clinical populations for this very reason. The improved bone volume observed in this study may correspond with the younger age of our samples, as bone deposition occurs to the greatest degree during development in childhood and adolescence, and it is difficult, but not impossible, to improve bone density past the 2nd decade in humans.[96]

The improvement in the crus compartment that did not reach significance in the UB and WB compartments, could be specific to the load-bearing nature of this region of the body. Perhaps for semaglutide to induce its beneficial effect on bone, a resistance stimulus is required, and had

resistance training been incorporated in this model, we could have visualized WB improvements in bone volume with semaglutide treatment. Interestingly, osteogenic proliferation and differentiation is upregulated in bone precursor stem cells treated with semaglutide, and this appears to be through the Wnt signaling pathway. While investigation of bone metabolism and signaling pathways was not a direction of this study, this may, in part explain the improvement in weightbearing bone volume. Obese adolescents typically have greater BMD than their lean counterparts. However, obesity at this life stage is also associated with elevated fracture risk.[97] While increases in bone volume are not directly related to structural integrity, the possible upregulation of the Wnt signaling pathway could be an indicator that semaglutide treatment can elicit the deposition of higher quality bone tissue that is able to ameliorate the negative consequences of obesity on bone.

6.3 How does semaglutide treatment impact skeletal muscle contractile function?

While known to produce muscle atrophy, the effect of GLP-1 RAs on muscle function is less studied. Smaller muscles are known to produce less force, but whether GLP-1 RAs like semaglutide produce weakness independent of muscle atrophy, and if so, by what mechanism is, to the best of our knowledge, currently undiscovered.

We performed multiple measures of contractile function, with some intended to look at the longitudinal effect of semaglutide on submaximal muscle function, and others designed to grasp its effect on maximal contraction at endpoint.

Modest doses of semaglutide do not inhibit submaximal contractile function

Overall, there is no apparent effect of semaglutide treatment at any timepoint on voluntary or involuntary measures of submaximal contraction. We performed weekly voluntary assessments of muscle function by testing forelimb grip strength and timing maximal cage hang duration. These measures are useful because the voluntary nature of them replicates what we would expect to see if there was any negative effect of semaglutide treatment on say, activities of daily living (ADL). There is a behavioural, or willingness, component to these functional tests, whereby letting go of either instrument does not yield any negative repercussions.

The main reported side effects of GLP-1 RA use in humans are GI in nature, including nausea, vomiting, diarrhea, and general lethargy.[12] These side effects are typically transient, which is why we chose to utilize a longitudinal measure of voluntary muscle function. In theory, if animals were feeling these side effects at intervention commencement, performance would dip

following baseline pre-intervention testing, which would be restored later in the intervention as the effects subsided. This was not observed and may be in part due to the more modest dosage schedule we utilized. Our endpoint involuntary measures of submaximal function corroborated our longitudinal findings, with no detrimental effect of semaglutide on submaximal contractile function.

Could there be a dose-response relationship of semaglutide on maximal force output?

SEMA-treated animals exhibited impaired maximal force output of the tibialis anterior (TA) muscle, which was abolished in the PRO group. When maximal force output was normalized to muscle cross-sectional area, this finding was absent, although given the trend observed at frequencies of 100 and 120Hz, this may have to do with the dose administered. At this dosage, impaired maximal absolute force in SEMA-treated animals may be explained by the reduced overall size of these animals, but it cannot be explained by muscle-specific atrophy, as the TA muscle was one of the only hindlimb muscles that was unaltered by semaglutide treatment.

Another potential explanation for the weakened absolute force output of the TA may be explained by a shift towards a type I muscle phenotype. In rodents, the TA is primarily glycolytic, consisting mostly of type IIx and type IIb fibers.[98] However, when the force frequency curve was normalized relative to maximal force output, SEMA-treated animals exhibited a force frequency curve more representative of a type I muscle, such as the soleus. . Type I muscles exhibit a greater proportion of maximal force output at lower frequencies of stimulation than type II. This is related to calcium (Ca^{2+})-handling and the rate of Ca^{2+} uptake by SERCA in these fiber types. The rate of SERCA Ca^{2+} uptake is dependent on the isoform, with SERCA2a being the predominant isoform in type I fibers, and SERCA1a the predominant type II isoform.[99] SERCA1a takes up Ca^{2+} ions much more rapidly than SERCA 2a, which contributes to the higher relative force output at lower stimulation frequencies in type I muscle fibers, as slower Ca^{2+} reuptake allows actin and myosin crossbridge-formation to last longer. Thus, reductions in maximal force output of the TA muscle may be explained by a shift toward a more oxidative fiber type.

In an attempt to translate these findings to a humanized population, semaglutide likely does not impair muscle contractile function needed to power ADL in a DIO, but otherwise healthy, model of adolescence. If administered in larger doses or at an increased frequency,

semaglutide could have a negative effect on submaximal contractile function, as there was a trend toward a steeper reduction in force output early on during fatiguing contractions. Likewise, the effect of semaglutide on submaximal contraction in models of aging or myopathy cannot be extrapolated from this data.

The reduction in maximal force output from semaglutide treatment may exhibit a dose-response relationship. While only absolute maximal force was impaired at this dosing schedule, the trend toward a reduction in specific force may become apparent in the presence of a more intense prescription. The TA is a weightbearing muscle important for locomotion and balance, and impaired maximal function in this adolescent model could relate to a negative performance effect of semaglutide administration, as maximal force output is more relevant to performance-based metrics.

6.4 How does semaglutide treatment impact skeletal muscle mitochondrial function?

Mitochondrial oxidative phosphorylation is a vital, life-necessitating process of energy generation; and the large density of mitochondria present in skeletal muscle corresponds with the large metabolic demands of this tissue. Thus, impairments in mitochondrial function can have stark consequences in skeletal muscle. Obese skeletal muscle exhibits reduced mitochondrial content per unit area, and upstream dysfunctions in both glucose and lipid metabolism contribute to impairments in substrate oxidation and elevated reactive oxygen species (ROS) generation.

While less is known regarding how obesity can affect skeletal muscle mitochondrial health in a younger cohort, clinical studies indicate that mitochondrial respiratory complex enzyme activity is unchanged in obese compared to lean children.[100] Thus, while we did not see an effect of semaglutide on total mitochondrial oxygen consumption or mH_2O_2 emission, it may be that these parameters are not compromised at this age, and that semaglutide could modulate mitochondrial function when a pronounced impairment is present.

We did observe enhanced sensitivity to ADP-stimulated respiration in SEMA- but not PRO-treated animals but aside from this, administration of semaglutide, with or without dietary modification, did not improve or worsen CHO or FA substrate oxidation or mH_2O_2 emission. Inclusion of a non-WD chow control would have been useful to assess whether in this model, at this timepoint, impairments in mitochondrial oxidative phosphorylation and/or elevated mH_2O_2

emission was occurring. But ultimately, what we observed was either no impact or a minor benefit of semaglutide on mitochondrial function.

CONCLUSIONS & FUTURE DIRECTIONS

Semaglutide is effective at stimulating weight loss and reducing the severity of weight-related comorbidities in overweight and obese adults. However, the potential for significantly reduced musculoskeletal quality and quantity makes the use of this drug in a clinical population optimizable for healthier long-term, sustainable weight loss. Semaglutide has begun to be used to treat obesity in childhood and adolescence, and the effects this drug may have during a vital time of growth and development are of concern. Protein is a macronutrient with anabolic properties that has been effective in supporting lean mass maintenance during conditions such as weight loss and bed rest. In this model, we showed that semaglutide treatment compared to no intervention leads to smaller body size, lower muscle mass, and reduced maximal force output. All three of these factors were able to be prevented by supplementing the diet with a high-quality protein source, such as whey and casein, in conjunction with semaglutide treatment.

We set out to find a dosing schedule that could minimize the negative outcomes of semaglutide administration while preserving meaningful reductions in adiposity, administering semaglutide at 40μg/kg 5 days per week. A conservative approach was taken in using a pharmacological weight-loss drug in an adolescent cohort. With this dose of semaglutide, bodyweight at 15 weeks of age was reduced. This dosing schedule did not negatively impact voluntary measures of muscle function, which can provide an indirect idea of feelings of lethargy. We also observed a non-significant reduction in specific force and greater initial reduction in force output during fatiguing contractions and significantly reduced maximal force. We believe that a larger dose or more frequent dosing schedule may have affected these parameters to a greater extent.

As such, the dose of semaglutide may yet need to be optimized for an adolescent model of obesity if the intent is to maximize adipose reductions and minimize muscle weakness. In the future, this could be achieved by establishing if a dose-response relationship is present between semaglutide and muscle contractile function. Once this has been elucidated and optimized for this age-group, use of other muscle mass- and strength-promoting interventions such as resistance

exercise or other nutraceutical supplementation in conjunction with, or independent of, protein supplementation may elicit high-quality weight loss in this age-group.

In the future, an investigation should take place to explain what is occurring at the molecular level, specifically with respect to muscle protein turnover. Investigating gene expression markers of muscle protein synthesis and breakdown will clarify what is regulating the atrophy witnessed across the majority of hindlimb muscles. Additionally, measuring BMD and markers of bone turnover will provide a better idea of what may be promoting the increased bone volume observed in the hindlimb region. Finally, although there was generally no effect of semaglutide treatment on measures of mitochondrial function, by measuring ETC protein content and then normalizing oxygen consumption to it, it will be possible to see if a difference in protein content could be masking alterations in mitochondrial oxygen consumption.

A limitation of this study was not including a lean control group. Obesity is associated with greater absolute muscle mass and force production, but lower muscle size and function when normalized to bodyweight. So any effects observed from semaglutide in this study can only be compared to the obese phenotype, and not to a healthy control. In the future, considering these findings against a lean cohort of males would further strengthen the current findings.

REFERENCES

1. Engin, A. The Definition and Prevalence of Obesity and Metabolic Syndrome. in *Obesity and Lipotoxicity* (eds. Engin, A. B. & Engin, A.) vol. 960 1–17 (Springer International Publishing, Cham, 2017).
2. Tremmel, M., Gerdtham, U.-G., Nilsson, P. & Saha, S. Economic Burden of Obesity: A Systematic Literature Review. *Int. J. Environ. Res. Public. Health* **14**, 435 (2017).
3. Wu, A. J. *et al.* Association of Changes in Obesity Prevalence With the COVID-19 Pandemic in Youth in Massachusetts. *JAMA Pediatr.* **176**, 198 (2022).
4. McTigue, K. M., Garrett, J. M. & Popkin, B. M. The Natural History of the Development of Obesity in a Cohort of Young U.S. Adults between 1981 and 1998. *Ann. Intern. Med.* **136**, 857 (2002).
5. Kiess, W. *et al.* Physiology of obesity in childhood and adolescence. *Curr. Paediatr.* **16**, 123–131 (2006).
6. Wannamethee, S. G. & Atkins, J. L. Muscle loss and obesity: the health implications of sarcopenia and sarcopenic obesity. *Proc. Nutr. Soc.* **74**, 405–412 (2015).
7. Chen, X. *et al.* Mitochondrial dysfunction: roles in skeletal muscle atrophy. *J. Transl. Med.* **21**, 503 (2023).
8. Schiaffino, S., Dyar, K. A., Ciciliot, S., Blaauw, B. & Sandri, M. Mechanisms regulating skeletal muscle growth and atrophy. *FEBS J.* **280**, 4294–4314 (2013).
9. Cao, J. J. Effects of obesity on bone metabolism. *J. Orthop. Surg.* **6**, 30 (2011).
10. Kim, D. *et al.* Effects of Once-Weekly Dosing of a Long-Acting Release Formulation of Exenatide on Glucose Control and Body Weight in Subjects With Type 2 Diabetes. *Diabetes Care* **30**, 1487–1493 (2007).

11. Hartz, A. Relationship of obesity to diabetes: Influence of obesity level and body fat distribution,. *Prev. Med.* **12**, 351–357 (1983).

12. Wilding, J. P. H. *et al.* Once-Weekly Semaglutide in Adults with Overweight or Obesity. *N. Engl. J. Med.* **384**, 989–1002 (2021).

13. Blundell, J. *et al.* Effects of once-weekly semaglutide on appetite, energy intake, control of eating, food preference and body weight in subjects with obesity. *Diabetes Obes. Metab.* **19**, 1242–1251 (2017).

14. Santanasto, A. J. *et al.* Impact of Weight Loss on Physical Function with Changes in Strength, Muscle Mass, and Muscle Fat Infiltration in Overweight to Moderately Obese Older Adults: A Randomized Clinical Trial. *J. Obes.* **2011**, 1–10 (2011).

15. Bikou, A., Dermiki-Gkana, F., Penteris, M., Constantinides, T. K. & Kontogiorgis, C. A systematic review of the effect of semaglutide on lean mass: insights from clinical trials. *Expert Opin. Pharmacother.* **25**, 611–619 (2024).

16. Chaston, T. B., Dixon, J. B. & O'Brien, P. E. Changes in fat-free mass during significant weight loss: a systematic review. *Int. J. Obes.* **31**, 743–750 (2007).

17. Thiebaud, D. *et al.* The Effect of Graded Doses of Insulin on Total Glucose Uptake, Glucose Oxidation, and Glucose Storage in Man. *Diabetes* **31**, 957–963 (1982).

18. Dirks, M. L. *et al.* One Week of Bed Rest Leads to Substantial Muscle Atrophy and Induces Whole-Body Insulin Resistance in the Absence of Skeletal Muscle Lipid Accumulation. *Diabetes* **65**, 2862–2875 (2016).

19. Zurlo, F., Larson, K., Bogardus, C. & Ravussin, E. Skeletal muscle metabolism is a major determinant of resting energy expenditure. *J. Clin. Invest.* **86**, 1423–1427 (1990).

20. Marso, S. P. *et al.* Semaglutide and Cardiovascular Outcomes in Patients with Type 2 Diabetes. *N. Engl. J. Med.* **375**, 1834–1844 (2016).

21. Yang, X. *et al.* The diabetes drug semaglutide reduces infarct size, inflammation, and apoptosis, and normalizes neurogenesis in a rat model of stroke. *Neuropharmacology* **158**, 107748 (2019).

22. Zheng, Z. *et al.* Glucagon-like peptide-1 receptor: mechanisms and advances in therapy. *Signal Transduct. Target. Ther.* **9**, 234 (2024).

23. Nauck, M. A. *et al.* Glucagon-like peptide 1 inhibition of gastric emptying outweighs its insulinotropic effects in healthy humans. *Am. J. Physiol.* **273**, E981-988 (1997).

24. Wren, A. M. & Bloom, S. R. Gut Hormones and Appetite Control. *Gastroenterology* **132**, 2116–2130 (2007).

25. Yu, M. *et al.* Battle of GLP-1 delivery technologies. *Adv. Drug Deliv. Rev.* **130**, 113–130 (2018).

26. Haase, C. L. *et al.* Weight loss and risk reduction of obesity-related outcomes in 0.5 million people: evidence from a UK primary care database. *Int. J. Obes.* **45**, 1249–1258 (2021).

27. Yanek, L. R. *et al.* Lean Mass and Fat Mass as Contributors to Physical Fitness in an Overweight and Obese African American Population. *Ethn. Dis.* **25**, 214–219 (2015).

28. Powers, S. K., Lynch, G. S., Murphy, K. T., Reid, M. B. & Zijdewind, I. Disease-Induced Skeletal Muscle Atrophy and Fatigue. *Med. Sci. Sports Exerc.* **48**, 2307–2319 (2016).

29. Hughes, V. A., Frontera, W. R., Roubenoff, R., Evans, W. J. & Singh, M. A. F. Longitudinal changes in body composition in older men and women: role of body weight change and physical activity. *Am. J. Clin. Nutr.* **76**, 473–481 (2002).

30. Cantini, G., Mannucci, E. & Luconi, M. Perspectives in GLP-1 Research: New Targets, New Receptors. *Trends Endocrinol. Metab.* **27**, 427–438 (2016).

31. Campos, R. V., Lee, Y. C. & Drucker, D. J. Divergent tissue-specific and developmental expression of receptors for glucagon and glucagon-like peptide-1 in the mouse. *Endocrinology* **134**, 2156–2164 (1994).

32. Herrou, J. *et al.* Narrative Review of Effects of Glucagon-Like Peptide-1 Receptor Agonists on Bone Health in People Living with Obesity. *Calcif. Tissue Int.* **114**, 86–97 (2023).

33. Johnson, K. C. *et al.* The long-term effect of intentional weight loss on changes in bone mineral density in persons with type 2 diabetes: results from the Look AHEAD randomized trial. *Arch. Osteoporos.* **18**, 97 (2023).

34. Josse, A. R., Atkinson, S. A., Tarnopolsky, M. A. & Phillips, S. M. Increased consumption of dairy foods and protein during diet- and exercise-induced weight loss promotes fat mass loss and lean mass gain in overweight and obese premenopausal women. *J. Nutr.* **141**, 1626–1634 (2011).

35. Jensen, M. D. *et al.* 2013 AHA/ACC/TOS Guideline for the Management of Overweight and Obesity in Adults: A Report of the American College of Cardiology/American Heart Association Task Force on Practice Guidelines and The Obesity Society. *Circulation* **129**, (2014).

36. Wing, R. R. & Phelan, S. Long-term weight loss maintenance. *Am. J. Clin. Nutr.* **82**, 222S-225S (2005).

37. McGuire, M., Wing, R. & Hill, J. The prevalence of weight loss maintenance among American adults. *Int. J. Obes.* **23**, 1314–1319 (1999).

38. Greenway, F. L. Physiological adaptations to weight loss and factors favouring weight regain. *Int. J. Obes.* **39**, 1188–1196 (2015).

39. Moon, J. & Koh, G. Clinical Evidence and Mechanisms of High-Protein Diet-Induced Weight Loss. *J. Obes. Metab. Syndr.* **29**, 166–173 (2020).

40. Wirunsawanya, K., Upala, S., Jaruvongvanich, V. & Sanguankeo, A. Whey Protein Supplementation Improves Body Composition and Cardiovascular Risk Factors in Overweight and Obese Patients: A Systematic Review and Meta-Analysis. *J. Am. Coll. Nutr.* **37**, 60–70 (2018).

41. Devries, M. C. & Phillips, S. M. Supplemental protein in support of muscle mass and health: advantage whey. *J. Food Sci.* **80 Suppl 1**, A8–A15 (2015).

42. Hoffer, L. J. Human Protein and Amino Acid Requirements. *J. Parenter. Enter. Nutr.* **40**, 460–474 (2016).

43. Rieu, I. *et al.* Increased availability of leucine with leucine-rich whey proteins improves postprandial muscle protein synthesis in aging rats. *Nutrition* **23**, 323–331 (2007).

44. Tang, J. E., Moore, D. R., Kujbida, G. W., Tarnopolsky, M. A. & Phillips, S. M. Ingestion of whey hydrolysate, casein, or soy protein isolate: effects on mixed muscle protein synthesis at rest and following resistance exercise in young men. *J. Appl. Physiol.* **107**, 987–992 (2009).

45. Kerasioti, E. *et al.* Antioxidant effects of whey protein on muscle C2C12 cells. *Food Chem.* **155**, 271–278 (2014).

46. Forman, H. J., Zhang, H. & Rinna, A. Glutathione: overview of its protective roles, measurement, and biosynthesis. *Mol. Aspects Med.* **30**, 1–12 (2009).

47. Landi, N., Ragucci, S. & Di Maro, A. Amino Acid Composition of Milk from Cow, Sheep and Goat Raised in Ailano and Valle Agricola, Two Localities of 'Alto Casertano' (Campania Region). *Foods Basel Switz.* **10**, 2431 (2021).

48. Boirie, Y. *et al.* Slow and fast dietary proteins differently modulate postprandial protein accretion. *Proc. Natl. Acad. Sci.* **94**, 14930–14935 (1997).

49. Pasiakos, S. M., McLellan, T. M. & Lieberman, H. R. The Effects of Protein Supplements on Muscle Mass, Strength, and Aerobic and Anaerobic Power in Healthy Adults: A Systematic Review. *Sports Med.* **45**, 111–131 (2015).

50. Ferguson-Stegall, L. *et al.* Aerobic Exercise Training Adaptations Are Increased by Postexercise Carbohydrate-Protein Supplementation. *J. Nutr. Metab.* **2011**, 1–11 (2011).

51. Shams-White, M. M. *et al.* Dietary protein and bone health: a systematic review and meta-analysis from the National Osteoporosis Foundation,. *Am. J. Clin. Nutr.* **105**, 1528–1543 (2017).

52. Katzmarzyk, P. T. Prevalence of class I, II and III obesity in Canada. *Can. Med. Assoc. J.* **174**, 156–157 (2006).

53. Van Pelt, R. E., Evans, E. M., Schechtman, K. B., Ehsani, A. A. & Kohrt, W. M. Contributions of total and regional fat mass to risk for cardiovascular disease in older women. *Am. J. Physiol.-Endocrinol. Metab.* **282**, E1023–E1028 (2002).

54. Kershaw, E. E. & Flier, J. S. Adipose Tissue as an Endocrine Organ. *J. Clin. Endocrinol. Metab.* **89**, 2548–2556 (2004).

55. Rexrode, K. M., Pradhan, A., Manson, J. E., Buring, J. E. & Ridker, P. M. Relationship of total and abdominal adiposity with CRP and IL-6 in women. *Ann. Epidemiol.* **13**, 674–682 (2003).

56. Giovannini, S. *et al.* Interleukin-6, C-Reactive Protein, and Tumor Necrosis Factor-Alpha as Predictors of Mortality in Frail, Community-Living Elderly Individuals. *J. Am. Geriatr. Soc.* **59**, 1679–1685 (2011).

57. Tallis, J., James, R. S. & Seebacher, F. The effects of obesity on skeletal muscle contractile function. *J. Exp. Biol.* **221**, jeb163840 (2018).

58. Frontera, W. R. & Ochala, J. Skeletal Muscle: A Brief Review of Structure and Function. *Calcif. Tissue Int.* **96**, 183–195 (2015).

59. Andersen, A., Lund, A., Knop, F. K. & Vilsbøll, T. Glucagon-like peptide 1 in health and disease. *Nat. Rev. Endocrinol.* **14**, 390–403 (2018).

60. Srikanthan, P. & Karlamangla, A. S. Muscle Mass Index As a Predictor of Longevity in Older Adults. *Am. J. Med.* **127**, 547–553 (2014).

61. Hulens, M. *et al.* Study of differences in peripheral muscle strength of lean versus obese women: an allometric approach. *Int. J. Obes.* **25**, 676–681 (2001).

62. Goodpaster, B. H., Theriault, R., Watkins, S. C. & Kelley, D. E. Intramuscular lipid content is increased in obesity and decreased by weight loss. *Metabolism* **49**, 467–472 (2000).

63. Khan, I. M. *et al.* Intermuscular and perimuscular fat expansion in obesity correlates with skeletal muscle T cell and macrophage infiltration and insulin resistance. *Int. J. Obes.* **39**, 1607–1618 (2015).

64. DeNies, M. S. *et al.* Diet-induced obesity alters skeletal muscle fiber types of male but not female mice. *Physiol. Rep.* **2**, e00204 (2014).

65. Schiaffino, S. & Reggiani, C. Fiber Types in Mammalian Skeletal Muscles. *Physiol. Rev.* **91**, 1447–1531 (2011).

66. Eshima, H. Influence of Obesity and Type 2 Diabetes on Calcium Handling by Skeletal Muscle: Spotlight on the Sarcoplasmic Reticulum and Mitochondria. *Front. Physiol.* **12**, 758316 (2021).

67. Tiidus, P. M., Tupling, A. R. & Houston, M. E. Carbohydrate and related metabolism. in *Biochemistry Primer for Exercise Science* 153–186.

68. Tiidus, P. M., Tupling, A. R. & Houston, M. E. Energy systems and bioenergetics. in *Biochemistry Primer for Exercise Science* 77–102.

69. Tiidus, P. M., Tupling, A. R. & Houston, M. E. Lipid metabolism. in *Biochemistry Primer for Exercise Science* 205–240.

70. Tiidus, P. M., Tupling, A. R. & Houston, M. E. Oxidative phosphorylation. in *Biochemistry Primer for Exercise Science* 107–139.

71. Friedman, J. E., Caro, JoséF., Pories, W. J., Azevedo, J. L. & Dohm, G. L. Glucose metabolism in incubated human muscle: Effect of obesity and non-insulin-dependent diabetes mellitus. *Metabolism* **43**, 1047–1054 (1994).

72. Kelley, D. E., Goodpaster, B., Wing, R. R. & Simoneau, J.-A. Skeletal muscle fatty acid metabolism in association with insulin resistance, obesity, and weight loss. *Am. J. Physiol.-Endocrinol. Metab.* **277**, E1130–E1141 (1999).

73. Abdul-Ghani, M. A. & DeFronzo, R. A. Pathogenesis of Insulin Resistance in Skeletal Muscle. *J. Biomed. Biotechnol.* **2010**, 1–19 (2010).

74. Draznin, B. Molecular Mechanisms of Insulin Resistance: Serine Phosphorylation of Insulin Receptor Substrate-1 and Increased Expression of p85α. *Diabetes* **55**, 2392–2397 (2006).

75. Bandyopadhyay, G. K., Yu, J. G., Ofrecio, J. & Olefsky, J. M. Increased Malonyl-CoA Levels in Muscle From Obese and Type 2 Diabetic Subjects Lead to Decreased Fatty Acid

Oxidation and Increased Lipogenesis; Thiazolidinedione Treatment Reverses These Defects. *Diabetes* **55**, 2277–2285 (2006).

76. Holloway, G. P., Bonen, A. & Spriet, L. L. Regulation of skeletal muscle mitochondrial fatty acid metabolism in lean and obese individuals. *Am. J. Clin. Nutr.* **89**, 455S-462S (2009).

77. Van Loon, L. J. C. & Goodpaster, B. H. Increased intramuscular lipid storage in the insulin-resistant and endurance-trained state. *Pflüg. Arch.* **451**, 606–616 (2006).

78. Pileggi, C. A., Parmar, G. & Harper, M. The lifecycle of skeletal muscle mitochondria in obesity. *Obes. Rev.* **22**, e13164 (2021).

79. Bakkman, L. *et al.* Reduced Respiratory Capacity in Muscle Mitochondria of Obese Subjects. *Obes. Facts* **3**, 1–1 (2010).

80. Brunetta, H. S. *et al.* Decrement in resting and insulin-stimulated soleus muscle mitochondrial respiration is an early event in diet-induced obesity in mice. *Exp. Physiol.* **104**, 306–321 (2019).

81. Bonen, A. *et al.* Triacylglycerol accumulation in human obesity and type 2 diabetes is associated with increased rates of skeletal muscle fatty acid transport and increased sarcolemmal FAT/CD36. *FASEB J.* **18**, 1144–1146 (2004).

82. Barbieri, E. & Sestili, P. Reactive Oxygen Species in Skeletal Muscle Signaling. *J. Signal Transduct.* **2012**, 1–17 (2012).

83. Espinosa, A. *et al.* Insulin-Dependent H2O2 Production Is Higher in Muscle Fibers of Mice Fed with a High-Fat Diet. *Int. J. Mol. Sci.* **14**, 15740–15754 (2013).

84. Fabre, O. *et al.* Defects in TLR3 expression and RNase L activation lead to decreased MnSOD expression and insulin resistance in muscle cells of obese people. *Cell Death Dis.* **5**, e1136–e1136 (2014).

85. Anderson, E. J. *et al.* Mitochondrial H2O2 emission and cellular redox state link excess fat intake to insulin resistance in both rodents and humans. *J. Clin. Invest.* **119**, 573–581 (2009).

86. Hamrick, M. W., Pennington, C., Newton, D., Xie, D. & Isales, C. Leptin deficiency produces contrasting phenotypes in bones of the limb and spine. *Bone* **34**, 376–383 (2004).

87. Choi, B. S.-Y. *et al.* Housing matters: Experimental variables shaping metabolism in obese mice. *Mol. Metab.* **98**, 102190 (2025).

88. Albuquerque, D., Nóbrega, C., Manco, L. & Padez, C. The contribution of genetics and environment to obesity. *Br. Med. Bull.* **123**, 159–173 (2017).

89. Sorli, C. *et al.* Efficacy and safety of once-weekly semaglutide monotherapy versus placebo in patients with type 2 diabetes (SUSTAIN 1): a double-blind, randomised, placebo-controlled, parallel-group, multinational, multicentre phase 3a trial. *Lancet Diabetes Endocrinol.* **5**, 251–260 (2017).

90. Zhang, L., Zhang, L., Li, L. & Hölscher, C. Semaglutide is Neuroprotective and Reduces α-Synuclein Levels in the Chronic MPTP Mouse Model of Parkinson's Disease. *J. Park. Dis.* **9**, 157–171 (2019).

91. Pan, X., Yue, L., Ban, J., Ren, L. & Chen, S. Effects of Semaglutide on Cardiac Protein Expression and Cardiac Function of Obese Mice. *J. Inflamm. Res.* **15**, 6409–6425 (2022).

92. Gabery, S. *et al.* Semaglutide lowers body weight in rodents via distributed neural pathways. *JCI Insight* **5**, e133429 (2020).

93. Farhang-Sardroodi, S. & Wilkie, K. P. Mathematical Model of Muscle Wasting in Cancer Cachexia. *J. Clin. Med.* **9**, 2029 (2020).

94. Shoji, H., Takao, K., Hattori, S. & Miyakawa, T. Age-related changes in behavior in C57BL/6J mice from young adulthood to middle age. *Mol. Brain* **9**, 11 (2016).

95.Ghag, N., Tam, J., Anderson, R. & Cheema, N. Cryopreservation Method for Preventing Freeze-Fracture of Small Muscle Samples. *BIO-Protoc.* **15**, (2025).

96.Rizzoli, R. & Bonjour, J.-P. Determinants of Peak Bone Mass and Mechanisms of Bone Loss: *Osteoporos. Int.* **9**, S17–S23 (1999).

97.Van Leeuwen, J., Koes, B. W., Paulis, W. D. & Van Middelkoop, M. Differences in bone mineral density between normal-weight children and children with overweight and obesity: a systematic review and meta-analysis. *Obes. Rev.* **18**, 526–546 (2017).

98.Augusto, V., Padovani, C. R. & Campos, G. E. R. Skeletal muscle fiber types in C57Bl6J mice. *J. Morphol. Sci.* **21**, 89–94 (2004).

99.Lamboley, C. R., Murphy, R. M., McKenna, M. J. & Lamb, G. D. Sarcoplasmic reticulum Ca^{2+} uptake and leak properties, and SERCA isoform expression, in type I and type II fibres of human skeletal muscle. *J. Physiol.* **592**, 1381–1395 (2014).

100.Cree-Green, M. *et al.* Insulin Resistance in Youth Without Diabetes Is Not Related to Muscle Mitochondrial Dysfunction. *J. Clin. Endocrinol. Metab.* **102**, 1652–1660 (2017).

SUPPLEMENTARY FIGURES

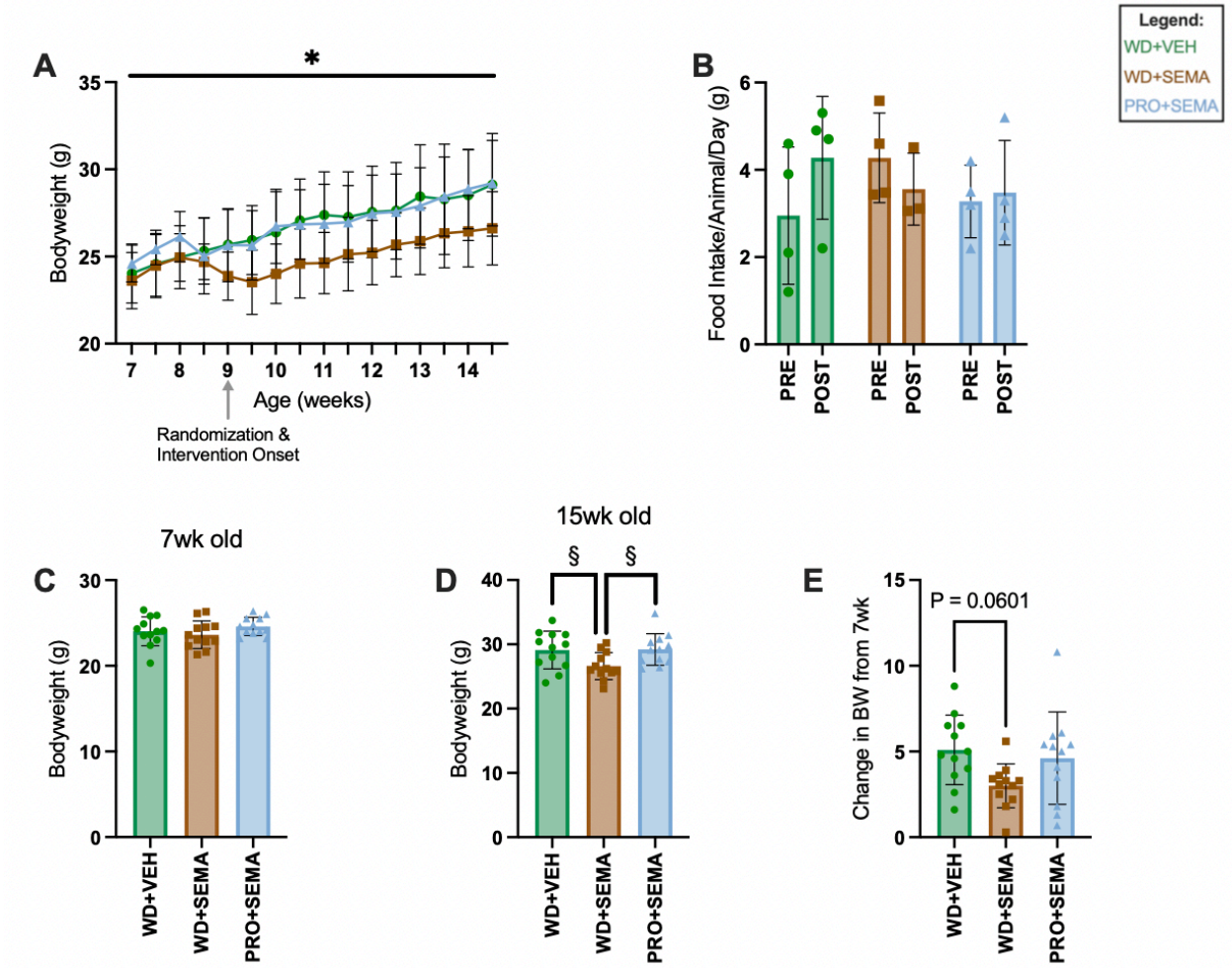

SFigure 1. Bodyweight at "pre" and "post" intervention timepoints. A) Whole-body weight was taken 2x/week (n=12). **B)** Approximate food intake pre- and post-intervention. All diets energetically provided 4.6kcal/g (n=4). **C)** Absolute bodyweight at 7wk old **D)** Absolute bodyweight at 15wk old (n=12). **E)** Change in bodyweight from baseline. Results represent mean ± SD. A two-way ANOVA was used to determine the difference between WD+VEH vs WD+SEMA vs PRO+SEMA for **A**. A one-way ANOVA was used to determine the difference between WD+VEH vs WD+SEMA vs PRO+SEMA for **B, C,** & **D**. When a significant interaction was present, post-hoc analysis was performed using the Benjamini, Krieger, and Yekutieli test. *P<0.05 main effect of time. §P<0.05.

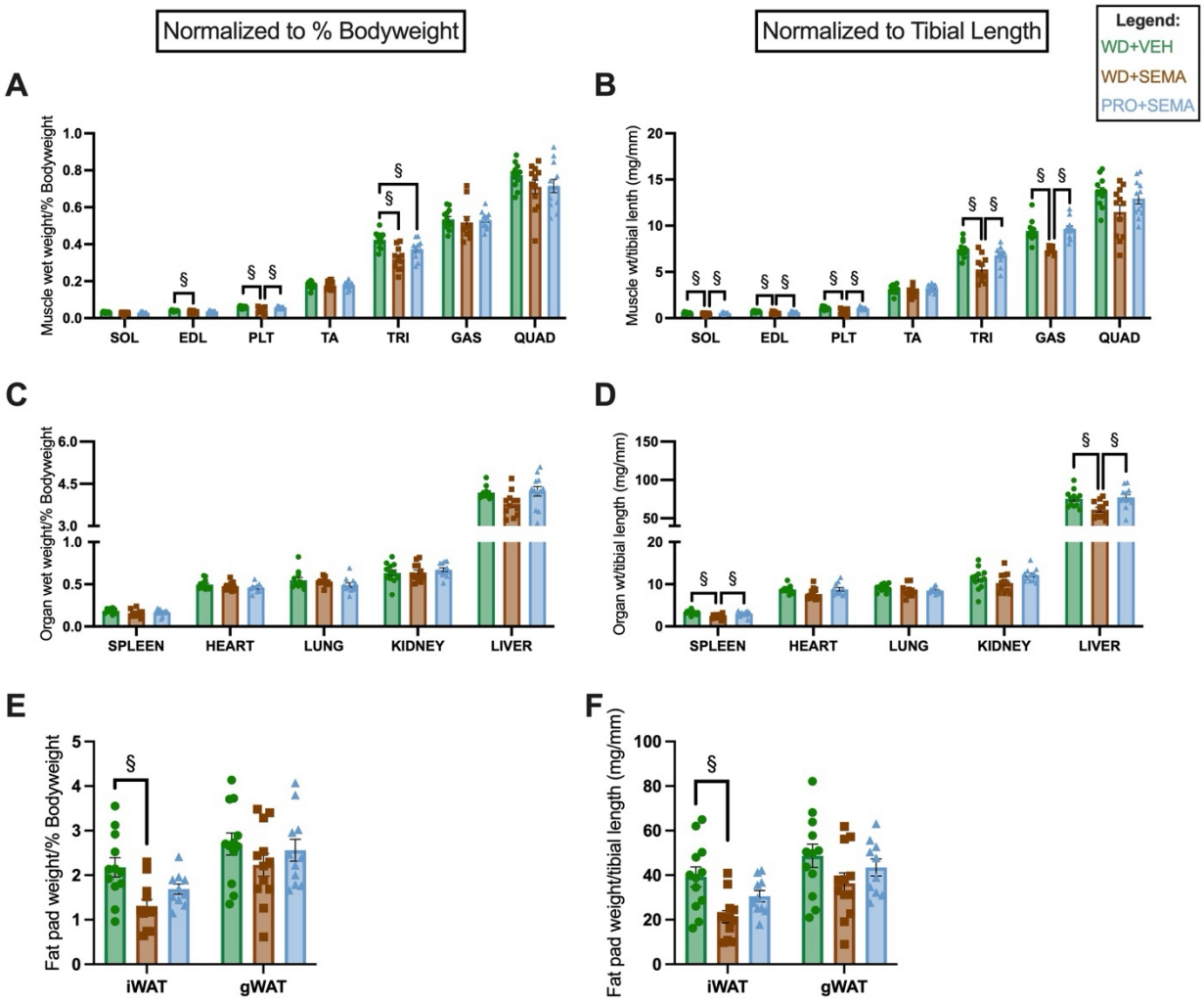

SFigure 2. Body morphometrics normalized to bodyweight and tibial length. A) & **B)** Hind- and fore-limb muscles (n-11-12). **C)** & **D)** Abdominal organ weights (n=11-12). **E)** & **F)** Subcutaneous (iWAT) and visceral (gWAT) fat pads (n=9-10). Results represent mean± SD. A one-way ANOVA was used to determine the difference between WD+VEH vs WD+SEMA vs PRO+SEMA. When a significant interaction was present, post-hoc analysis was performed using Benjamini, Krieger, and Yekutieli test. $^{§}P<0.05$.

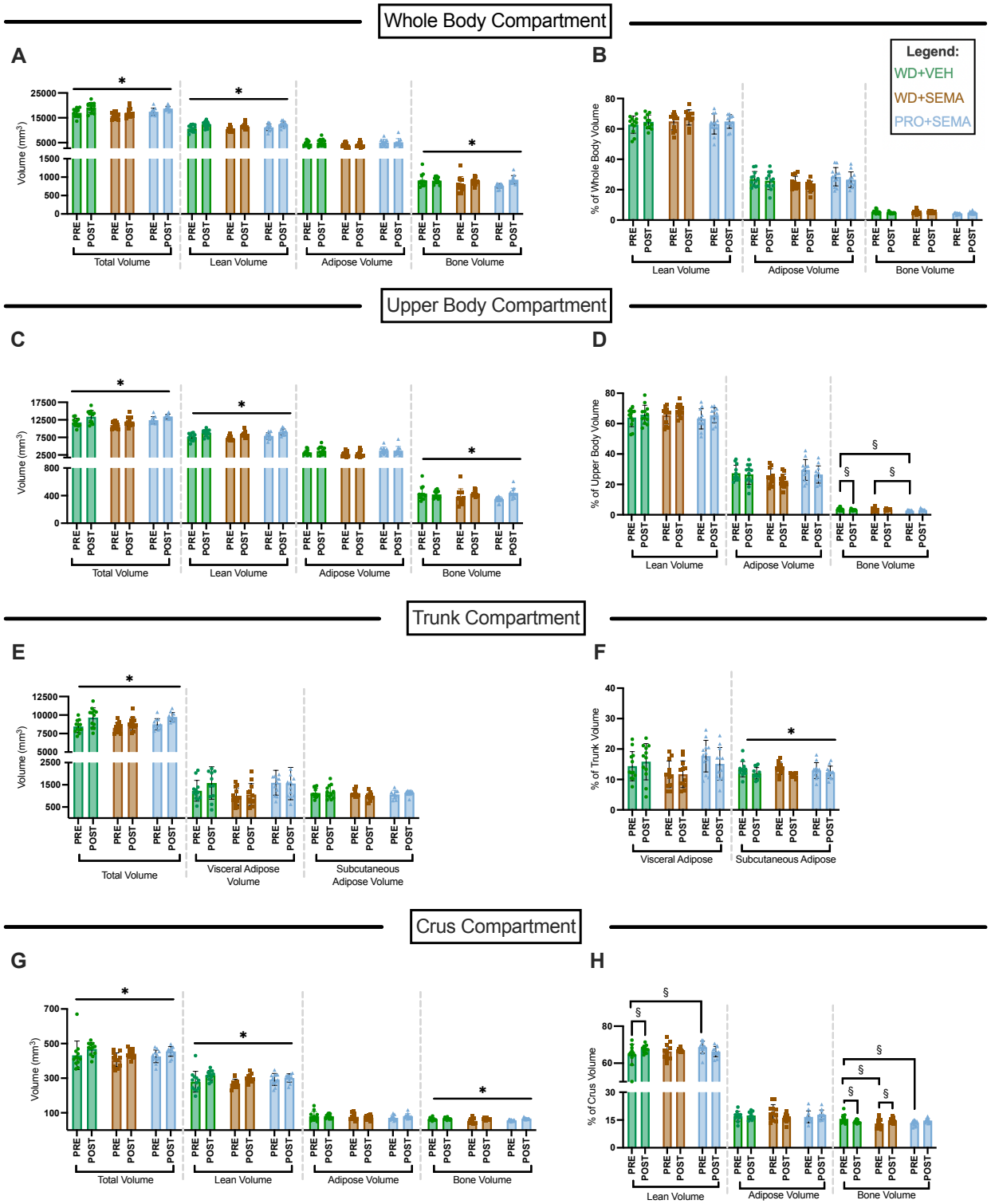

SFigure 3. Comparison of pre- vs post- intervention changes in body composition. A) Whole-body (WB) compartment total, lean, adipose, and bone volumes (n=11-12). **B)** Proportion of lean, adipose, and bone volume comprising the WB compartment (n=11-12). **C)** Upper-body (UB) compartment total, lean, adipose, and bone volumes (n=11-12). **D)** Proportion of lean, adipose, and bone volume comprising the UB compartment (n=11-12). **E)** Trunk compartment total, visceral adipose, and subcutaneous adipose volumes (n=10-12). **F)** Proportion of visceral and subcutaneous adipose making up total trunk adipose volume (n=10-12). **G)** Crus compartment total, lean, adipose,

and bone volumes (n=11-12). **H)** Proportion of lean, adipose, and bone volume comprising the crus compartment (n=11-12). Results represent mean ± SD. A two-way ANOVA was used to determine WD+VEH vs WD+SEMA vs PRO+SEMA. When a significant interaction was present, post-hoc analysis was performed using Benjamini, Krieger, and Yekutieli test. *P<0.05 = main effect of time. §P<0.05.

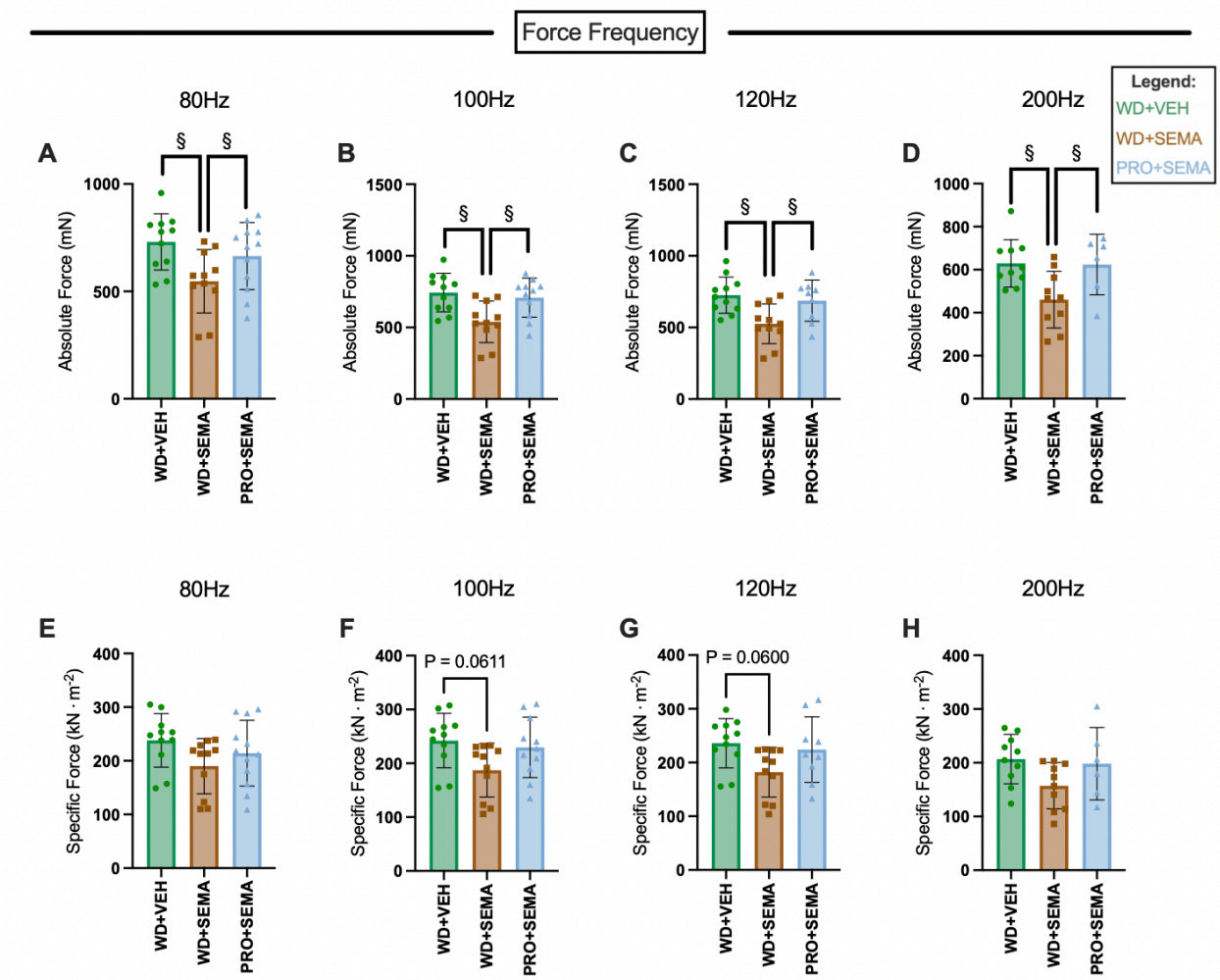

SFigure 4. Sub-analysis of individual force frequency contractions. A–D) Final 4 contractions (80, 100, 120, & 200Hz respectively) of force frequency (FF) protocol (n=10-12). **E-H)** Final 4 contractions of FF protocol, calculated by dividing the absolute force by muscle cross-sectional area (n-10-12). Results represent mean ± SD. A one-way ANOVA was used to determine WD+VEH vs WD+SEMA vs PRO+SEMA. When a significant interaction was present, post-hoc analysis was performed using Benjamini, Krieger, and Yekutieli test. $^{§}P<0.05$.

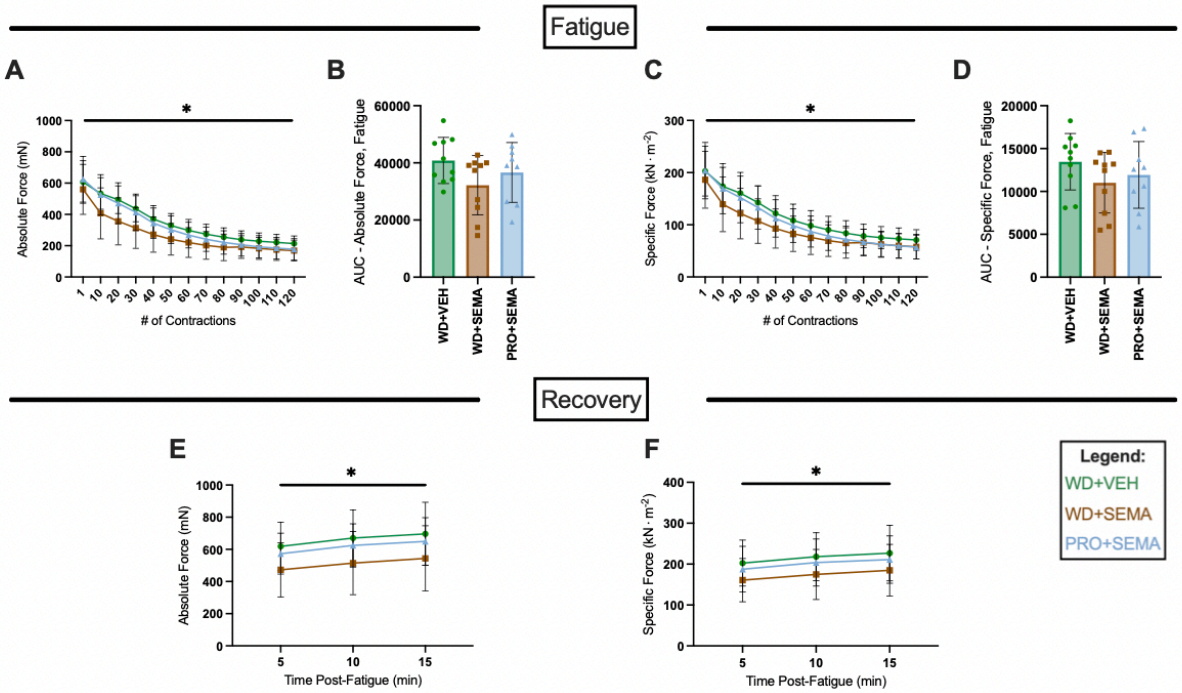

SFigure 5. Involuntary submaximal measures of muscle contraction. Absolute **(A)** and specific **(C)** muscle fatiguability. Area under the curve of absolute **(B)** and specific **(D)** fatigue protocol force output (n=9-10). Absolute **(E)** and specific **(F)** force output during recovery following fatigue (n=9-10). Results represent mean ± SD. A two-way ANOVA was used to determine WD+VEH vs WD+SEMA vs PRO+SEMA for **A), C), E),** & **F)**. A one-way ANOVA was used to determine WD+VEH vs WD+SEMA vs PRO+SEMA for **B)** & **D)**. *P<0.05 main effect of time.

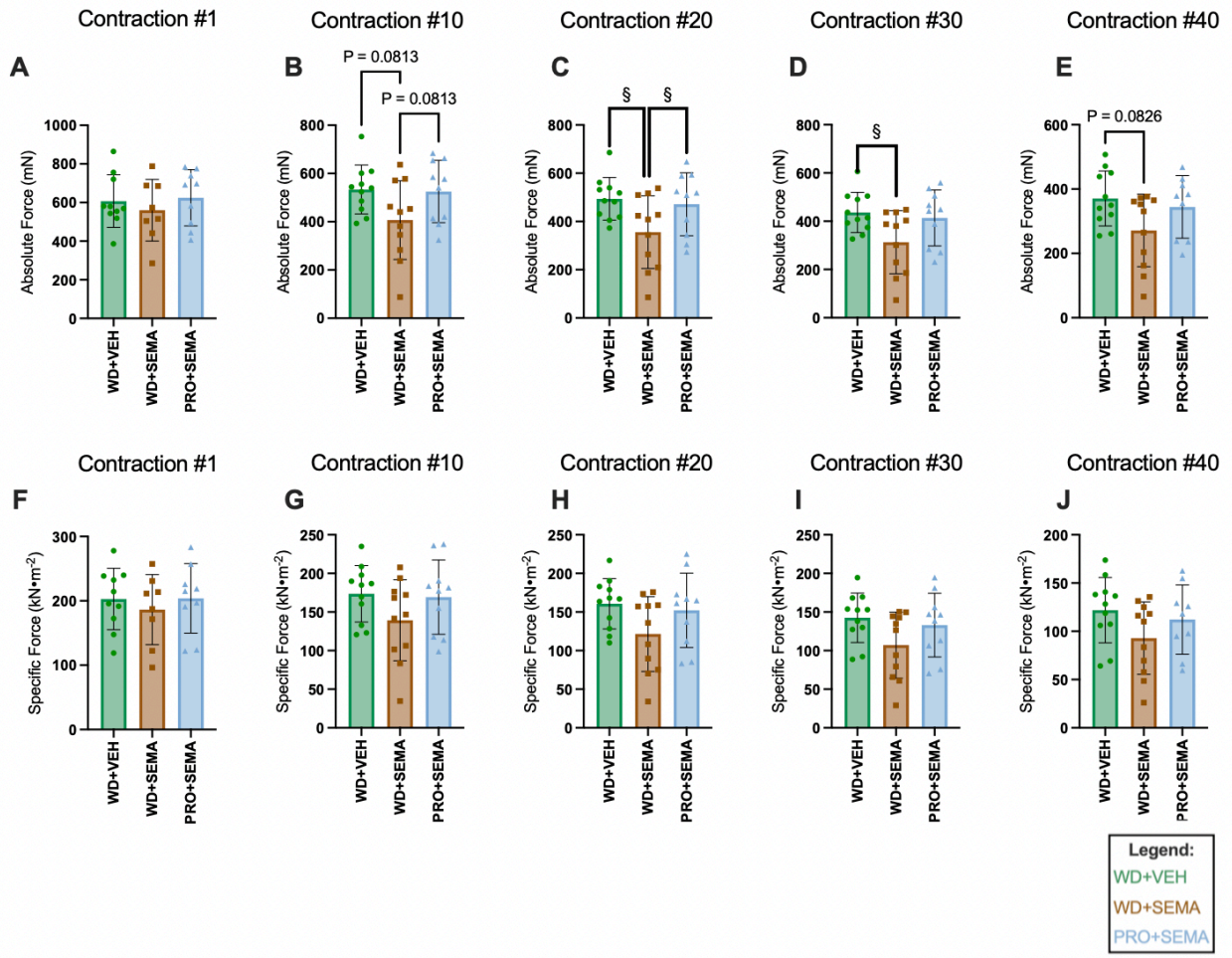

SFigure 6. Sub-analysis at different fatigue protocol timepoints. A-E) Absolute force of initial fatiguing contraction and every 10th subsequent contraction for first 1/3rd of fatigue protocol (n=9-10). **F-J)** Each respective contraction from **A-E)** normalized to muscle CSA. Results represent mean ± SD. A one-way ANOVA was used to determine WD+VEH vs WD+SEMA vs PRO+SEMA. When a significant interaction was present, post-hoc analysis was performed using Benjamini, Krieger, and Yekutieli test. $^{§}P<0.05$.

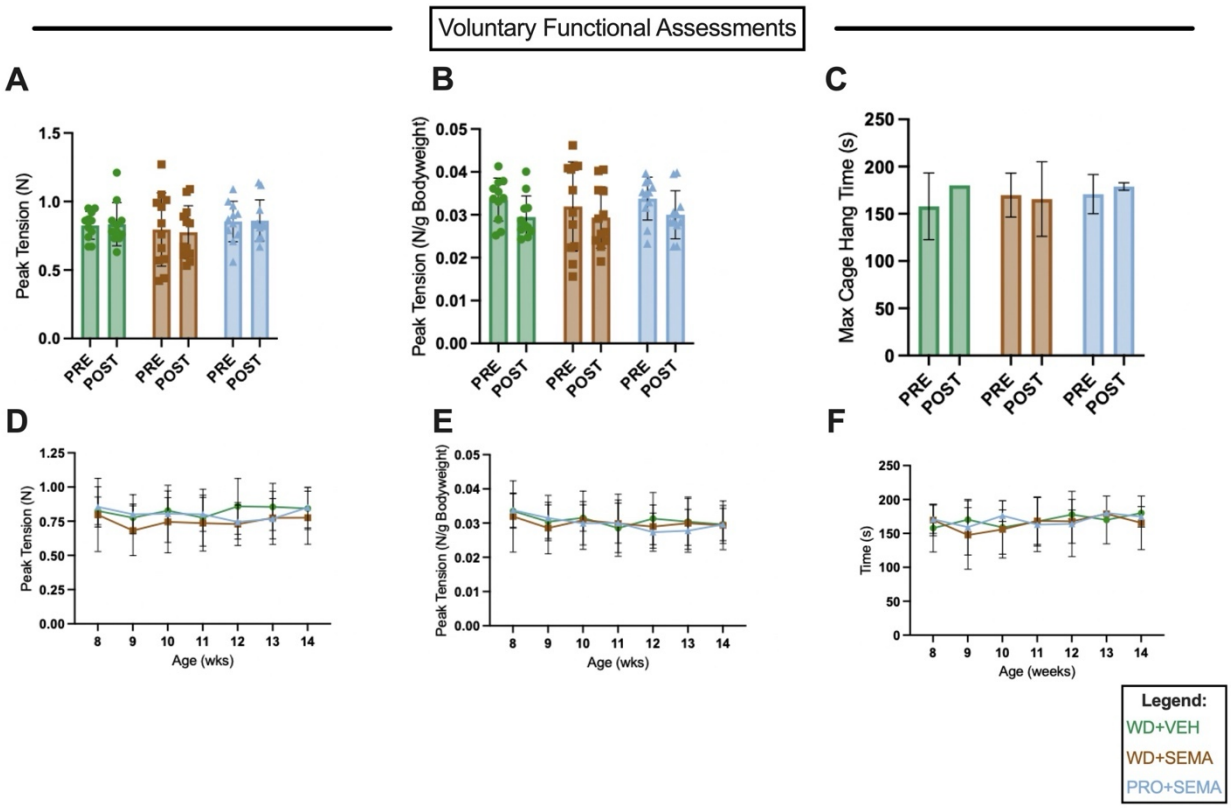

SFigure 7. Longitudinal measures of voluntary muscle function. A) & **D)** Absolute forelimb grip strength was assessed weekly using the "peak tension" function on a grip strength meter. **B) & E)** Absolute grip strength normalized to bodyweight. **C) & F)** Maximum cage hang time was assessed weekly by placing animal on a cage top and turning it upside down. This measurement was capped @ 180s (3 minutes). Under certain instances, all animals in a group reached 180s for cage hang time. When this occurred, no error bars were drawn. Results represent mean ± SD. A two-way ANOVA was used to determine WD+VEH vs WD+SEMA vs PRO+SEMA.

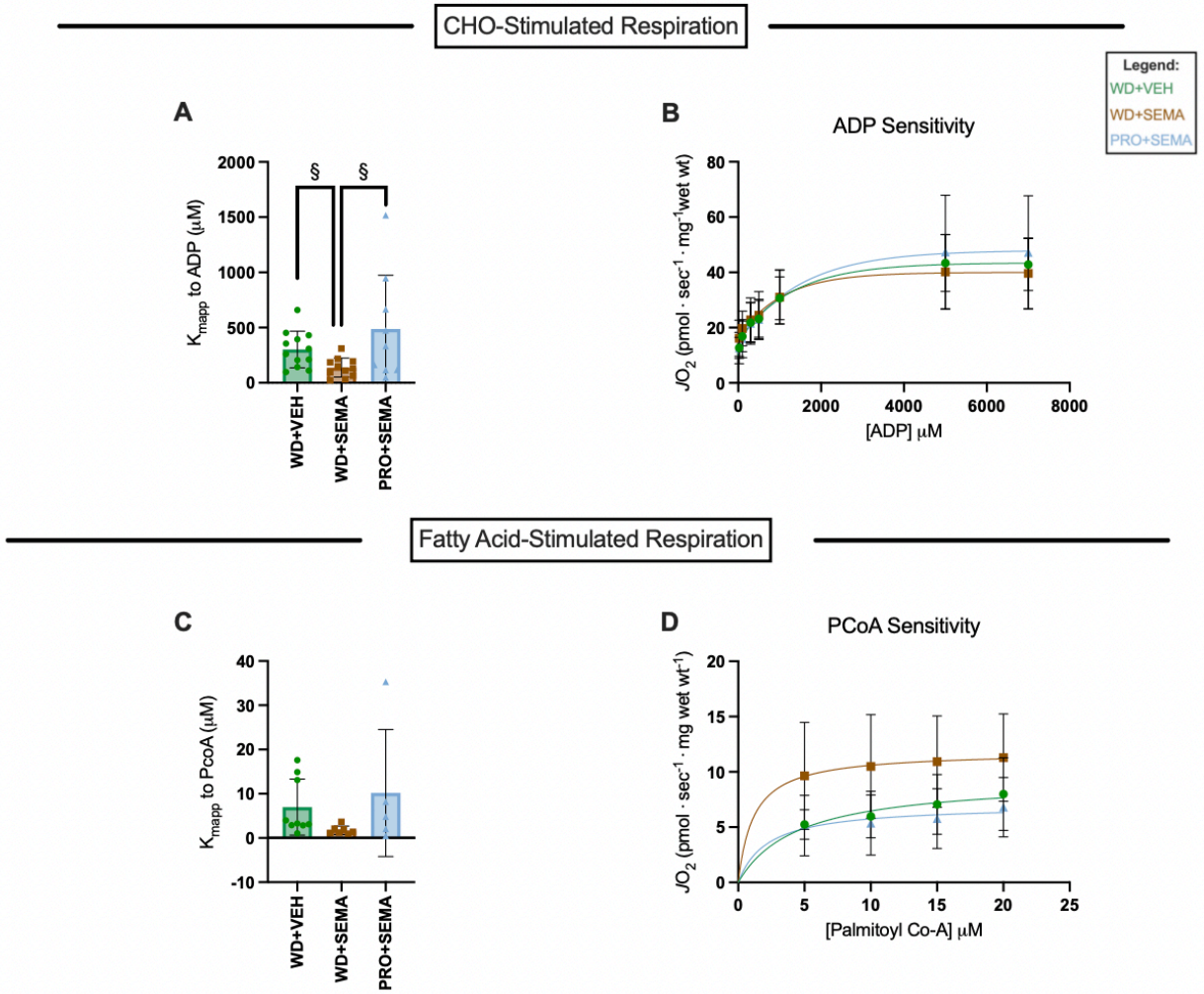

SFigure 8. TA muscle sensitivity to respiration stimulated by different substrates. A) K_{mapp} reflects the substrate concentration at which ADP-stimulated respiration is at half of its maximal capacity (n=9-12). **B)** Michaelis-Menten graph depicting change in K_{mapp} to ADP (n=9-12). **C)** K_{mapp} reflects the concentration at which PCoA-stimulated respiration is at half of its maximal capacity (n=9-12). **D)** Michaelis-Menten graph depicting change in K_{mapp} to PCoA (n=9-12). Results represent mean ± SD. A one-way ANOVA was used to determine WD+VEH vs WD+SEMA vs PRO+SEMA for **A)** & **C)**. A non-linear regression (curve fit) was used to depict Michaelis-Menten Kinetics for **B)** & **D)**. WD+VEH When a significant interaction was present, post-hoc analysis was performed using Benjamini, Krieger, and Yekutieli test. $^{\S}P<0.05$.

APPENDIX A – DETAILED METHODS

Glucose Tolerance Tests

Glucose Tolerance Test (GTT) SOP

IMPORTANT: mice must be fasted for at least 5hr prior to the baseline tail vein collection measure is taken. Remove food from cages and leave note so animal facility is aware this has been done for a reason.

Equipment required

- → Heating pad
- → Heat lamp (heat sources allow veins to dilate + make tail vein blood collection easier)
- → Empty cage to be situated on heating pad, to allow mice to warm up
- → "n" empty cages where mice shall be placed between each tail vein collection
- → Mouse restraint
- → Glucose solution
- → Glucometer
- → Glucose test strips
- → Timers – as many as you are performing GTT's
- → EMLA cream
- → Q-tips – to spread EMLA cream
- → Scale
- → Pipette box
- → Calculator
- → 1mL syringes
- → 23-gauge needles – for tail vein blood collection
- → 26-gauge needles – for IP injection of glucose bolus
- → Silver nitrate applicators – if bleeding doesn't stop, apply to tail vein on area of cut
- → Gloves
- → Sharps container

1. Mice must be fasted prior to GTT. 5hr recapitulates an overnight fast in humans best (Nighttime is active time for mice, fasting during this period leads to significantly catabolic state).
2. To fast mice, remove food and place in a clean cage with fresh bedding, a home, and water. Set timer for 5hr.
3. Obtain baseline blood glucose.
4. Allow mice to warm up in empty cage (no bedding) on heating pad. Keep cage half on/half off, to allow them to cool off if they get too hot.
5. EMLA cream should be applied ~15min before 1st glucose test. Apply to sides of tail where veins are. Works to assist w/ pain and blood vessel vasodilation.
6. For each tail vein collection, secure mouse in mouse restraint. ~1/2 way up tail, along vein, pierce the skin @ ~30-degree angle w/ 23-gauge needle, just enough for the entire bevel to enter the tail. Remove the bevel and allow enough blood to pool to collect on glucose test strip. Glucometer should be set up with test strip inserted and screen on. If

screen turns off, press any button to wake it up. Collect blood on marked sides of glucose test strip and write the measure down on corresponding datasheet. For subsequent tail vein collection, move proximally up the tail vein towards the body, or the other vein on opposite side of the tail (veins are on the side, not underneath!).
    - The heat lamp directly pointed at a tail can help w/ vasodilation and blood collection. Ensure animals are not burned as they cannot move out of the lamplight while restrained.
7. Once baseline measure has been taken, administer glucose bolus intraperitoneally. Calculate volume based off bodyweight and dosage. Dose is 1.5g/kg
    - Volume (uL) = BW * 7.5
8. Set timer for 30min, and collect blood every 30min for until 120min (2hr) has passed.
9. To do >1 mouse at a time, stagger by ~5min, each with their own timer and maybe cage.

MicroCT Scanning Procedure

Taking X-ray:

1. Turn on scanner and monitor, open Bruker Skyscan program.
2. On the bottom right of the screen you will see a panel, to change parameters right click each button.
    - Change filter to 0.5 AI, if you look at the microCT panel, you will now see "soft tissues and bones" selected, with 50 kV and 996uA.
    - Changing the filter will also change the exposure time to 30ms.
3. Adjust Flat-field corrections, this needs to be done at the beginning of every day. Make sure there is no animal or bed in the microCT.
    - Turn on TV icon and X-ray
    - Wait 3-5 minutes before making flat-field corrections for x-ray to stabilize.
    - Ensure flat-field corrections is off, look at the left corner of image it should say "ff" which indicates it is on or "flat-field off". Double click on "ff" to turn it off. When flat field is off and the TV icon is on, the screen will look like a grey honeycomb.
    - With flat-field off, the red line (xray saturation) should be relatively straight indicating there is nothing in the chamber, and the <u>average profile values</u> should be 50-70%
        - **if average profile values are not between 50-70%, then exposure times need to be changed***
    - If you're happy with the average profile values, go to options and update flat-field
    - Turn flat-field on, you should now see a white screen, the average profile values, min and max should be ~90%.
4. Turn off x-ray and insert the animal bedding.
5. Turn on x-ray and TV icon
    - The red saturation line should be flat where there is only air, and decrease when it passes the animal bed.
    - The minimum saturation should be ~30% while max should be ~90%.
6. Turn on the lightbulb icon to monitor the mouse in the bedding.
7. With the TV icon on, move the mouse using the right on left buttons on the microCT monitor or the green up and down buttons on the bottom right of your screen until animal is best positioned in your field of view.
8. Click blue circular arrow icon to set up your scanning parameters.

- Make a new folder for each mouse
- Click step and shoot, rotation should be 0.75 degrees and averaging 4 frames.
- Click 360 rotation.
- Click X-ray off after scanning.
- Partial width = 100%
- After scanning, don't send files to any other program

9. Once the scan is complete, go to actions à send to reconstruction, this will send file to Nrecon

NOTE

→ **Flatfield corrections: Flat-field corrections are background corrections that will improve image quality by ensuring the background is always represented in the same grayscale level and will normalize pixel response variations that would otherwise give rise to various types of artifacts**

→ ***Reset flatfield corrections everyday or if scanning parameters have changed! ***

Myosin Heavy-Chain Fiber Typing Immunofluorescence

All section/slide incubations for this procedure are done at room temperature (RT), on the shaker (~~220rpm~~), and with 50-100µL of solution (only large sections/areas require 100µL). Make sure slides are as flat/level as possible when they are in the incubation container. Also, when blotting slides, even though it is important to remove as much of the solution as possible, the Kimwipes will leave fabric fibers on the sections which show up very brightly blue on the microscope. So, avoid touching the pap pen area with the Kimwipe. Finally, make up antibody dilutions immediately before they are applied.

Set-up

1. Container
   - Put wet paper towel on top of lid covered by parafilm held up by tape (this ensures slides won't dry out).
2. PBS
   - 1 tablet/100mL ddH_2O.
   - Filter, keep at room temperature.
3. Blocking
   - 10% Goat Serum (in freezer in 400µL aliquots).
     - If staining cocktail – 1mL blocking per slide.
       1. 900µL PBS and 100µL Goat Serum
4. Primary (make immediately before use).
   - Primary cocktail (leave on rocker away from light for 2hr)
     - MHCI (BA-F8) @ 1:25 – IgG2b: blue
     - MHC IIa (SC-71) @ 1:500 – IgG1: green
     - MHCIIb (BF-F3) @ 1:50 – IgM: red
     - ~~MHCIIx (6H1) @ 1:100 – IgM: red~~ – this will not be done, so these fibers will appear black.
     - NOTE: these dilutions are for hybridomas at ~50µg/µL.
5. Secondary (make immediately before use).
   - Secondary cocktail (leave on rocker away from light for 1hr)
     - Alexa Fluor 350 IgG_{2b} 1:1000 (blue)

- Alexa Fluor 488 IgG_1 1:1000 (green)
- Alexa Fluor 568 IgM 1:1000 (red)

Procedure

1. Air dry slides for 10MIN at room temperature and outline sections in pap pen (optional).
2. Incubate sections for 1hr in blocking solution.
3. Blot dry slides. Incubate in primary antibodies appropriately diluted in blocking solution (see above). Give the stock antibody tubes a quick shake/inversion before pipetting. Leave away from light, rock for 2hr.
4. Wash slides 3x5MIN in a Columbia jar with 1xPBS.
5. Blot dry slides. Incubate in secondary antibodies appropriately diluted in blocking solution for 1hr at room temperature in the dark. (NOTE: precipitate forms in the stock tubes, which shows up as bright spots on the microscope; centrifuge for 15s before pipetting out of stock tubes. Ensure as little light as possible makes contact with the secondary antibodies and sections from this point forward).
6. Wash slides 3x5MIN in a Columbia jar with 1xPBS. Take the mounting medium, nail polish, and cover slips.
7. Apply 15µL Prolong to each slide and mount with a number 1 coverslip. (Perform this step in the microscope room in almost total darkness). The coverslip can be pressed gently to remove bubbles, but do not apply pressure directly above sections as it will squish them.
8. Tack the corners of the coverslip down with nail polish and place in a labelled, light-proof slide box.
9. Slides can be imaged after nail polish has dried (~5-10MIN), but next-day imaging seems to work better as the Prolong is allowed to set. Slides should be imaged no more than 2 days after staining.

In situ TA Force Production

A good rule of thumb is to have practiced this surgery at least 10-15 times and be able to get consistent data with previous literature. If you are doing a new model establish your own normal values in a pilot data set.

Protocol

Create a folder to save files for each animal - Setup: Autosave Folder, open folder you created; click “current folder”
Setup: Instant Stim
Pulse Frequency: 1Hz
Pulse Width: 0.2ms
Number of Pulses: 1
Train Frequency: 0.1Hz
Run Time: 1 second
** I have a train frequency that does 3 twitches with a delay between that I find most useful for optimizing current
Open Live Data monitor and set time to 10 minutes
Once TA has been sutured at the distal tendon and tied to force transducer, insert needle electrodes in the fascia underneath the TA. Note: do not insert needles directly into muscle belly.
Optimize Current

Range:10mA -100mA (if you can get the right placement this can go to 10mA, but if you struggle can go to 10% of 100mA). If you placed the electrodes well you will be able to stimulate the sciatic nerve with very little current (20% of 10mA).
Run instant stim
Adjust range to ensure all muscle fibres are being recruited – obtain 3 twitches in a row where force does not increase (run instant stim and increase current between twitches (wait about 30 seconds in between twitches)
Set supramaximal current by increasing current by 15%
Optimize Resting Length
Increase/decrease length until maximal twitch force is achieved, wait about 30 seconds in between twitches to avoid twitch potentiation.
On average ~10week old female mice have ~10 baseline tension for reference. This can change with age, sex, breed, and disease.

Once optimal current and length have been set, record muscle length and protocol is ready to begin. This step is crucial as the in-situ set-up can have human variability in how high you cut the TA. Recording length ensures consistency.

Load **"TA In Situ Force Frequency"** sequence
Frequencies of 1Hz, 10Hz, 20Hz, 30Hz, 40Hz, 50Hz, 60Hz, 80Hz, 100Hz, 120Hz, 200Hz
Initial Delay: 0.2ms
Pulse Frequency: ____Hz (above frequency)
Pulse Width: 0.2ms
Duration: 300ms
1 minute in between
Wait 5 minutes
Load **"TA Fatigue"** sequence
120 contractions at 60Hz with a delay of 0.2ms between each
Wait 5 minutes
Load **"TA Recovery"** sequence
1 tetanic contraction will be sent every 5MIN for 15MIN
Harvest muscle and before freezing **MAKE SURE TO RECORD MUSCLE WEIGHT.**
Data will be normalized to muscle CSA.

mH_2O_2 Buffer Recipes, Protocols, and Analyses

Amplex Ultra Red – Preparation

- → Total volume per experiment: 1000μL
- → Total volume per tube: 1050μL

Stock AUR ingredients required:

- → 5mM Amplex Ultra-Red (Invitrogen A36006)
- → 5000 IU/mL Cu/Zn Superoxide dismutase (SOD1; Sigma S9697)
- → 10mM Blebbistatin (BLEB; Cayman)
- → 0.5M EGTA (aliquots in freezer)
- → 20mM Creatine anhydrous

Final concentrations for AUR Stock

→ 10μM AUR
→ 5uM BLEB
→ 25U/mL Cu/Zn SOD1
→ 1mM EGTA
→ 20mM Creatine anhydrous

Work fairly quickly given AUR and BLEB should not be stored on ice. Keep AUR and BLEB out of light when not using. Wrap beaker in foil and cover with lid when mixing components.

Preparation of AUR Stock A (20mM Cr)

1. Prepare 5mM AUR. Add 666.6ul of DMSO to 1mg AUR. Vortex gently. Place tube in drawer out of light. (Don't place on ice, DMSO will freeze).
2. Prepare 10mM BLEB. Add 1.71mL DMSO to 5mg BLEB. Prepare in black tube, keep off ice.
3. Prepare 5000IU/mL SOD1 from 30KU/mL stock. Add 3mL to Sigma bottle, mix well, move to 15mL Falcon tube. Add an additional 3mL to Sigma bottle, moving this to the 15mL Falcon tube (6mL total). pH to ~7. **Make sure you use 1M KOH to pH, titrate incrementally, 1μL at a time**. Make 850μL aliquots, label with date of preparation and title "5000IU/mL SOD1", and freeze.
4. Prepare 10μM AUR stock. Mix together
    - 160.6mL Buffer Z. Note: sucrose buffers lower oxidant emission
    - 421.19mg creatine anhydrous
    - 325μL of 5mM AUR
    - 812.5μL of 5000IU/mL SOD1
    - 80.3μL of 10mM BLEB
    - 325μL of 0.5M EGTA
    - Aliquot 1050 uL in black tubes and store at -80°C

H_2O_2 Standard curve for AUR

1. H_2O_2 dilution (serial dilution)
    - H_2O_2 is light sensitive. Keep in dark when possible.
    - Use H_2O_2 purchased within last 6 months (stored in fridge, wrapped in foil).
    - One standard curve per batch is acceptable, but re-make curve if batch approaches 6 months of age. Discard if curve no longer consistent with original curve.
        - Good in -20C freezer up to 6 months.
    - Use stock 3% w/w H_2O_2: 3g H_2O_2/100mL solution (1mol H_2O_2/34.01g) = 0.0882mol H_2O_2/0.100L = .882mol H_2O_2/1L = 0.882M H_2O_2
        1) 4310μL ddH_2O + 100uL 3% w/w H_2O_2 >>>> 20mM H_2O_2. Use in dilution step 2).
        2) 3980μL ddH_2O + 20μL of 20mM H_2O_2 >>>>>> 100μM H_2O_2. Use in dilution step 3) for 20μM.
        3) 3200μL ddH_2O + 800μL 100μM H2 H_2O_2 >>>>> 20μM H_2O_2. Use in table below.

4) 2000µL ddH_2O + 2000µL 20µM H_2O_2 >>>>>> 10µM H_2O_2. Use in table below.
5) 2000µl ddH_2O + 2000µL 10µM H_2O_2. >>>>>> 5µM H_2O_2. Use in table below.

NOTE:

→ H_2O_2 is light sensitive.
→ Prepare large volumes to minimize pipetting/dilution errors.
→ Do not vortex – H_2O_2 is unstable and dismutates spontaneously over time. Agitation may worsen. Flip tube in hand several times.
→ Make this right before you are about to start standard curve

1. Add AUR, HRP, (oligomycin) and other substrates (G/M/S/G-3-P……) into the cuvette as per your protocol.

NOTE:

→ You only need to pick one protocol (i.e. substrate combination: pyruvate/malate or succinate) to perform background on. Sofhia Ramos performed experiment to show that each substrate combination does not change background fluorescence that much.
→ Make sure you add total volume of ADP to the titrate as well – does not matter what concentration you use.

2. H_2O_2 titration: NOTE: [final H_2O_2] depends on final volume in the cuvette, which will vary depending on your protocol.
    - **BACKGROUND COLLECTION: collect for 3MIN minimum**
    - **(VERIFY LAST 0:30 OF BACKGROUND LOOKS LINEAR)**

Make sure to clean the pipette tip by pipetting up and down in a beaker of ddH2O after each addition, and wipe pipette tip with Kim wipe. This avoids excess additions of H2O2 as you progress.

If for 1000µL… Titrate very fast, 45-60 sec		**If for 600ul…** Titrate very fast, 45-60 sec	
[H_2O_2] (µM)	Add (µl))	[H_2O_2] (µM)	Add (µl))
5	3.33	5	2.0
5	3.33	5	2.0
10	3.33	10	2.0
10	5	10	3
20	5	20	3
20	5	20	3
20	10	20	6

3. Repeat 3x. Average all 3 standard curves to make one equation for analyses in Excel if values are consistent. See next page for acceptable ranges of values and general considerations…
    - NOTE: Prepare a standard curve for project – make sure you save some AUR buffer for any redo's for standard curve you need to do.

General Considerations:

→ **<u>In general, collect background of 3MIN and collect 45s-60s for each H_2O_2 titration.</u>**
→ You will have 8 points in the Standard Curve. Consult experienced personnel on judgement for quantifying steady state fluorescence.
→ During analysis, it can be common to drop points if the standard curve begins to form a curvilinear response. Check curve closely following analyses. Aim for at least 4 data points in the final curve.
→ Finally, the accuracy of dilutions has an enormous effect on the lowest H_2O_2 points of the standard curve. It is not uncommon for new trainees to see scattered points at the low end. The stocks must be re-made with new curves prepared if this is the case.
→ APRIL 2020: we compared normalizing each titration of H_2O_2 to its own drift calculation and it gives the same results as normalizing each H_2O_2 titration to the drift calculation from the background. In drift calculation use the last 0:30 of 3MIN background for drift calculation so long as it is linear – this can change to less points if only last 10-15s are linear in the background.

<u>Ranges:</u>

→ **SLOPE: LOW 1millon- LOW 2millon (**newer bulbs will give you closer to low 2 million)**
→ Bulb should be changed if slopes are seeing less than 1millon- always check bulb usage hours if you are getting lower slope. Max bulb usage time is 400hr.
  - **<u>Always check bulb usage hours before you start a study</u>**.
  - If you get a very high slope (ie 2.5 million) it might be a new bulb but re-run standard curve to be sure it was not an H_2O_2 dilution error.
→ **Y-INTERCEPT: do not go above 5000 if slope is around 1 million, 8000 if slope is closer to 2 million (subject to change based on group discussions)**.
  - **<u>You need positive value – needs to be as close to 0 as possible</u>**
  - If all y-intercepts are positive, then go to the values closest to 0 (and below cutoffs listed above) and average these intercepts. **Use your judgement.**
  - If all y-intercept are negative, redo standard curves. But negative values close to 0 might be acceptable as well **(subject to group discussion)** – **use your judgement.**

mH_2O_2 Protocols

Pyruvate & Malate (Complex I FET)

35µM CDNB (5µL od 10.5mM CDNB Stock)

SLOT	ASSAY BUFFER	PRE-EXPERIMENT		SUBSTRATES		ADP		ADP		ADP	
1	20mM Creatine-AUR	**1U HRP** 2µL of 500U/mL Fiber	3 min	**10mM Pyruvate** 5µL of 2M **2mM Malate** 2µL of 1M	1 min	**25µM** 5µL of 5mM	2 min	**100µM** 1.5uL of 50mM	2 min	**500uM** 0.8µL of 500mM	2 min
2											

Succinate (Complex I RET)

SLOT	ASSAY BUFFER	PRE-EXPERIMENT		SUBSTRATES		ADP		ADP		ADP	

1 2	20mM Creatine-AUR	**1U HRP** 2µL of 500U/mL Fiber	3 min	**10mM Succinate** 5µL of 2M	5 min	**25µM** 5µL of 5mM	2 min	**100µM** 1.5uL of 50mM	2 min	**500uM** 0.8µL of 500mM	2 min

mH_2O_2 Analysis

Phase 1: Export Traces

1. Go to lab computer where H_2O_2 experiments were completed and open Felix software.
2. Open H_2O_2 file, right click protocol and click "Export Trace." Save all files in a folder and use a USB to transfer data over to a personal computer and back up data on One Drive (or any other location where you keep your data).
3. Once data is on personal computer where you wish to analyze, right click file you wish to analyze and click "Export with Excel".
4. Highlight first 4 rows and click delete.
5. All that should be remaining in the file is data in Column A and Column B. Column A will contain time data (independent variable) while column B will contain fluorescence intensity data (dependent variable), the index of H_2O_2 emission. Copy all Column A and Column B data and paste it into the H_2O_2 analysis template

Phase 2: Setting up and understanding template sheet

1. Open H_2O_2 analysis template provided by a lab member and ensure the following criteria

Phase 2: Setting up and understanding template sheet

1. Open H_2O_2 analysis template provided by a lab member and ensure the following criteria are met:

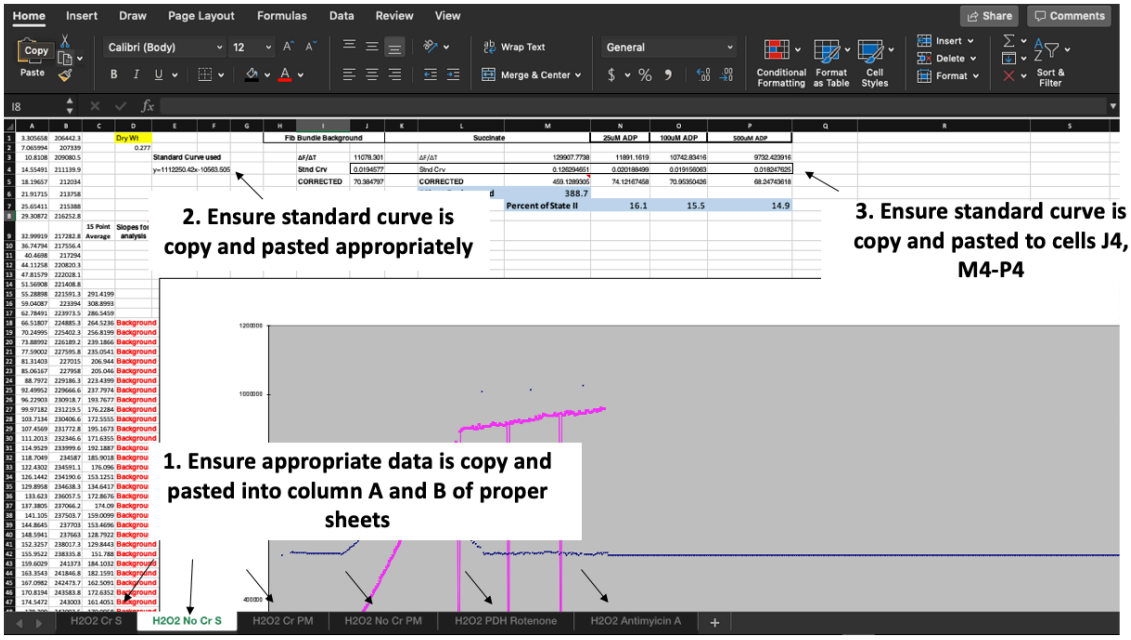

2. Once values are pasted into columns A and B the template will automatically create a 15 point or 10 point slope calculation in column C and generate a graph. See below for interpretation of data..

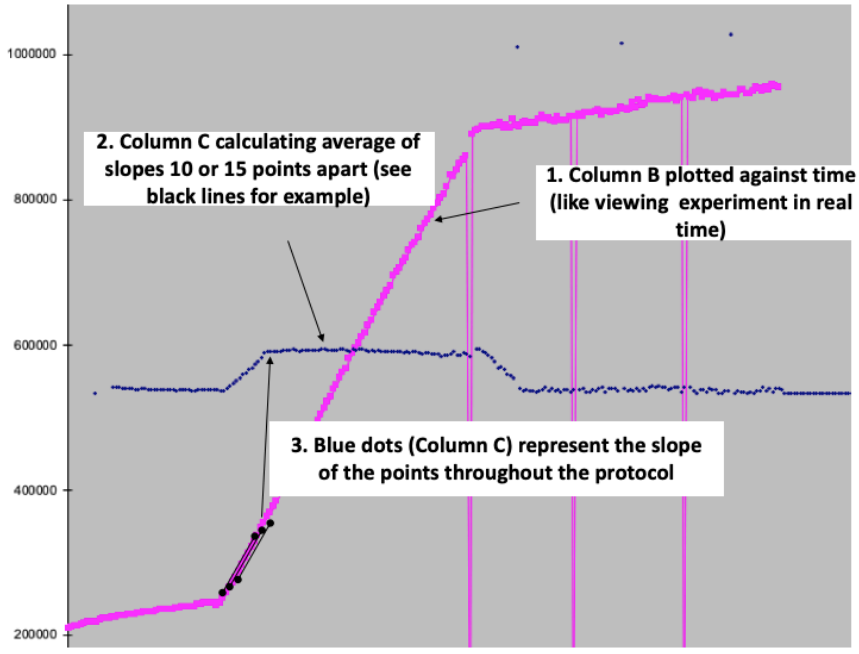

Phase 3: Analyze H_2O_2 Traces

→ Every protocol has slightly different patterns of H_2O_2 emission and therefore slightly different regions to be analyzed. Although different regions will be selected per protocol, the fundamental premise remains – **take large averages of max substrate emissions.** Some protocols can be a "judgment call" but this SOP will attempt to walk the reader through the best choices.

Pyruvate Malate

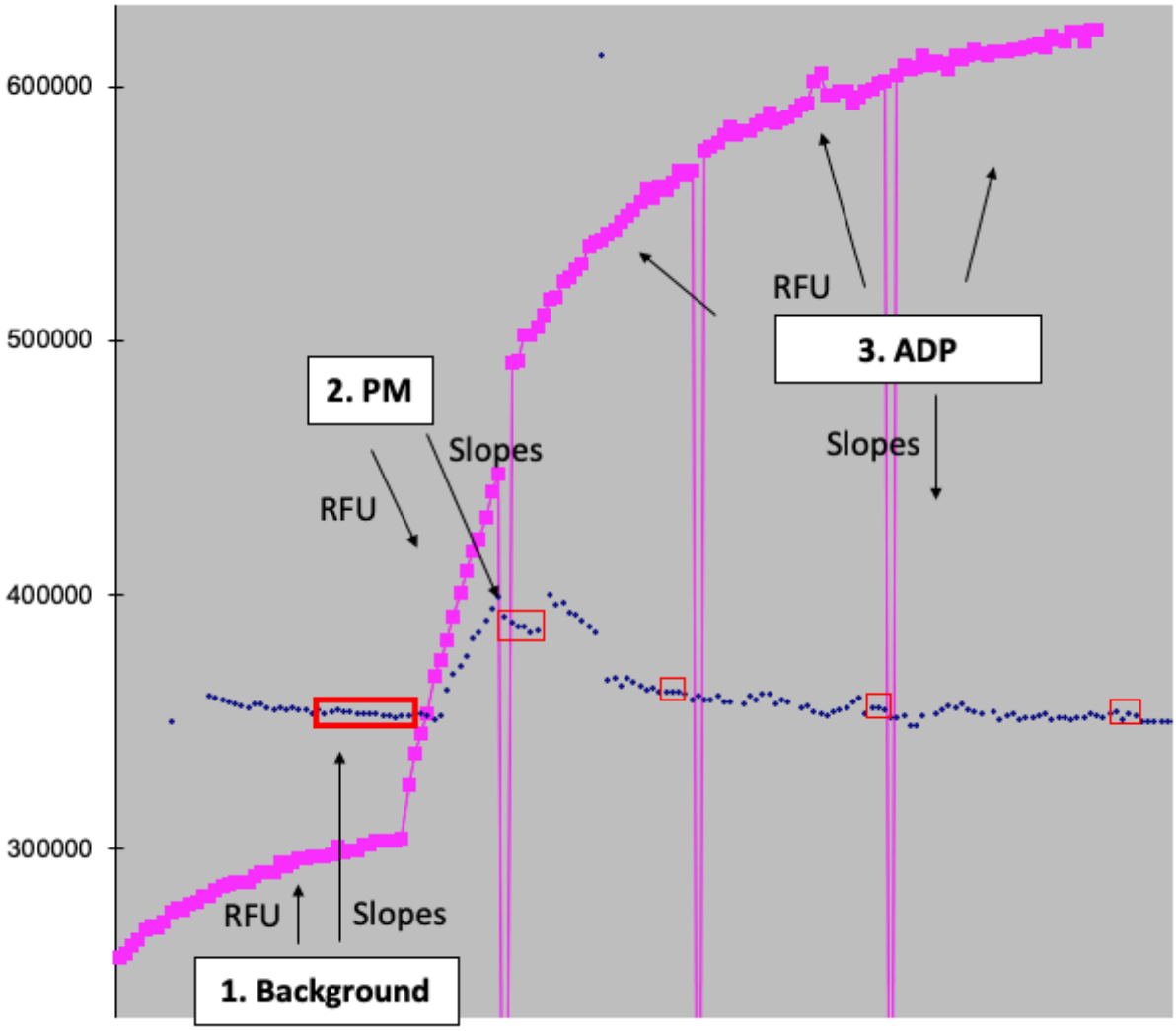

1. Background should be 2-3 minutes, PM 1 minute, ADP 2 minutes each
2. NOTE: PM is increasingly difficult because PM generates so much H_2O_2 that the longer the protocol runs, the more the fiber could be dying due to cell damage. This protocol requires a 1-minute titration and a narrow window to select for averages compared to succinate. **Be extra careful you are NOT averaging slopes of recording data from a previous titration.**
3. Data copied are in cells J5-P5 (corrected rates).

Succinate

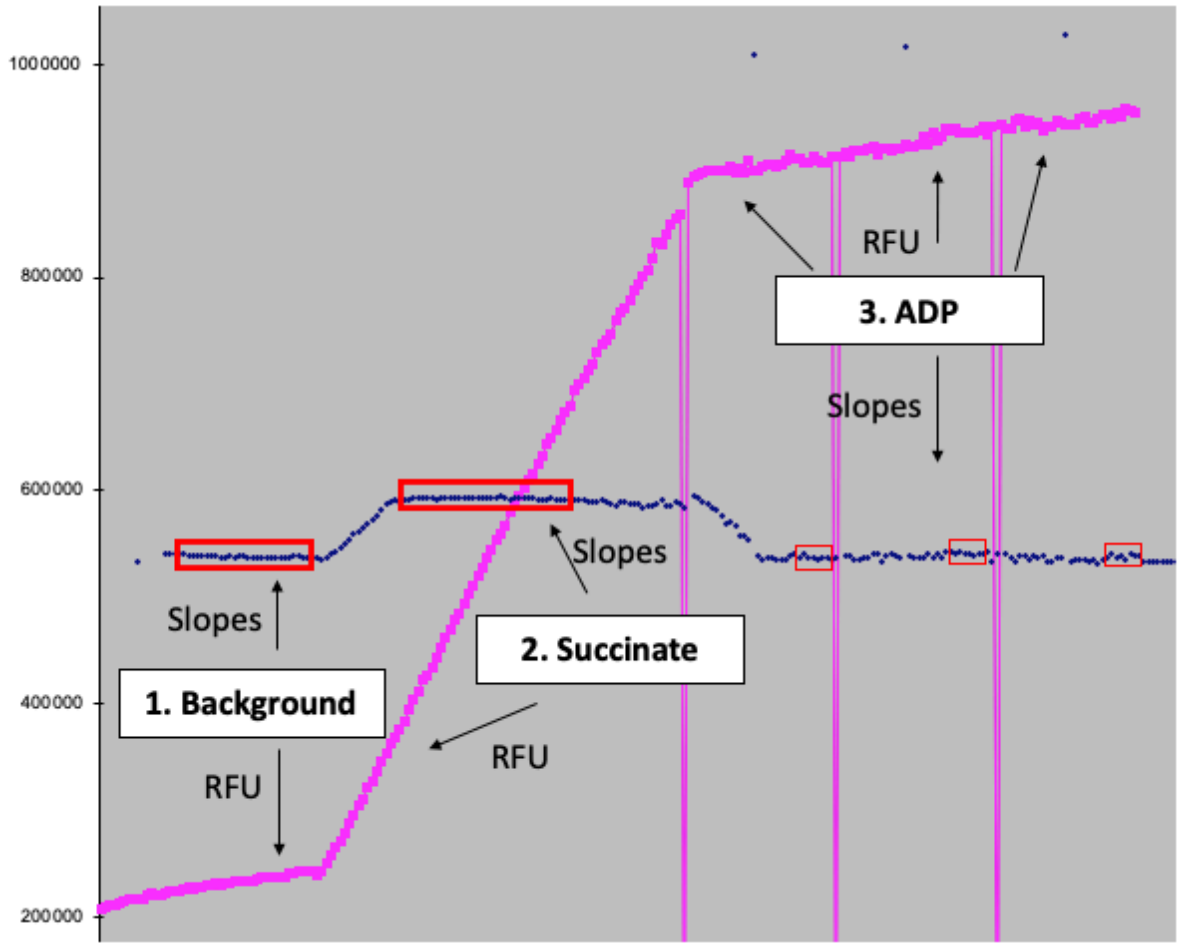

1. Background should be 2-3 minutes, succinate 5 minutes, ADP 2 minutes each
2. Make sure you are referencing column C to ensure you are measuring correct slopes calculated from RFU data (column B). **Be extra careful you are NOT averaging slopes of recording data from a previous titration.**
3. Data copied are in cells J5-P5 (corrected rates).

NOTE: All graphs were generated using control mice from LD's Cancer Cachexia thesis. All protocols may not look identical but general trend should be similar.

Bioenergetics Buffer Recipes

BIOPS BUFFER (Extracellular)

Chemical	Stock Solution	Molecular Weight	Final Concentration	Addition to *2 Litre* Final Volume
CaK_2EGTA*	100mM		2.77mM	55.4mL
K_2EGTA*	100mM		7.23mM	144.6mL
Na_2ATP		555.1 605.24	5.77mM	6.41g 6.98g
$MgCl_2 \cdot 6H_2O$		203.3	6.56mM	2.67g
Taurine		125.1	20mM	5.02g

Na_2Phosphocreatine		327.14	15mM	9.81g
Imidazole		68.1	20mM	2.72g
Dithiothreitol (DTT)		154.2	0.5mM	0.154g
MES Hydrate		195.2	50mM	19.52g

*__ALWAYS__ double check molecular weights for supplier-specific chemicals (n=m/M.W.)

BIOPS contains the following ion concentrations		**EXTRACELLULAR RANGE**
Ca^{2+} free	0.1uM	Rat: 7.6mM Mouse: 1.3mM
Mg^{2+} free	1mM	
Na^+	41mM	Human: 133-143mM
K^+	20mM	Human: 4.5mM
Cl^-	13mM	Rat: 160mM Mouse: 95-120mM
MgATP	5mM	
Ionic Strength	160mM	
Osmolality	295 mOsm	

*Ionic strength is the sum of all ions
*Buffers do not perfectly reflect extracellular conditions
*Species-specific extracellular ranges exist
*Ranges are expressed as mmol/L (refer to ion concentration summary chart)

CaK_2EGTA: Dissolve 2.002g of $CaCO_3$ in 100mM hot (80°C) solution of EGTA (7.608g of EGTA in 200mL ddH_2O). Add 2.3g of KOH and adjust pH to 7.0 using KOH. Freeze unused portions.

K_2EGTA: Dissolve 7.608g EGTA and 2.3g KOH into 200mL ddH_2O. Adjust pH to 7.0 using KOH. Freeze unused portions.

To make BIOPS:

1. Add approximately 1500mL of ddH_2O to 2000mL beaker
2. While constantly stirring add stock solutions of CaK_2EGTA and K_2EGTA
3. Weigh and add all powder chemicals
4. Adjust pH to 7.2 using KOH pellets
5. Using graduated cylinder, bring total volume to 2000mL
6. Filter and then aliquot into 50mL falcon tubes
7. Freeze falcon tubes

Notes Re: BIOPS Buffer

→ BIOPS is designed to mimic the extracellular environment.

→ BIOPS should be a relaxing media to prevent basal Na^+/K^+ flux that stimulates electrical signals in muscle - this is the purpose of having high K^+ (K^+ counteracts action potentials).
→ BIOPS prevents cell shrinkage or swelling.
  - Keep Ca^{2+} low and ATP available.
  - Keep it cold.
  - Saponin removes cell membrane ~15MIN into permeabilization.

<u>CaK_2EGTA</u>

→ Need some Ca^{2+}, but too much kills cell (calpain and caspase activation, mitochondrial swelling).
  - Not enough Ca^{2+}: cannot prime all dehydrogenases and ETC (keep them active).
  - As an example, PDH requires Ca^{2+} to be activated: Ca^{2+} binds PDP (pyruvate dehydrogenase phosphatase), not PDH itself.
  - SR may have lost normal regulation, so need for EGTA to maintain low Ca^{2+}.

→ K^+ relaxes fibers so they stay flaccid while separating (prevents spontaneous depolarization).
→ EGTA is a cationic non-specific chelator – it can chelate Ca^{2+} and Mg^{2+}; binds divalent cations (that is why it cannot chelate Na^+ or K^+); EGTA has a higher affinity for chelating Ca^{2+} (prevents Ca^{2+} from going too high).
  - EGTA buffers Ca^{2+} and keeps Free Ca^{2+} low.
  - Mitochondria can swell over time if you do not have EGTA to buffer Ca^{2+}.
  - Amount of Ca^{2+} and amount of EGTA determines Free Ca^{2+} (refer to sample calculation e.g. McGuigan et al. *Can. J. Physiol. Pharmacol.* 69:1733 – 1749, 1991)

<u>Na_2ATP</u>

→ Na^+ is exchanged with Mg^{2+} from $MgCl_2$ (ATP naturally binds to Mg^{2+} creating Mg•ATP in the buffer).
  - ATP relaxes fiber in buffer – therefore, it relaxes myosin with ATP.
  - ATP supports metabolism while separating fibers in BIOPS.
  - BIOPS contains 41mM of Na^+, which is less than the known extracellular ion concentration of 133-143mM – this may be to ensure that fibers are not excessively activated (remain somewhat relaxed) – see ion concentration chart in separate file.

<u>$MgCl_2$</u>

→ Mg^{2+} is needed for metabolism because it is required in the ETC for ATP production (cofactor for ATP synthase).
  - Any enzyme that hydrolyzes or makes ATP needs Mg^{2+}.
  - EDTA preferentially chelates Mg^{2+} over Ca^{2+} (this is why EDTA is <u>NOT</u> added).

<u>Taurine</u>

→ Sulphur-based, inert compound used to balance osmolarity; could be an antioxidant.
→ Cation chelator (keeps Ca^{2+} and Mg^{2+} in balance).

<u>PCr</u>

→ Needed for energy production and phosphate shuttling mechanism between mitochondria and cytoplasm; keeps energy exchange higher.
  - PCr loss likely occurs during permeabilization, which requires addition to buffer.

<u>Imidazole ** might do many things</u>

→ Preservative and antioxidant that prevents bacterial growth in BIOPS, might inhibit contraction.
→ Potentially causes hyperpolarization of mitochondrial membrane.

Dithiothreitol (DTT)

→ Two thiol groups → very common antioxidant; if no antioxidants are present, many enzymes can form disulfide bonds and become inactivated by ROS.
  - Therefore, it must be at very low concentrations.

2-(N-Morpholino) ethanesulfonic acid (MES) Hydrate

→ Buffers protons, a substitute for the natural *in vivo* bicarbonate buffer.
→ "S" refers to sulfonic acid, which buffer protons.
→ Acids exist in equilibrium as negative and positive. Therefore, sulfonic acids will buffer H^+ as a natural part of their equilibrium.
  - MES effective pH range: 5.5-6.7
  - HEPES pH range: 6.8-8.2 ← this may be more ideal

Cytoplasmic Ca^{2+} low, Mg^{2+} high

→ This prevents Ca^{2+}-induced mitochondrial swelling and ensures high Mg^{2+} for ATP synthase and ATPases throughout the cell, given Mg^{2+} is a cofactor for ATP.
→ Therefore, EGTA is used (and not EDTA) to keep Ca^{2+} low and Mg^{2+} high (EGTA is a strong Ca^{2+} chelator and a weak Mg^{2+} chelator) – EDTA is the opposite.
→ Must prevent mitochondrial swelling (keep low Ca^{2+} so it does not die, need Mg^{2+} for metabolism while separating and permeabilizing fibres).
→ Free Mg^{2+} is a calculation of what is left from $MgCl_2$ after being bound to ATP that was added to the buffer and chelated weakly by EGTA.
  - The same is true of free Ca^{2+} and EGTA.

Importance of total osmolarity

→ Do not want to swell or shrink the cytoplasm and mitochondria while you are separating (osmolarity is anything that draws water).
→ Calculated based on concentration of every component of the buffer – every component is water soluble (contributes to osmolarity), not just the salts.
→ Extracellular osmolarity is 295mOsm, just like BIOPS buffer.

Importance of total ionic strength

→ Maintaining protein shapes throughout cell through ionic bonds.
→ Ionic strength is total ions in a cell.

MiRO BUFFER (Intracellular)

Chemical	Stock Solution	Molecular Weight	Final Concentration	Addition to *2 Litre* Final Volume
EGTA		380.4	0.5mM	0.38g
$MgCl_2 \cdot 6H_2O$		203.3	3mM	1.22g
K-Lactobionate*	0.5M	358.3 free acid	60mM	240mL
Taurine		125.1	20mM	5.02g
KH_2PO_4		136.1	10mM	2.72g
HEPES		238.3	20mM	9.54g
Sucrose		342.3	110mM	75.3g
BSA		154.2	1g/L	2.0g

*__ALWAYS__ double check molecular weights for supplier-specific chemicals (n=m/M.W.)

MiRO contains the following ion concentrations		**INTRACELLUAR RANGE**
Ca^{2+} free	0.0uM	Human: 30nM – 60nM SR: 5.7-20mmol/L Free Ca^{2+} in SR 0.2-0.5mM Rat: 7.76-11.11 ueq/g dry wt
Mg^{2+} free	2.1mM	
Na^{+}	0.0mM	Human: 6-13mM Rat: 7.10-21.9mmol/L
K^{+}	90mM	Human: 130 – 164mmol/L Rat: 117 – 149mmol/L
Cl^{-}	6mM	Rat: 4.97-16.57mmol/L
PO_4^{3-}	10mM	
EGTA free	0.46mM	
Ionic Strength	95mM	
Osmolality	330 mOsm	

*Ionic strength is the sum of all ions
*Buffers do not perfectly reflect extracellular conditions
*Species-specific intracellular ranges exist
*Ranges are expressed as mmol/L (refer to ion concentration summary chart)

K-Lactobionate: Dissolve 71.6g lactobionic acid in 300mL ddH_2O, adjust pH to 7.0, adjust final volume to 400mL with ddH_2O

To make MiRO:

1. Add approximately 1500mL of ddH_2O to 2000mL beaker
2. While constantly stirring add stock solution of K-Lactobionate
3. Weigh and add all powder chemicals
4. Adjust pH to 7.2 using KOH pellets
5. Using graduated cylinder, bring total volume to 2000mL
6. Filter and then aliquot into 50mL falcon tubes
7. Freeze falcon tubes

Notes Re: MiRO Buffer

Lactobionate/Taurine

→ Osmotic regulators (hold onto water); prevent shrinking or swelling of mitochondria by maintaining osmolarity.

→ Cells have higher mOsm than extracellular (MiRO and Buffer Z need to be saltier than BIOPS – that is what mitochondria are accustomed to).
→ They are also weak antioxidants.

K-Lactobionate
→ Main source of K^+ in MiRO buffer.

HEPES
→ Buffer (effective range @ pH 6.8-8.2).

Sucrose
→ Membrane stabilizer
→ Antioxidant

KH_2PO_4
→ Provides inorganic phosphate for ATP synthesis

BSA
→ Osmolarity, Antioxidant, Buffer.

Cytoplasmic Ca^{2+} low, Mg^{2+} high (same as BIOPS, but ALSO…)
→ This prevents Ca^{2+}-induced mitochondrial swelling and ensures high Mg^{2+} for ATP synthase and ATPases throughout cell given Mg^{2+} is a cofactor for ATP.
→ Therefore, EGTA is used (and not EDTA) to keep Ca^{2+} low and Mg^{2+} high (EGTA is a strong Ca^{2+} chelator and a weak Mg^{2+} chelator) – EDTA is the opposite.
→ Not only do you need high Mg^{2+} to drive ATP synthase but also to maintain steady state respiration by supporting ATPases (potentially other pathways that use ATP) throughout the cell that regenerate ADP for the mitochondria.
→ Without Mg^{2+} in the buffer, ATP would not be synthesized or utilized, and respiration would not be steady state

BUFFER Z (Intracellular)

Chemical	Molecular Weight	Final Concentration	Addition to *500mL* Final Volume
K-MES	233.33	105mM	12.26g
KCl	74.55	30mM	1.12g
KH_2PO_4	136.08	10mM	0.7g
$MgCl_2 \cdot 6H_2O$	203.3	5mM	0.51g
EGTA	380.35	1mM	0.19g
BSA		5mg/mL	2.5g

*__ALWAYS__ double check molecular weights for supplier-specific chemicals (n=m/M.W.)

Buffer Z contains the following ion concentrations		**INTRACELLULAR RANGE**
Ca^{2+}	0.0uM	Human: 30nM – 60nM SR: 5.7-20mmol/L Free Ca^{2+} in SR 0.2-0.5mM Rat: 7.76-11.11 ueq/g dry wt

Mg^{2+} (total, not free)	5mM	
Na^+	0.0mM	Human: 6-13mM Rat: 7.10-21.9mmol/L
K^+	145mM	Human: 130 – 164mmol/L Rat: 117 – 149mmol/L
Cl^-	40mM	Rat: 4.97-16.57mmol/L
PO_4^{3-}	10mM	
EGTA free	1mM	

*Buffers do not perfectly reflect extracellular conditions
*Species-specific intracellular ranges exist
*Ranges are expressed as mmol/L (refer to ion concentration summary chart)

To make Buffer Z:

1. Add approximately 400mL of ddH_2O to 1000mL beaker
2. Weigh and add all powder chemicals
3. Adjust pH to 7.2 using KOH pellets
4. Using graduated cylinder, bring total volume to 500mL
5. Filter and then aliquot into 50mL falcon tubes
6. Freeze falcon tubes

NOTES RE: BUFFER Z (alternative to MiRO)

Special notes

→ Principles listed above for BIOPS and/or MiRO are the same for Buffer Z, regarding $MgCl_2$, EGTA, BSA, KH_2PO_4 and MES.

→ Buffer Z is used for H_2O_2 emission because it does not contain any antioxidants or sucrose.

BSA benefits

1. Buffers protons
2. Buffers FFA
3. Buffers ROS (it is loaded with cysteines and histidines which can react with ROS to buffer it)
4. Contributes to osmolarity of cell

Special note: K^+ source

→ BUFFER Z uses K-MES, not K-Lactobionate (as in MiRO)

Special note: Cl^- (from KCl)

→ Intracellular Cl^- is supraphysiological; this does not seem to affect respiration (see figure 1A of Perry and Kane et al. *Diabetes* 2013. Note Mitomed is similar to MiRO in figure).

→ Cl^- above 30mM can cause mtCK to dissociate from inner membrane space according to Oroboros blue book. However, our lab still obtains good respiration and H_2O_2 with Cr compared to without.

Oroboros Respiration Protocols

Mouse TA – 20 mM Cr (PM)				
Substrate	Event Code	STOCK	Titration Volume (µL)	Final Concentration in Chamber
Buffer Z Lights Out BLEB Fiber	F10 BLEB Fiber	20 mM Cr 10 mM BLEB	1	5 µM
Stop stir bar, turn on lights and verify fiber is in chamber/not stuck on side wall Hit F10 (lights out)				
100% O_2	O		Injection	250-275 µM
Pyruvate Malate	P M	2M 1M	5 4	5 mM 2 mM
ADP	25µM D	5mM	10	25 µM
ADP	100µM D	50mM	3	100 µM
ADP	300µM D	50mM	8	
ADP	500µM D	50mM	8	500 µM
ADP	1mM D	500mM	2	1 mM
ADP	5mM D	500mM	16	5 mM
ADP	7mM D	500mM	8	7 mM
Glutamate	10mM G	2M	10	10 mM
Cyto c	Cyto C	4 mM	5	10 µM
Succinate	20mM S	2 M	20	20 mM

MOUSE TA – 20 mM Cr (PCoA)				
Substrate	Event Code	STOCK	Titration Volume (µL)	Final Concentration in Chamber
Buffer Z Lights Out BLEB Fiber	F10 BLEB Fiber	20 mM Cr 10 mM BLEB	1	5 µM
Stop stir bar, turn on lights and verify fiber is in chamber/not stuck on side wall Hit F10 (lights out)				
100% O_2	O		Injection	250-275 µM
L-Carnitine Malate	LC M	500mM 1M	4 4	1mM 2mM
ADP	500µM D	500mM	20	5mM
Palmitate-CoA	20µM PCoA	10mM	1	5µM
Palmitate-CoA	20µM PCoA	10mM	1	10µM
Palmitate-CoA	20µM PCoA	10mM	1	15µM
Palmitate-CoA	20µM PCoA	10mM	1	20µM
Palmitate-CoA	40µM PCoA*	10mM	4	40µM
Palmitate-CoA	60µM PCoA	10mM	4	60µM
Palmitate-CoA	80µM PCoA	10mM	4	80µM
Palmitate-CoA	100µM PCoA	10mM	4	100µM
Malonyl-CoA	0.5µM MCoA	1mM	1	0.5µM
Malonyl-CoA	1µM MCoA	1mM	1	1µM
Malonyl-CoA	2.5µM MCoA	1mM	3	2.5µM
Malonyl-CoA	5µM MCoA	1mM	5	5µM
Malonyl-CoA	7.5µM MCoA	1mM	5	7.5µM
Malonyl-CoA	10µM MCoA	1mM	5	10µM
Malonyl-CoA	20µM MCoA**	1mM	20	20µM
Cyto c	Cyto C	4mM	5	10µM

- * Keep adding 4uL (20uM) PCoA at a time until plateau is reached
- ** Keep adding 2ouL (10uM) MCoA at a time until plateau is reached

Permeabilized Fiber Preparation

Pre-surgery

1. For every fiber bundle you make you will need:
    - 1x 0.5mL tube for wet weights
    - 1x 1.5mL Eppendorf tube for permeabilization
    - 1x 1.5mL tube for wash
    - *Keep all tubes and buffers on ice
2. In a 5mL tube, make 10mg/mL Saponin solution by dissolving a small amount of saponin in distilled water.
    - Vortex gently and place on rocker until ready for use.
3. Fill all 0.5mL tubes with 500uL of BIOPS
4. Fill all permeabilization tubes with 1.5mL freshly thawed BIOPS (or BIOPS from fridge with fresh EGTA…see "Other Things to Consider") and *40ug/mL saponin (6uL in 1.5mL BIOPS).
    - *Different saponin concentrations may be used depending on species/tissue type but 40ug/mL is standard for rodent.
5. Fill all wash tubes with 1.5mL freshly thawed MiRO (or from fridge…same as above).
6. Using a 50mL falcon tube, weigh out ~ 0.05g of creatine (this number will change based on the number of chambers you need with creatine), add the correct amount of MiRO to make a 20mM Creatine MiRO Solution.
    - Place on rocker as creatine takes some time to dissolve.
7. Label and fill 1x 5mL tube with 3.5mL BIOPS for every muscle that will be harvested during surgery.
8. Proceed to "O2k Setup" Section, after O2k's are setup, you are ready for surgery.

Post-Surgery

1. Separate fibers in BIOPS quickly and carefully.
    - Change ice block/ice pack frequently (~every 10MIN), as buffer should never be allowed to warm up.
2. Place separated fibers in corresponding 0.5mL tube with BIOPS and proceed to wet weight procedure.

Bundle Wet Weights

1. Fill a 1.5mL tube with BIOPS until a "dome" of liquid covers the top.
2. Place tube in holder on scale and tare.
3. With fine forceps, remove first bundle from Eppendorf and, using a Kim wipe, blot the bundle to remove excess liquid.
    - Try to blot no more than 3 times and try to turn the bundle the same way each time to get consistent blotting.
4. Very carefully, place bundle in Eppendorf on scale, ensuring forceps don't draw up any liquid.
5. Wait for scale to stabilize and record weight.
6. Until accuracy is proven, weigh each bundle twice and take average if within 0.2mg, repeat weighing if weights are more variable.
7. When done weighing, place back in 0.5mL Eppendorf tube until all bundles have been weighed.

Permeabilization

1. Once all bundles are weighed, switch to permeabilization tubes (tubes containing saponin) using forceps or a gel loading pipette tip.
2. Place on nutator in the fridge for 30MIN.
    - Ensure all Eppendorfs have the liquid mixing by checking the air bubble is moving.
    - If air bubble appears stuck, invert Eppendorf 1-2x to allow for movement, and place back on nutator.
3. After 30MIN, transfer bundles to corresponding wash tubes using gel loading pipette tip.
4. Place bundles in wash on nutator in the fridge for an additional 15MIN.
    - Permeabilized bundles can remain in the fridge in wash for up to 2hr, but will start to lose viability after that point.
5. After 15MIN wash, proceed to "Running an Experiment"

Using the O2k

O2k Setup

1. Turn machine on using the switch on the back.
2. Open up DatLab and a connection box should pop up.
    - For O2k 1 and O2k 2:
        - O2k 1 – USB: E-0085
        - O2k 2 – Com 3: C-0024
3. When connection box pops up ensure the top blue bar says E-0.0085.

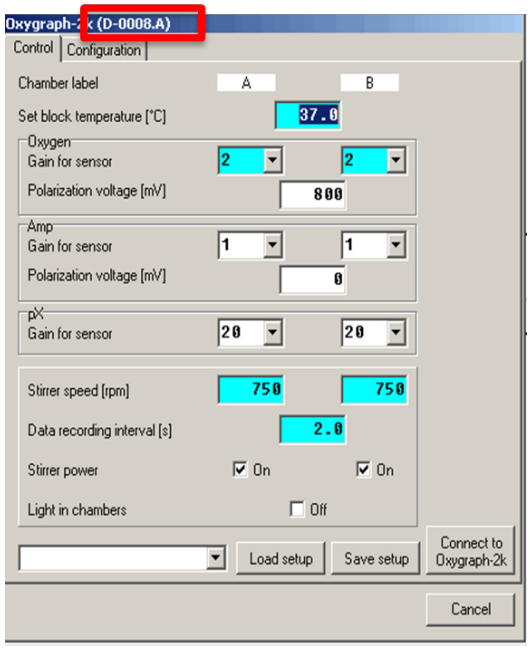

    - If it does not, click the configuration tab, click "select communication port" and select USB.
    - Click the control tab and click "Connect to Oxygraph-2k".
    - A screen will pop up asking you to change the file name, save file in location of choice.
    - An "Edit Experiment" screen will appear, click "Save".
    - After O2k-1 is connected, open DatLab again and an error screen will appear, change the serial port to "Com 3" and click OK.

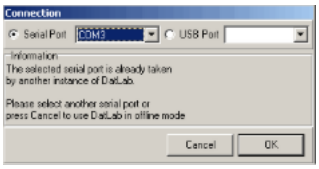

- Follow steps d-f for O2k 2.
- For O2k 3 and O2k 4:
  - O2k 3 – Com 3: D-0008
  - O2k 4 – Com 4: D-0098
  - Follow steps b-g for O2k 3 and O2k 4

4. Remove stoppers and place with top down on top of the O2k.
5. Turn on the aspirator and remove ethanol from chambers…keep aspirator AWAY from membrane inside the chamber.
   - The best way to ensure this is to only touch the bottom of the chamber on the side opposite the membrane to avoid contact.
6. Fill chambers with water and then aspirate again.
   - When cleaning chambers, don't let chambers stay dry for long, always replace liquid immediately.
7. Repeat rinse with ethanol.
8. Finish with 3 rounds of water rinses and leave spinning in water until ready to load buffers.
   - ***If this is the first experiment of the day do Volume Calibration before loading buffers**.
9. Load chambers with 2.1mL Cr-Buffer Z (or just regular Buffer Z if no creatine is wanted).
10. Push stoppers down and adjust height with plastic wrench so both stoppers are at same height.
11. Wait for both O_2 Concentration and O_2 Slope to reach steady state, then proceed with "Air Calibration".

Volume Calibration

1. Volume calibrate chambers at the start of each day, it is not necessary to do in-between rounds of experiments.
   - **** For cell culture experiments, you will need to volume calibrate for each experiment**.
   - *****VOLUME CALIBRATION IS SUPER IMPORTANT- you will need to ensure that the volume chamber when sealed is 2.1mL in order for concentration calculations to hold true.**
2. Add 2.1mL water to each chamber.
3. Using the Allen Key in the O2k Accessory kit, loosen the collar on the stopper and push all the way to the top.
4. Slowly lower stopper into chamber until the first drop of liquid comes out the top of the capillary in the stopper.
5. Push the collar all the way to the bottom and tighten with Allen Key.

Air Calibration (this is to allow all machines to start at the same point)

1. When a steady state has been achieved, click on the blue Y_1 box in the top right corner of chamber A.

2. Holding down the shift button, use your mouse, click and drag across the steady O_2 concentration line to create a "mark".
3. Click "F5." (Air cal should be at 180-200. If not, there is likely a problem with the membrane. Check solubility factor)** NOTE: THE SOLUBILITY FACTOR FOR BUFFER Z AND MIRO IS 0.92 (THIS IS BASED ON BUFFER COMPOSITION)

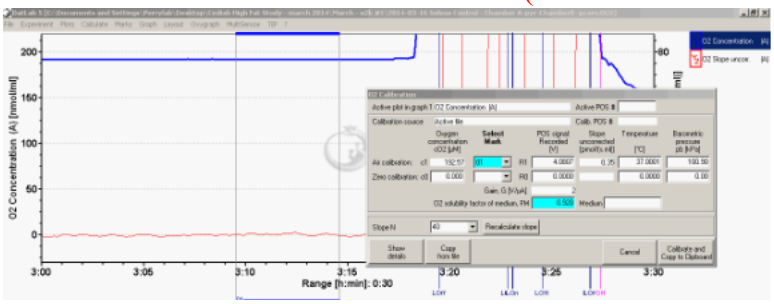

4. Select 01 in the "Select Mark" box for the "Air Calibration" line.

Running an Experiment

1. When fibers are done washing and chambers have been air phased, remove stoppers and place on top of O2k.
2. Add 5uM BLEB and stop the stir bar, pressing F11 for Chamber A and F12 for Chamber B.
3. Add fiber and loosely place stopper on chamber, not sealing it.
4. Turn stir bars back on by clicking F11 and F12, respectively.
5. Add ~10mL O_2 with syringe through capillary in stopper.
6. Wait until O_2 concentration reaches ~370 and remove stopper, O_2 concentration will continue to rise. When the levels begin to fall, push stopper in all the way, ensuring a tight seal between chamber and stopper.
7. Check there is no air bubble in the chamber.
    - If no air bubble, press F10 to shut off lights.
    - If there is an air bubble, remove stopper, add more buffer, and repeat steps 5-8.
8. Wait for background to reach a steady state…this usually takes 10MIN+ (see "Important Considerations, then proceed with respective protocol (remember to always achieve a steady state after the addition of a substrate).
    - See "Important Considerations" for important tips on setting up syringes/beakers and substrates.
9. To record when you add a substrate, click "Control", and left click the mouse at the timepoint on the graph you added a substrate, you can then make an "event".
    - A screen will pop up allowing you to name your event. You can pick whether it is for Chamber A, Chamber B, or both.
    - Do this after the addition of each substrate.
10. At the end of the experiment, turn lights on by clicking F10 and stop stir bars.
11. Remove tissue if being saved and place in labeled Eppendorf.
12. Turn stir bars back on and proceed with cleaning.
    - 3 water washes.
    - 3 ethanol washes.
    - 1 water wash.
    - Add 70% ethanol and leave in chamber.

- Rinse stoppers in sink with water and ethanol.
- Place stoppers loosely in chamber with caps on and turn off machine.

Analyzing Data

1. Open file you wish to analyze and click “F3”.
2. In the box labeled “Background Correction”, click “Copy from File”.
3. Select the O2k file that contains your most recent background curve for that machine (See “Background Curve” section).
    - Note: you can also manually enter the slope and y-intercepts from your background curve in each file.
4. Click save.
5. In the top right corner of Chamber A, click on Y_2 so the red box is highlighted.
6. Using the technique to “Make a Mark” like was done for air calibration, make marks for each steady state following a substrate addition as well as your background steady state.
    - If you make a mark and wish to delete it, hold shift, right click the mouse, and drag over the mark you wish to delete, then let go and the mark will disappear.
7. Once all marks are made, click “Layout” at the top of the screen and select “05 Flux per Volume Corrected”.
    - Your data is now corrected using the background curve you imported.
8. Click F2 and select copy to clipboard, your data can now be pasted into excel.
9. Repeat steps 5-8 for Chamber B

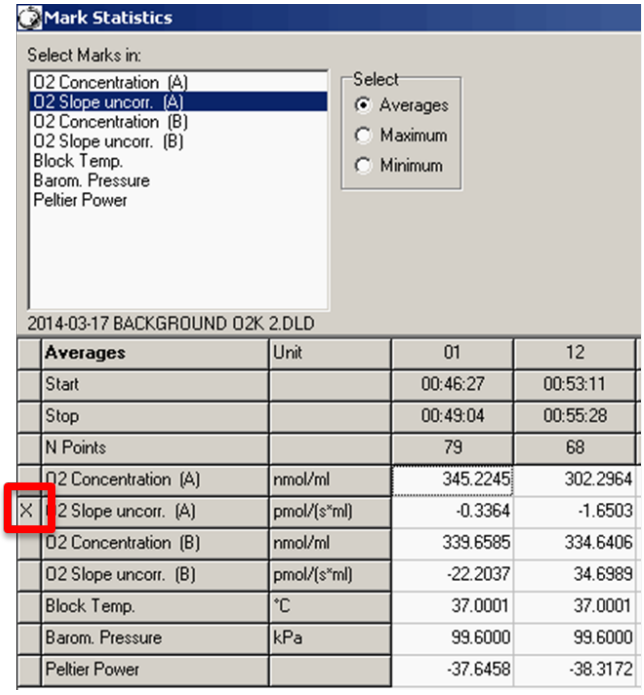

	Averages	Unit	01	12
	Start		00:46:27	00:53:11
	Stop		00:49:04	00:55:28
	N Points		79	68
	O2 Concentration (A)	nmol/ml	345.2245	302.2964
X	O2 Slope uncorr. (A)	pmol/(s*ml)	-0.3364	-1.6503
	O2 Concentration (B)	nmol/ml	339.6585	334.6406
	O2 Slope uncorr. (B)	pmol/(s*ml)	-22.2037	34.6989
	Block Temp.	°C	37.0001	37.0001
	Barom. Pressure	kPa	99.6000	99.6000
	Peltier Power		-37.6458	-38.3172

- Note: while clicking F2 and pasting will export both Chamber A and Chamber B data…the data is not accurate unless you see the “X” beside that chamber in the pasted data (glitch in the system).

POS Service and Membrane Mounting

Membranes should be changed and electrode should be cleaned when data appears excessively noisy or air calibration curves have dropped below normal
**See O2k Manual for detailed instructions and pictures
***It takes some practice to efficiently change membranes without getting air bubbles stuck. If you see one before you replace the anode into the O2K – repeat mounting the procedure**

POS Service

1. IMPORTANT: Ensure to touch somewhere on the sides of the O2K to de-static oneself before removing sensors.
2. Pull back the blue sheath and slowly remove sensor from inside the system.
3. Unplug the wire from the port on the O2K (should be plugged in to the port labeled O_2).
4. Remove the black cap from the sensor and keep in a safe place, this may be reused.
5. Using the black "membrane mounting tool" use the open end of the smaller piece to squeeze and remove the membrane ring off the sensor head.
6. Use clean forceps to remove the membrane from the top of the sensor, discard the old membrane.
7. Rinse sensor 1-2x with distilled water, covering sensor until dome of water appears and then dump water off.
8. If gold cathode looks dirty (not shiny but dark grey in colour), it must be cleaned with extreme care.
    - Using the "O2K Polishing Cloth" in the O2K accessory kit, add a small amount of "polishing powder" to the top of the cloth and wet with distilled water.
    - Place the top of the sensor face down on the cloth and very gently make small circles using the cloth and powder to clean the cathode, continue until cathode appears gold and shiny again.
9. Rinse sensor 1-2x with distilled water.
10. The anode also becomes oxidized over time, changing it from a cream colour to a dark grey colour. When this happens it must be cleaned with 25% ammonia.
11. Under a fume hood, cover sensor with 25% ammonia until a dome appears, leave for 10MIN.
12. Repeat 1-2x until grey colour disappears, if anode is very dark it may require overnight treatment with ammonia and/or a higher % ammonia solution.
13. If leaving overnight in ammonia, seal ammonia in with membrane (see below), and make sure sensor is protected from light.
14. After cleaning, rinse 1-2x with water to ensure all traces of ammonia are removed.

Membrane Mounting

1. If this is the first time mounting a membrane, fill "electrolyte solution" up to the 10mL mark with distilled water
    - This is simply 1M KCl (you can also dissolve 1.49g KCl in 20mL water)
2. Cover sensor with electrolyte until a "dome" appears
3. With forceps, remove a membrane from the membrane box, avoiding contact with the skin removing the paper from either side of the membrane.
4. Using the wider piece of the membrane mounting tool, place membrane flat on the ledge inside the tool.
5. Pull down the sheath on blue POS connector and place membrane mounting tool on top of sensor, letting go of sheath so it locks in place with the membrane lying flat on top of the electrolyte solution

6. Place membrane ring around circle on the end of the smaller piece of the membrane mounting tool.
7. Using a good amount of force, push the smaller piece of the membrane mounting tool straight down on top of the membrane so the membrane ring locks in place.
8. Remove both pieces of the membrane mounting tool (pull back sheath to remove bigger piece).
9. Check for air bubbles under the membrane, if there are considerable air bubbles you must restart at step 2 with a new membrane.
10. Once membrane is mounted with no air bubbles, cover the sensor with the black rubber cap and make sure the entire gold cathode is visible.
11. Plug connector wire into O_2 port, pull back sheath on POS and place sensor back in place in the O2k.
12. Let DatLab run with the machine on for 24hr to allow new membrane to equilibrate.
    - File will start off very noisy but by the end of 24hr, it should be a flat line. If file is still noisy, remove sensor and check membrane.

*Over time the black caps get looser, if you notice the chamber leaking after replacing the membrane, replace the black cap to obtain a tighter seal.

Background Curves

1. Set up O2k as you would for a normal experiment (see "O2k Setup"), loading chambers with 2.1mL of Buffer Z.
2. When a steady state is achieved for the air phase, complete air calibration (see "Air Calibration").
3. Add O_2 to chambers until O_2 levels reach ~370 (hyper-oxygenate), remove stoppers to ensure no air is trapped in stoppers.
4. When O_2 levels start to drop, push stoppers in all the way and make sure there is no air bubble within the chamber.
5. Allow for a background steady state to be achieved.
6. Using the "zeroing powder" (dithionite) in the O2k accessory kit, mix a few grains of dithionite with distilled water and vortex.
7. Add 1uL of dithionite solution to each chamber once a steady state is achieved.
    - It is impossible to know how much dithionite to add, you want the oxygen concentration to drop 30-40 units with each addition so with your first addition add 1uL, see how much it drops, and add more if necessary.
    - Dithionite **degrades over the course of the experiment** so towards the end of the titration you will need a larger volume to get the same reduction in oxygen,
8. After each addition, wait for a steady state to be achieved, continue with dithionite additions until O_2 concentration reaches ~0. **When O_2 looks to be reaching zero add a large amount of dithionite (~20uL) to ensure O_2 levels are at 0.**
9. Once O_2 has reached zero, create a mark measuring O_2 concentration at the zero level in the same way you would make your air calibration mark.
10. Click F5 and insert "02" in the zero calibration "Select Mark" box.

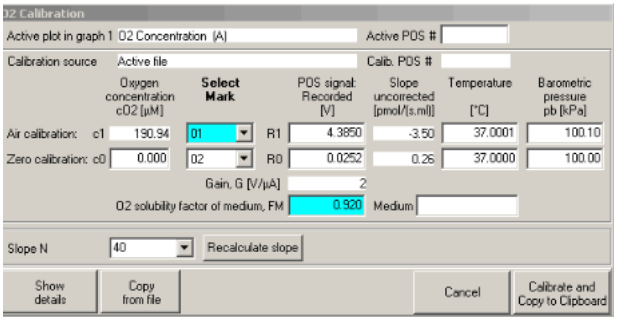

- Note: "01" should already be inserted in the "Air Calibration Select Mark Box"

11. Click "Calibrate and Copy to Clipboard".
12. Click on the red Y_2 box in the upper right corner of each chamber to switch to "Respiration Mode", using the method for making marks (see "Air Calibration"), make marks for each steady state that occurs after a dithionite addition (including the background steady state).
13. With Chamber A highlighted (click anywhere on the chamber A box), select "F2" and then select "copy to clipboard".
14. In Excel, paste the data you have just copied from DatLab.
15. Using the "O_2 Concentration (A)" and "O_2 Slope Uncorr. (A)" data, create a graph with concentration on the y-axis and slope on the x-axis.
    - By having 7-10 points to use, you can drop outliers that do not fit the straight-line model.
16. Repeat steps 13-15 for Chamber B.
17. Record the slope and y intercept for each chamber.
18. Back in your DatLab file, click "F3". In the section that says "Background Correction", insert your y intercept for each chamber in the a° boxes and the slopes in the b° boxes, and click save.

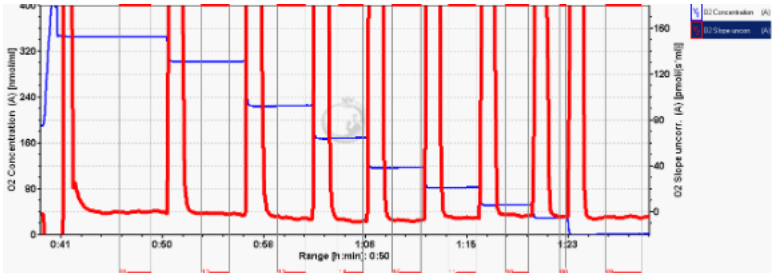

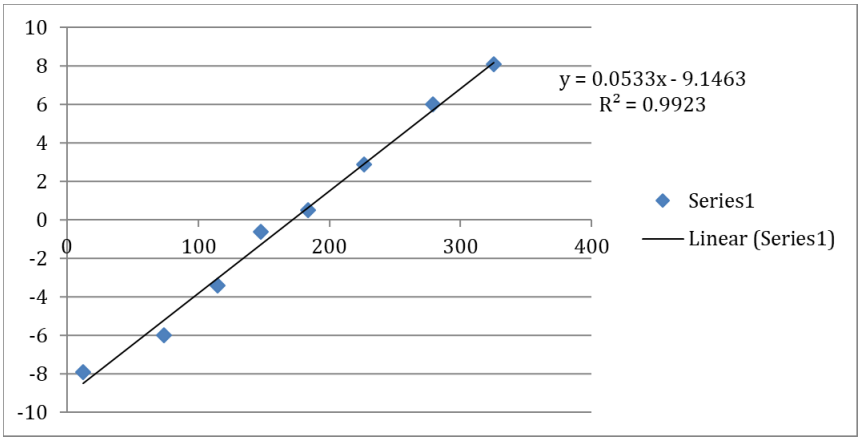

1. Typical ranges for equation of the line are:
    - 0.03 to 0.07 (slope)
    - -3 to -8 (Y-Intercept)

Important Considerations

Buffers

1. Buffers must be thawed fresh each day for actual data collection. When thawed, write the date of thawing on the tube, and place any left-over in the fridge. For practice, buffers in the fridge can be reused…if it was thawed <2 days prior, it is fine to use as is. If it was thawed 3 days prior or more (up to 1 week….throw out buffers that are more than a week old) it must be topped up with EGTA. To do this, pour buffer into graduated cylinder to get accurate volume. Thaw a 0.5M EGTA from the freezer and add corresponding volume to get the following final concentrations:
    - BIOPS: 10mM
    - MiRO: 0.5mM
    - Buffer Z: 1mM

Substrates

1. When making substrates, pH to 7.1 and aliquot into small volumes, enough for 6 chambers for 1 protocol. When running experiments, thawed substrates cannot be put back in the freezer, they must be placed in fridge and can be used for up to 1 week after thawing.
2. **ADP must be thawed fresh each day, do not reuse for actual data collection (OK for practice).
3. Pyruvate must be made fresh each day, make 2M solution in a 1.5mL Eppendorf by combining powder and water, throw out at the end of each day.

Syringes and Beakers

1. Each protocol being followed should have its own separate syringe and beaker filled with water. Syringes should be rinsed with water prior to use and should be wiped with a Kim wipe after being put in the chamber to remove residual buffer. When switching substrates, syringes should be rinsed thoroughly with water.

Steady States

1. It is very important to ensure a steady state is achieved before each subsequent addition in order to get accurate data. When waiting for background steady state (after adding fiber, but before adding any substrates) wait until respiration has leveled out ABOVE zero. If the background is below zero, respiration will be a negative and all data will be corrected for a negative rate. This may take 10MN+ to achieve proper steady state.
2. After adding glutamate/pyruvate/malate, respiration often tends to slowly increase. Again, make sure you have an accurate steady state so you do not end up overestimating this rate and getting a lower rate with your first substrate addition (may need to wait 5MIN+).
3. If data is very noisy, make a large mark over steady state as opposed to trying to find a small flat line. Taking a larger area average will give a more accurate reading.

Oxygen Levels

1. Do not let oxygen levels drop below 150. If oxygen is below 200, make next addition and wait for steady state, once respiration has achieved steady state, loosen stopper, and re-oxygenate up to 370. Push stopper back in and wait for steady state. Often when

reoxygenating, respiration rates steady state higher than before reoxygenation, if this happens, take an average of the rate before reoxygenation and after reoxygenation and then proceed with adding next addition.